

**THE TIME COURSE OF CHANGES IN SKELETAL MUSCLE METABOLITES DURING
MUSCLE REPAIR, AS DETECTED BY PROTON NUCLEAR MAGNETIC RESONANCE
SPECTROSCOPY.**

BY

ROSS E. BAKER

A Thesis
Submitted to the Faculty of Graduate Studies
in Partial Fulfilment of the Requirements
for the Degree of

MASTER OF SCIENCE (M.Sc.)

Department of Human Anatomy and Cell Science
University of Manitoba
Winnipeg, Manitoba

(c) May 1999



National Library
of Canada

Acquisitions and
Bibliographic Services

395 Wellington Street
Ottawa ON K1A 0N4
Canada

Bibliothèque nationale
du Canada

Acquisitions et
services bibliographiques

395, rue Wellington
Ottawa ON K1A 0N4
Canada

Your file Votre référence

Our file Notre référence

The author has granted a non-exclusive licence allowing the National Library of Canada to reproduce, loan, distribute or sell copies of this thesis in microform, paper or electronic formats.

The author retains ownership of the copyright in this thesis. Neither the thesis nor substantial extracts from it may be printed or otherwise reproduced without the author's permission.

L'auteur a accordé une licence non exclusive permettant à la Bibliothèque nationale du Canada de reproduire, prêter, distribuer ou vendre des copies de cette thèse sous la forme de microfiche/film, de reproduction sur papier ou sur format électronique.

L'auteur conserve la propriété du droit d'auteur qui protège cette thèse. Ni la thèse ni des extraits substantiels de celle-ci ne doivent être imprimés ou autrement reproduits sans son autorisation.

0-612-41678-X

Canada

**THE UNIVERSITY OF MANITOBA
FACULTY OF GRADUATE STUDIES

COPYRIGHT PERMISSION PAGE**

**THE TIME COURSE OF CHANGES IN SKELETAL MUSCLE METABOLITES
DURING MUSCLE REPAIR, AS DETECTED BY PROTON NUCLEAR MAGNETIC
RESONANCE SPECTROSCOPY.**

BY

ROSS E. BAKER

**A Thesis/Practicum submitted to the Faculty of Graduate Studies of The University
of Manitoba in partial fulfillment of the requirements of the degree
of
Master of Science**

Ross E. Baker©1999

Permission has been granted to the Library of The University of Manitoba to lend or sell copies of this thesis/practicum, to the National Library of Canada to microfilm this thesis and to lend or sell copies of the film, and to Dissertations Abstracts International to publish an abstract of this thesis/practicum.

The author reserves other publication rights, and neither this thesis/practicum nor extensive extracts from it may be printed or otherwise reproduced without the author's written permission.

To My Mom and Dad, the bearers of my soul.

ABSTRACT

Duchenne muscular dystrophy (DMD) is characterized by progressive deterioration of muscles due to the lack of dystrophin. To date there is no effective method for monitoring DMD progression without reverting to biopsies and subjective muscle strength testing. With the discovery of the mdx mouse muscular dystrophy, similar to DMD, and the accessibility and use of nuclear magnetic resonance (NMR), ¹H-NMR may prove valuable to monitor progression and track therapy. *Ex vivo* and extract ¹H-NMR studies from this laboratory indicate that the resonances contributed by taurine and other metabolites are indicators of repair and disease progression. Following these metabolites may provide information to interpret the repair sequence by non-invasive means. Experiments were designed to test whether ¹H-NMR can detect the phases of myofiber repair 0-14 days (d) after an imposed injury to C57 mouse tibialis anterior (TA) muscle. Muscle crush injury was employed to produce synchronous muscle repair. Water-soluble metabolites were extracted from TA crushed, uncrushed and control muscle samples using perchloric acid. One-dimensional spectra were acquired from double-coded extracts on a narrow bore 500 MHz spectrometer using sodium 3-trimethylsilyl-propionate as a quantitative chemical shift reference. Control extracts were expected to dominate all peaks. However phasic metabolites like acetate, an unknown metabolite, choline, carnitine and glutamate exhibited significant time dependent changes in crushed samples that correlated with specific stages of repair. The concentrations of progressive metabolite such as lactate, creatine and taurine decreased immediately following the imposed crush injury before progressively returning to control levels by day 14 of the experiment. As well, taurine peaks (3.26 and 3.41 ppm) exhibited varying degrees of chemical shift, perhaps from pH sensitivity to lower buffering metabolites and cellular infiltration. Our results support the notion that ¹H-NMR can differentiate stages of skeletal muscle regeneration at specific marker metabolites over a time course of change. As well, the present results support taurine's role as a sarcolemmal stabilizer.

ACKNOWLEDGMENTS

“[T]his kind of stone [the magnet] restores husbands to wives and increases elegance and charm in speech. Moreover, along with honey, it cures dropsy, spleen, fox mange, and burns....[W]hen placed on the head of a chaste woman [the magnet] causes its poison to surround her immediately, [but] if she is an adulteress she will instantly remove herself from bed for fear of an apparition....There are mountains made of such stones and they attract and dissolve ships made of iron.”

- Bartholomew the Englishmen. (encyclopedist), 13th century A.D.

(From: The Experts Speak. The Definitive Compendium of Authoritative Misinformation. Cerf C. and Navasky V., 1984)

If nothing else my Master of Science degree has taught me the importance of patience, sound analysis and synthesis of scientific research (It seems Bartholomew dismissed a few scientific principles).

I would like to thank all individuals that contributed to completion of my Masters degree. As we know nothing in science (as in life) is complete without contributions from our peers.

First I would like to express a very grateful ‘Thank You’ to my advisor, Dr. Judy Anderson. Her scientific capabilities and thoughts command the foremost respect, I am fortunate to have had the experience of learning under her watchful eye.

Dr. Archie Cooper, Dr. Jim Peeling and Dr. Elliott Scott contributed significantly to the final draft of my thesis. I appreciate their rigorous review of my thesis. I learned some important lessons about drafting a scientific report that I hope will serve me well in the future.

The Department of Human Anatomy and Cell Science provided me with a unique education that will assist my career. The teaching and administrative experience is gratefully appreciated. Without monetary support this degree would have been very difficult to complete. I would like to thank the Anatomical Research Fund, the University of Manitoba Graduate Student Fellowship and the Muscular Dystrophy Association (through Dr. Anderson). Thank You.

I made many friends while studying at the University of Manitoba. Jason Taylor has rewarded me with many memorable events. I wish him success in all his future endeavours. Speaking of memorable events Mike Weber has entertained me (in a good way) since the first day he arrived in the lab, have fun Orest! It has been a pleasure having Ryan Skrabek in the lab, I am sure he has a bright future to look forward to (he likes Labrador Retrievers). I would also like to acknowledge Marla Wilson, Tracy Harrower and Melissa Jones, you rock at floor hockey!

A special thank you to Terry Wolowiec, Dr. Laura McIntosh, Dr. Andrea Moor and Cynthia Vargas. Your tireless support and help, and your friendship will always be appreciated and revered.

My stay in Winnipeg has been made more precious because of friends like Steve and Correna Peck. I consider you family and thank you for all the great times and breaks from my occasional ennui.

The friend I have in Charis Kepron is unequivocal. A great listener and a beautifully intelligent companion. Cheers.

LIST OF FIGURES AND TABLES

Chapter 3

Figure 3.1 Crush Injury.

Figure 3.2 Tagged Crush Site.

Figure 3.2 Muscle Sample Schematic.

Chapter 4

Figure 4.1 Averaged Spectra.

Figure 4.2 1D-TOCSY Spectrum.

Figure 4.3 Pure t-Butanol Spectrum and Skeletal Muscle Spectrum Overlaid.

Figure 4.4 Pure Mevalonic Acid, Pure t-Butanol and Skeletal Muscle Spectra Overlaid.

Figure 4.5 Contamination Samples Spectra.

Figure 4.6 Representative ¹H-NMR Spectrum Indicating Metabolites.

Table 4.1 Summary of Duncan's New Multiple Range Test.

Figure 4.7(A-N) Metabolite Changes Over the Time Course of Repair.

Figure 4.8 Crush-Injured Skeletal Muscle Sample Data Expressed as the % Difference
From Control Muscle Sample Data.

Figure 4.9 Lactate and Taurine Moiety Ratios.

Figure 4.10 Chemical Shift of Taurine.

Figure 4.11 Uncrushed Muscle Sample Changes Compared to Crushed Muscle and
Control Muscle Sample Changes.

Appendix A

Figure A-1 Spectrum Acquired from a Skeletal Muscle Sample Spiked with Mevalonic
Acid.

Figure A-2 Spectrum Acquired from a Skeletal Muscle Sample Spiked with Taurine.

Figure A-3 Spectrum Acquired from a Pure Sample of Taurine.

Table A-1 Taurine Yield Data (trial 1).

Table A-2 Taurine Yield Data (trial 2).

Appendix B

Table B-1 Crushed Mean Area Data Including Standard Deviation, Group Size, Age.

Table B-2 Control Mean Area Data Including Standard Deviation, Group Size, Age.

Table B-3 Uncrushed Mean Area Data Including Standard Deviation, Group Size, Age.

Table B-4 Analysis of Variance Tables for each Metabolite Studied.

TABLE OF CONTENTS

Abstract	ii
Acknowledgments	iii
List of Figures and Tables	iv
Chapter 1 - Introduction	1
<i>Section 1</i>	1
SKELETAL MUSCLE - STRUCTURE	
1.0 Basic Skeletal Muscle Organization	2
1.01 The Myofiber	2
1.02 Skeletal Muscle Connective Tissues	2
1.1 Skeletal Muscle Cytoskeleton	3
1.11 Basic Skeletal Muscle Histology	3
1.12 Contacts Within and Between Myofibrils	5
1.12a The M Region or M Line	5
1.12b The Z Disc or Z Line	7
1.12c Intermediate Filaments	8
1.13 Peripheral Myofibrils and the Sarcolemma	9
1.13a Costameres and Dystrophin	9
1.13b Transmembrane Plaques	10
1.14 Laminin and the Extracellular Matrix	12
<i>Section 2</i>	13
SKELETAL MUSCLE - METABOLISM	
2.0 Energy Metabolism	14
2.1 Lipid Metabolism	16
2.11 Cholesterol Biosynthesis	18
2.12 Control of Cholesterol Biosynthesis and Transport	20
2.2 Protein Metabolism	21
<i>Section 3</i>	24
SKELETAL MUSCLE - DEGENERATION AND REGENERATION	
3.0 Inflammation	24
3.01 Intrinsic Phase	26

3.02 Cell-Mediated Phase	27
3.021 Acute Inflammation	28
3.021a Vascular Response	28
3.021b Cellular Response	29
3.021c Acute-Phase Response	31
3.022 Chronic Inflammation	32
3.1 The Response of Normal Skeletal Muscle to Injury	32
3.2 The Response of Dystrophic Skeletal Muscle to Injury	37
 <i>Section 4</i>	 38
PROTON NUCLEAR MAGNETIC RESONANCE SPECTROSCOPY	
The Magnet	40
The Probe and Magnetic Field Stability	40
4.0 Spectroscopy Basics	42
4.01 Nuclei and Spin	43
4.02 Nuclear Magnetic Resonance Frequency	43
4.03 Chemical Shift and Proton J-Coupling	44
4.1 Pulse NMRS Techniques	45
4.11 The Pulse	46
4.12 Relaxation	47
4.13 Saturation and Peak Suppression	48
4.14 Exponential Multiplication	49
4.2 Advanced NMRS Techniques: 1D-TOCSY	50
4.3 Instrumental Sensitivity	50
 Chapter 2 - Research Hypotheses and Significance	 53
 Chapter 3 - Materials and Methods	 55
3.0 Animals	55
3.1 Muscle Crush Surgery and Skeletal Muscle Recovery	55
3.11 Crush Surgery	55
3.12 Sample Collection	56
3.2 Sample Preparation	58
3.21 Perchloric Acid Extraction	58
3.3 ¹ H-NMR Spectroscopy	60
3.4 Pure Compounds	61
3.5 One-Dimensional Total Correlation Spectroscopy (1D-TOCSY) Parameters	62

3.6 Spectral Analysis	63
3.7 Statistical Analysis	63
Chapter 4 - Results	68
4.1 Spectral Acquisition	68
4.2 Experimental Results	69
4.2A An Unknown Metabolite Peak at 1.25ppm	69
4.2A1 Averaged Spectra	70
4.2A2 1D-TOCSY	70
4.2A3 Pure t-Butanol in D ₂ O	71
4.2A4 Skeletal Muscle Extracts Spiked with Mevalonic Acid and HMG-CoA	71
4.2A5 Contamination	72
4.2B Significant Metabolite Concentrations and Changes	72
4.2B1 Comparison of Damaged Muscle to Control Muscle	73
4.2B2 Comparison of Regenerating Muscle to Control Muscle	74
4.2B3 Comparison of Damaged Muscle and Regenerating Muscle	75
4.2B4 Comparison of Control Muscle Samples	75
4.3 Chemical Shift of Taurine	76
Chapter 5 - Discussion	97
5.1 A Compound Similar to Tertiary Butyl Alcohol	98
5.11 Averaged Spectra	98
5.12 The 1D-TOCSY Experiment	99
5.13 Tertiary Butyl Alcohol, Mevalonic Acid and HMG-CoA	100
5.2 Control Skeletal Muscle Samples	101
5.3 Crush-Injured Skeletal Muscle	102
5.31 Comparison of Damaged Muscle to Control Muscle	103
5.32 Comparison of Regenerating Muscle to Control Muscle	103
5.4 Taurine and Stability of the Sarcolemma	106
5.5 Cholesterol Biosynthesis and New Membrane Formation	108
5.6 Acetate and Experimental Precision	109
5.7 Uncrushed Skeletal Muscle Samples	112
5.8 Conclusions	113
5.9 Significance	114
Future Research	115
References	117
Appendix A - ¹H-NMRS Yield of Taurine	128

CHAPTER 1 - INTRODUCTION

Section 1

SKELETAL MUSCLE-STRUCTURE

Skeletal muscle has been described as the most highly organized and structurally specialized of all tissue types (Watermann-Storer, 1991). The characteristic arrangement of its contractile proteins and modifications in both the distribution and morphology of its organelle systems makes skeletal muscle as body's specialist in producing voluntary movement from metabolic energy. Basically, skeletal muscle is responsible for body movement and locomotion. It attaches to the bony skeleton and in some situations the overlying dermis of the skin, e.g. muscles of facial expression. The functional cellular unit of muscle tissue is the myofiber which produces and maintains those proteins responsible for the contractile nature of this tissue. Skeletal muscle's role in mechanical movement and locomotion requires exceptional strength and resilience at the molecular level (Watermann-Storer, 1991) as it must maintain its structural integrity through continual cycles of contraction and relaxation. Although a resilient and plastic structure, when skeletal muscle is damaged by disease or strenuous exercise, either adaptive or disruptive changes may occur (Watermann-Storer, 1991).

Structural integrity of skeletal muscle is accomplished through muscle connective tissues and a highly organized intracellular and extracellular cytoskeleton that is maintained by various cytoskeletal proteins, many with functions specific to skeletal muscle. Disassembly or disruption at any level of this cytoskeleton could result in serious

functional deficits, which may be the case for many if not all forms of muscular dystrophy identified to date.

Comprehension of the skeletal muscle cytoskeleton is essential in order to make sense of molecular myopathies. The following section reviews skeletal muscle's myofiber and connective tissues. This review emphasizes cytoskeletal architecture in relation to fiber integrity from the **M** line and **Z** discs of the intracellular matrix to the ultimate association across the sarcolemma with the extracellular matrix, specifically laminin.

1.0 BASIC SKELETAL MUSCLE ORGANIZATION

1.01 The Myofiber

A myofiber is a multinucleated, elongated, cylindrical cell that may or may not extend the entire length of a particular muscle. One fiber is composed of many myofibrils. The myofiber itself is arranged with many other myofibers to constitute a fascicle or bundle. It is the parallel arrangement of fascicles and connective tissue sheaths which forms the muscle observed in gross dissection.

1.02 Skeletal Muscle Connective Tissues (Bloom and Fawcett, 1975)

Muscle connective tissues are important for the transmission of forces from

myofibers to tendon; as well, they confer structural integrity to the muscle when producing work. Therefore connective tissues are as important to muscle function as the myofiber itself. There are three levels of connective tissues: the epimysium, the perimysium and the endomysium. The epimysium or deep fascia is a tough, thick outer covering that separates and binds muscles together. It is continuous with the tendon of the muscle and is connected to the perimysium. Within the muscle the perimysium binds the fascicles together and provides a pathway for major blood vessels and nerves to pass through the muscle belly. Deep to this tough perimysial covering exists a loose, more delicate network of collagen fibrils, some being connected to the endomysium, where arterioles and venules are located with intramuscular nerve branches (Banks, 1993). The endomysium is that connective tissue covering which invests each myofiber. Internal to the endomysial investment, the myofiber is further circumscribed by the external lamina (EL or basement membrane, as it is referred to in many scientific reports related to skeletal muscle regeneration). “External lamina” will be used in this thesis as not to cause confusion with the epithelial basement membrane

1.1 SKELETAL MUSCLE CYTOSKELETON

1.11 Basic Skeletal Muscle Histology

Traditional histology describes skeletal muscle as a repeating assembly of myosin-thick and actin-thin filaments arranged in a myofibril-registered pattern of cross striations.

The cross striations are viewed with a polarizing microscope as alternating light and dark bands. The dark band is referred to as the **A** (anisotropic) band and the light band is the **I** (isotropic) band. The **A** band length is unchanging in muscle activity, while the **I** band length decreases with contraction and increases in a relaxed state. A sarcomere is defined as the contractile unit of skeletal muscle and is separated from contiguous sarcomeres of the same myofibril by two successive **Z** discs (sometimes called the **Z** line). Therefore one sarcomere includes an **A** band and half of the two adjacent **I** bands.

The **Z** disc is a dense line that bisects the middle of the **I** band (which contains only actin filaments). As well as demarcating the lateral boundary of each sarcomere, the **Z** disc is the site whereby the actin filament lattice is maintained and each myofibril forms registered connections with adjacent myofibrils. Peripheral myofibrils in a fiber cross section communicate with or attach to the sarcolemmal costameres through **Z** discs alongside adjacent myofibrils.

The **A** band, which appears darker than the **I** band as it is a thicker protein rod composed of many parallel myosin filament rods, has a lighter zone (the **H** zone) at its center that is microscopically visible in a relaxed myofiber. A dense line referred to as the **M** line bisects this lighter zone. The **M** line is the result of a number of bridges that connect myosin filaments at their centers and maintain an organized arrangement of the thick filaments.

This describes skeletal muscle in a most basic sense, but to fully comprehend the scope of skeletal muscle myopathy we need a much more detailed picture of skeletal muscle anatomy. In fact we need to look at the formation of these skeletal muscle

structures viewed by light microscopy and understand how they are organized. A basic comprehension of the skeletal muscle cytoskeleton at the molecular level is required when reading through current literature. It is helpful to visualize how the intracellular matrix of skeletal muscle is connected in parallel to its extracellular matrix.

1.12 Contacts Within and Between Myofibrils

1.12a *The M Region or M Line*

The **M** region, bisecting the **H** zone, is the site of linkage between myosin thick filaments. This link is accomplished with primary M bridges, secondary M bridges and M filaments (see McComas, 1996, pg. 14, figure 1.8).

The primary M bridges appear under the electron microscope as three to five lines running perpendicular to the longitudinal axis of a myofiber between the myosin filaments. They are numbered relative to the M1 set at the center. The M4, M4' set is one set located bilateral to the midline M1 set. The M6, M6' set is bilateral to the M4 lines. It is hypothesized that these M bridges add stability to the A band by cross-connecting myosin filaments (Stromer, 1995). The primary M bridges have been described in the literature as existing in a three-line (M1, M4 and M4') pattern, or a four-line (weak M1) pattern or the M region may be altogether absent (Stromer, 1995). The varying patterns are a function of muscle fiber type, age, species and muscle tissue type. The potential absence of the M bridges in some fiber types is indicative of a nonessential

function or at least the existence of other linkages.

Additional linkages include secondary M bridges and M filaments. The M filaments, as described by Luther and Squire (1978) are arranged parallel to myosin and connect the previously described primary M bridges at their centers. The secondary M bridges are thought to connect M filaments to each other.

Immunocytochemistry and immunofluorescence studies by various researchers have revealed the constituents of some of these linkages. For example, the creatine kinase isoform MM-CK has been isolated to the sarcoplasm (majority) and the M4, M4' lines of the primary M bridges (Walliman et al., 1983). Myomesin and the M protein are two other skeletal muscle proteins that have been isolated to the M region. Specifically, the M protein has been demonstrated as the major constituent of the M6, M6' lines and possibly of the M1 line or M filaments (Strehler et al., 1983). Grove et al. (1984) and Carlsson et al. (1990) localized myomesin to the M region. Bahler et al. (1985) provided further evidence supporting myomesin and M protein localization at myosin's center. The specific role of any of these proteins in the organization of the M region structures is not known nor are there standing hypotheses in the literature. The apparent complexity of the M line and H zone may be due to a redundancy in nomenclature.

A fourth protein associated with the M region is skelemin (Price and Gromer, 1993). Price and Gromer (1993) observed that anti-skelemin antibody stained M regions within myofibrils and an intermyofibrillar band between M regions of adjacent myofibrils. Price and Gromer's (1993) work indicate skelemin may form linked rings around the periphery of the myofibrillar M region thereby providing a link between

myofibrils and the intermediate filament (IF) cytoskeleton. Thus, throughout cycles of contraction and relaxation skelemin may contribute to the structural integrity of striated muscle by binding myofibril to myofibril.

1.12b *The Z Disc or Z Line*

As previously described, the **Z** disc is the dark line seen under light microscopy at the center of each **I** band. It demarcates the boundaries of a sarcomere and has been described as a dynamic structure involved in determining some of the mechanical properties of muscle (Goldstein et al., 1991). Actin filaments, like myosin, rely on associated proteins for structural support to maintain proper position within a sarcomere. The **Z** disc is thought to be composed of a number of skeletal muscle proteins including: α -actinin, desmin, vimentin, synemin, paranemin, Cap Z, Z-nin, Z protein, zeugmatin, filamin and vinculin. Of these **Z** disc filaments α -actinin is thought to be the cross-connecting **Z** filament found in the central domain of the **Z** disc (Stromer, 1995). α -Actinin draws actin filaments into a square lattice at the **Z** disc (McComas, 1996). The **Z** filaments, such as desmin, vimentin and synemin are the intermediate filaments located at the periphery of the **Z** disc, linking adjacent **Z** discs together and peripheral myofibrils to the sarcolemma. Cap-Z, Z-nin, Z protein, zeugmatin, filamin and vinculin, the other listed **Z** filament proteins, have each been isolated to the **Z** line and thus represent integral **Z** line proteins. Their specific contributions to **Z** line structure is unknown.

1.12c *Intermediate Filaments*

The group of intermediate filaments (IF) are named due to early observations that described the diameter of these filaments is between that of actin (6 nm) and myosin (16 nm). The first IF protein to be purified and localized to the **Z** disc was desmin. Since desmin's discovery, three other IFs have been characterized which include vimentin (Granger and Lazarides, 1979), synemin (Granger and Lazarides, 1980) and paranemin (Breckler and Lazarides, 1982). Paranemin is present in embryonic skeletal muscle but is lost in fully differentiated adult muscle (Breckler and Lazarides, 1982).

All four of these IFs share the same distribution and are located in the peripheral domain of the **Z** disc (Lazarides et al., 1981). The filaments essentially wrap around each **Z** disc to connect it to neighboring **Z** discs within a myofiber (Tokuyasu et al., 1983). Tokuyasu et al. (1983) further demonstrated how desmin links to the sarcolemma, mitochondria, nucleus and the sarcoplasmic reticulum. Wang et al. (1983) identified transverse and peripheral longitudinally arranged IFs between **Z** discs and proposed a mechanical role for the longitudinal IF in limiting extreme length changes of sarcomeres.

So far we have seen how **M** region structures, such as M bridges and M filaments, cross connect myosin filaments while maintaining myosin's position within a myofibril and establish registry with **M** regions of adjacent myofibrils through proteins like skelemin. We have also seen how actin filaments are cross connected at the **Z** disc via α -actinin and how adjacent myofibrils are held in register by a number of intermediate filaments, especially desmin. The result is the maintenance of a muscle's registered

appearance and structural integrity.

The next logical step is to understand how skeletal muscle's myofibrillar contractile machinery affixes to the sarcolemma and in so doing, how it transfers contractile force to the extracellular matrix.

1.13 Peripheral Myofibrils and the Sarcolemma

1.13a *Costameres and Dystrophin*

Costameres are robust structures essential for force transduction to the substratum (Danowski et al., 1992). Extrinsic or intrinsic degradation of costameres can significantly alter the functional and structural integrity of muscle fibers (Taylor et al., 1995). Craig and Pardo (1983) describe the costamere component of skeletal muscle as rib-like filamentous bands running between peripheral myofibrils and the sarcolemma. Furthermore they have been described as occurring intermittently along the myofibril within the I band at the level of the Z disc registry (Craig and Pardo, 1983; Taylor et al., 1995). Costameres are thought to consist of: dystrophin and γ -actin; the adhesion proteins, β -spectrin, talin, vinculin, clathrin and ankyrin; and the IF proteins, desmin and vimentin. A second costamere-like network has been demonstrated for the M region that extends from peripheral myofibrils to the sarcolemma. This network involves links between skelemin, the intermediate filament cytoskeleton and the sarcolemma.

Many investigators have reported the significant role dystrophin plays in

maintaining the resilience and plasticity of skeletal muscle. Following the discovery of the Duchenne Muscular Dystrophy (DMD) gene (Hoffman et al., 1987), dystrophin was localized intracellularly immediately beneath the sarcolemma. It was later found to form costameric cytoskeletal networks in normal muscle, while it was absent in DMD muscle. In 1987 Koenig et al. proposed a model for dystrophin when they cloned the dystrophin complementary DNA. Koenig et al. (1987) suggests dystrophin is long and presents four separate functional domains which are called the actin-binding (N-terminal), rod, cysteine-rich and C-terminal domains. It is thought that γ -actin binds to the N-terminal domain of dystrophin and the cysteine-rich domain (including the first half of the C-terminal domain) binds to a group of dystrophin associated proteins (DAPs) immediately connected to the sarcolemma and the extracellular matrix. Precisely how each costameric protein contributes to subsarcolemmal networks, the structures they form with dystrophin and their exact location will be better understood “when research tools with higher resolution are developed and utilized” (Stromer, 1995).

1.13b *Transmembrane Plaques:*

When dystrophin was first dissociated from the sarcolemma and purified, many other proteins were co-purified along with it. Later many of these proteins were described by Ervasti et al. (1990) and Yoshida and Ozawa (1990) under the name dystrophin associated proteins (DAPs) or dystrophin glycoprotein complex (DGC). Some of these DAPs are transmembranous or extracellular glycoproteins, while others are

nonglycosylated membrane proteins present intracellularly. In 1994, Yoshida et al. fractionated these DAPs into three separate complexes, each composed of several proteins. These complexes are called the dystroglycan complex, the sarcoglycan complex and the syntrophin complex. All three of these complexes directly associate with dystrophin beneath the sarcolemma at different loci. The dystroglycan complex is composed of α -dystroglycan, an extracellular glycoprotein and β -dystroglycan, a transmembrane glycoprotein. The sarcoglycan complex is composed of transmembranous glycoproteins which include α -, β -, γ - and δ -sarcoglycans. The syntrophins ($\alpha 1$ -, $\alpha 2$ -, $\beta 2$ -) are located intracellularly. In the absence of dystrophin, as is the case for Duchenne Muscular Dystrophy (DMD), a severe reduction of all DGC proteins occurs with concurrent disruption of linkage between the extracellular matrix (ECM) and the cytoskeleton (Brown and Lucy, 1993; Ohlendieck et al., 1993; Matsumara and Campbell, 1994; Tachi et al., 1997). Such a disruption between the ECM and the cytoskeleton eventually leads to activity-induced myofiber death (Brown and Lucy, 1993).

Primary deficiencies of the components of the DGC cause several forms of myopathy resembling DMD (Ozawa et al., 1998). A few of the muscular dystrophies and their missing DGC component include: Duchenne MD (dystrophin), Becker MD (C-terminal of dystrophin present only), Emery-Dreifuss MD, Facio-Scapulo-Humeral MD (FSHD1, FSHD2), Limb-Girdle Dominant MD (LGMD1A, LGMD1B, LGMD1C) and Limb-Girdle Recessive MD (LGMD2A; LGMD2B; LGMD2C, γ -sarcoglycan; LGMD2D, α -sarcoglycan; LGMD2E, β -sarcoglycan; LGMD2F, δ -sarcoglycan; LGMD2G). A

complete list is published yearly in *Neuromuscular Disorders* (e.g. *Neuromuscular Disorders* 8 (1998), I-VII).

1.14 Laminin and the Extracellular Matrix (ECM)

The ECM surrounding a myofiber is composed of the external lamina (basement membrane) and interstitial connective tissues. The interaction of sarcolemmal proteins with ECM components produce important effects contributing to cell morphology, biosynthetic pathways, gene expression and cytoskeletal organisation. Laminin is a glycoprotein localized to the lamina lucida of the EL immediately opposite the sarcolemma. It functions to mediate attachment between the sarcolemma and type IV collagen of the EL. A second EL glycoprotein acting similar to laminin is fibronectin although laminin is more abundant. The remaining components of the EL include collagen, and a muscle-specific heparan sulfate proteoglycans that serves as a receptor for ECM elements (Campos et al., 1993). Laminin- α 2 (merosin) which is specific to skeletal muscle binds α -dystroglycan, which in turn binds to β -dystroglycan. The cytoplasmic tail of β -dystroglycan binds the C-terminal domain of dystrophin intracellularly which is an important structural link across the sarcolemma (Campbell, 1995, Durbeej et al., 1998).

In summary, this review of the cytoskeleton has concentrated on only those proteins that form important links between the intracellular and extracellular matrices. Connections between actin and myosin filaments with merosin in the ECM have been discussed such that proper skeletal muscle function is intimately tied to the integrity of

these linkages. One of these linkages includes actin filaments bound to each other by α -actinin at the level of the **Z** disc which in turn are bound to parallel actin filaments in the same myofibril and adjacent myofibrils by the IFs desmin, vimentin and paranemin. Peripheral myofibrils bind to costameres by way of desmin, adhesion proteins (β -spectrin, vinculin, etc.) and α -actin which in turn binds the N-terminal domain of dystrophin. Dystrophin is further bound to the DGC (β -dystroglycan) which links the ICM with merosin in the ECM, thus completing this important trans-sarcolemmal link. Absence of any of these linker proteins can have significant effects on the integrity of skeletal muscle, hence the importance of these cross-linking cytoskeletal proteins for proper muscle function (Campbell, 1995).

Section 2

SKELETAL MUSCLE - METABOLISM

Skeletal muscle metabolism refers to the incorporation of carbohydrate, lipid and protein as it applies to energy production and maintenance of homeostasis and structural integrity within a myofiber. Numerous texts and scientific reports have detailed the metabolic workings of skeletal muscle, e.g. McComas, 1996; Voet and Voet, 1990, and include lengthy descriptions of its metabolism. Rather than presenting a reiteration of those detailed texts, this section focuses on proton nuclear magnetic resonance spectroscopy ($^1\text{H-NMRS}$)-visible skeletal muscle metabolites such as lactate, alanine, glutamate, succinate, phosphocreatine, creatine, choline, carnitine, taurine, glycine and

tricarboxylic acids like mevalonic acid (MA) and 3-hydroxy-3-methylglutaryl-CoA (HMG-CoA). These particular metabolites contribute to an NMRS "fingerprint" for skeletal muscle (Smith and Blanford, 1995). The information this "fingerprint" provides in relation to energy, lipid and protein metabolism will be discussed.

2.0 ENERGY METABOLISM:

As the body's specialist in producing movement, muscle depends on ATP to provide the energy necessary to function. Since muscle has less than a second's worth of stored ATP, energy must be readily available, abundant and renewable in order to maintain prolonged activity (Banks, 1993; McComas, 1996). This is accomplished through glycolysis and the TCA cycle. Specifically, ATP is needed for the detachment of myosin crossbridges from actin filaments, integral ion pumps (Na^+/K^+ , Ca^{2+}) for sustaining excitability and terminating contraction, general cellular maintenance and replenishment of energy stores (Alberts et al., 1994).

Myofibers have a storage system for immediate ATP replenishment. During brief periods of low-grade activity, ATP reacts with creatine to form phosphocreatine (PCr).



At rest, the phosphocreatine store is four times greater than ATP levels (McComas, 1996), although some reports indicate PCr stores to be thirty times greater than ATP (Banks, 1993). During periods of activity ATP constantly degrades to ADP, while PCr constantly rephosphorylates ADP by the muscle specific enzyme creatine kinase to make

more ATP. The ATP used to form PCr comes from glucose metabolism through glycolysis and the TCA cycle.

When glucose is metabolized in the presence of oxygen it results in the generation of energy (in the form of ATP), CO₂ and H₂O. Aerobically, glucose undergoes glycolysis to form pyruvic acid and in the process releases ATP. The pyruvate, formed in the cytosol of a myofiber, is subsequently taken up by the mitochondria where it is decarboxylated with coenzyme A to form acetyl-CoA. Acetyl-CoA combines with oxaloacetate to make citric acid which enters the TCA cycle (see Voet and Voet, 1990, p. 508). In the TCA cycle the degradation process, in association with the respiratory chain, generates much more ATP per molecule of glucose than the glycolytic pathway.

A unique feature of glycolysis is the potential for the production of ATP in the absence of oxygen. In this setting ATP is produced by the glycolytic breakdown of glucose; however pyruvate is converted to lactate instead of carbon dioxide and acetyl-CoA. The cost of this anaerobic generation of energy is a diminished amount of ATP, insufficient formation of creatine phosphate and the accumulation of lactate. The lactate excess is associated with an oxygen debt that must be satisfied when lactate is converted back to pyruvate. As well, lactate leaks from the myofiber and causes local vasoconstriction which exacerbates the primary oxygen debt (Banks, 1993). As the ratio of oxygen supply to contractile activity increases, lactate converts back to pyruvate which undergoes oxidation to produce ATP, CO₂ and H₂O in the TCA cycle. The excess lactate produced under anaerobic conditions is used in the liver as a gluconeogenic precursor. In the liver, lactate is converted to pyruvate which enters the TCA cycle or is directed

towards glucose synthesis. Higher than normal lactate levels in muscle are likely due to a heightened glucose consumption and increased glucose uptake (Moreno and Arús, 1996) or perhaps the result of inhibition or sluggish gluconeogenesis in the liver.

Although muscle can oxidize glucose delivered through the circulation, most high-intensity contraction energy (at least after the initial first use of PCr) comes from the degradation and metabolism of glycogen stored in myofibers. Glycogen is degraded to glucose and energy is generated as described above. Conversely, energy for resting muscle and low-intensity contraction arises from the metabolism of lipids to acetyl-CoA and from the ensuing TCA cycle and the respiratory chain.

2.1 LIPID METABOLISM:

Lipids perform vital roles in energy generation and in certain aspects of cellular structure and function. Approximately 90% of the fat in our bodies is in the form of triacylglycerols and is stored in specialized cells called adipocytes (Matthews and van Holde, 1990). In storage, fat serves as a physical cushion for organs against shock, e.g. perirenal fat surrounding the kidneys, and it is a capable thermal insulator, e.g. marine mammals. Through the metabolism of triacylglycerols, a relatively large amount of energy is generated compared to that released from carbohydrate metabolism. As well, lipids have significant structural and functional roles in membranes, as vitamins and as metabolic regulators, e.g. phosphatidylinositol. This section addresses the role of carnitine and choline in the overall scheme of lipid metabolism. As these compounds are

visible with $^1\text{H-NMRS}$ it is important to understand, at a basic level, what an increase or decrease in the level of these metabolites might signify.

Carnitine is synthesized in skeletal muscles from the essential amino acids lysine and methionine, which are abundant in these tissues (Hunt and Groff, 1990; Carter et al., 1995). Carnitine is not an essential nutrient; however it does perform several important functions. The most studied function is its role as a carrier molecule for the transport of long-chain fatty acids into the mitochondria for oxidation and energy production. This is essential for β -oxidation, since fatty acids and their CoA derivatives cannot cross the mitochondrial membrane alone (Carter et al., 1995). Once inside the mitochondria, fatty acids are oxidized to acetyl-CoA which is then oxidized in the TCA cycle in a process similar to the oxidation of acetyl-CoA generated from pyruvate.

Other functions of carnitine include: 1. its role as an energy store (acetylcarnitine, as for sperm and mononuclear phagocytes) (Carter et al., 1995; Kurth., 1994); 2. removal of faulty metabolized acyl-CoAs to prevent CoA sequestration; 3. stabilization of red blood cell membranes; and 4. enhancement of Ca^{2+} transport within cells. Therefore, carnitine contributes to energy metabolism, regulates free CoA levels and modulates many membrane activities within cells.

It might be expected that decreased carnitine levels disrupt fatty acid β -oxidation; however, less than 2% of the total amount of carnitine is required to drive the enzymes of the mitochondrial fatty acid transport system. A substantially decreased carnitine level is required before any effect on β -oxidation is observed (Carter et al., 1995). Conversely, a moderately low carnitine level will likely hinder the regulation of free CoA in cells.

Choline is a major constituent of two phospholipids, phosphatidylcholine and sphingomyelin which constitute half of the four major phospholipids present in plasma membranes such as the sarcolemma (Alberts et al., 1994). Phosphocholine, choline and glycerophosphocholine are all present under the same peak in a ¹H-NMR spectrum of skeletal muscle. Increased levels of these metabolites may be indicative of upregulated phospholipid synthesis for membrane repair.

2.11 Cholesterol Biosynthesis

There has been a great deal of interest in the past few decades in the biosynthesis, utilization, transport and deposition of cholesterol in health and disease. As well as being a vital constituent of biological membranes, cholesterol is also the precursor for steroid hormones and bile acids. This segment of the thesis addresses the biosynthesis and incorporation of cholesterol into plasma membranes, in particular the sarcolemma of skeletal muscle.

The lipid bilayer of mammals is composed of exceptionally large amounts of cholesterol. A proportion as high as one cholesterol molecule for every phospholipid molecule is observed in plasma membranes (Alberts et al., 1994). The structure of cholesterol lends rigidity to membranes and enhances the permeability-barrier properties of the bilayer.

A cholesterol molecule consists of a polar head group, a rigid steroid ring structure and a nonpolar hydrocarbon tail. Cholesterol orients in the bilayer with its

hydroxyl group adjacent to the polar groups of membrane phospholipids, e.g. phosphatidylcholine, phosphatidylethanolamine, phosphatidylinositol and sphingomyelin. The rigid steroid ring interacts with the phospholipid hydrocarbon tail closest to the polar head group; thus, cholesterol partly immobilizes this region of the phospholipid. In so doing, cholesterol renders this part of the plasma membrane rigid, which acts to decrease the membrane permeability to small water-soluble molecules (Alberts et al., 1994). By making the lipid bilayer less fluid, the high concentration of cholesterol also prevents hydrocarbon chains from interacting and undergoing phase transitions, thereby resisting structural deformity (Alberts et al., 1994; Matthews and van Holde, 1990).

Most tissues in our body are capable of producing cholesterol, but the two most active cholesterol-synthesizing organs are the liver and the intestinal epithelium. Together these organs provide greater than 90% of endogenously synthesized plasma cholesterol which accounts for about 2/3 of the total cholesterol store in our bodies (Hunt and Groff, 1990).

Although acetate is directed to pathways such as the TCA cycle for energy production (Voet and Voet, 1990), acetate also forms the entire carbon backbone of cholesterol once it has been converted to acetyl-CoA in the cell (Matthews and van Holde, 1990; Voet and Voet, 1990). Of the many steps involved in the synthesis of cholesterol from acetyl-CoA, only the major events will be reviewed below.

The first few steps of cholesterol biosynthesis occur in the cytosolic compartment of cells. As stated above acetyl-CoA (from acetate) is the primary building block of cholesterol. Acetyl-CoA is also synthesized from pyruvate or β -oxidation of fatty acids in

the mitochondria. Mitochondrial acetyl-CoA is converted to citrate and transported into the cytosol where it is cleaved back to acetyl-CoA and oxaloacetate. The oxaloacetate is further converted to malate which is used in lipid biosynthetic pathways.

With formation of a cytosolic acetyl-CoA pool, cholesterol synthesis occurs in 4 stages: 1. a cytosolic stage where HMG-CoA is formed from three molecules of acetyl-CoA; 2. the rate limiting step which involves the reduction of HMG-CoA to mevalonic acid (MA) by HMG-CoA reductase in the membrane of the endoplasmic reticulum; 3. the formation of squalene from MA by several cytosolic enzymes; and 4. the cytosolic formation of cholesterol from squalene involving 20 enzymatic steps, 11 enzymes, 2 cofactors, 2 separate electron transport systems and molecular oxygen (Faust et al., 1988; Voet and Voet, 1990; Matthews and van Holde, 1990; Edwards, 1991).

[For a more detailed account of cholesterol biosynthesis and specific reactions refer to the following texts: Faust et al., 1988; Voet and Voet, 1990; Matthews and van Holde, 1990; and Edwards, 1991]

2.12 Control of Cholesterol Biosynthesis and Transport

As dietary cholesterol levels increase, endogenous synthesis tends to decrease. A decrease in synthesis is the result of the short-term, negative feedback regulation by cholesterol of HMG-CoA reductase. Cholesterol regulates the enzyme's catalytic activity directly and in the long term regulates its synthesis and degradation (Voet and Voet, 1990; Matthews and van Holde, 1990). Homeostasis is maintained by mechanisms that

coordinate dietary cholesterol and endogenously-synthesized cholesterol in the liver with cellular utilization of cholesterol. This mechanism involves high levels of intracellular cholesterol which inhibit low-density lipoprotein (LDL) receptor synthesis, thereby preventing the cellular uptake of cholesterol or cholesterol esters from LDL. Needless to say, cholesterol biosynthesis and transport are tightly regulated in the circulation between the liver and peripheral tissues.

In summary, peripheral tissues such as muscle have two ways of obtaining cholesterol for membranes: 1. it is produced *de novo* from acetyl-CoA within cells, or 2. it is obtained from LDL produced in the liver (and to a lesser extent the intestine). Muscle normally acquires cholesterol from circulating very low density lipoprotein (VLDL) that is removed in muscle capillary beds and converted to intermediate density lipoprotein (IDL) and then to LDL. Cholesterol is cleaved from LDL in the cytosol and enters the sarcoplasmic reticulum of the myofiber where it is subsequently used for sarcolemmal synthesis.

2.2 PROTEIN METABOLISM:

The metabolism of proteins is integral for living systems. Dietary protein is essential because of its constituent amino acids which can contribute to: the synthesis of numerous body proteins, the synthesis of many important nonprotein nitrogen-containing molecules, e.g. phosphatidylcholine and phosphatidylethanolamine, or the production of energy through oxidation (Hunt and Groff, 1990). Free amino acids in the plasma and

within cells arise not only from digestion and absorption of dietary protein but also from the degradation of tissue proteins. Amino acids from tissue degradation and diet combine to form an amino acid "pool" in the plasma with smaller pools forming in various tissues including skeletal muscle. The skeletal muscle pool includes certain NMRS-visible metabolites such as alanine, glutamate, glycine, glutamine and taurine. The basis of the relation between these metabolites and skeletal muscle function follows.

Alanine and glutamine are two amino acids that are synthesized *de novo* in muscle. Alanine is believed to be synthesized from the transamination of pyruvate to glutamate and glutamine can be formed from any two amino acids that are capable of being oxidized (Hunt and Groff, 1990). In muscle, oxidized amino acids transfer their amino groups to α -ketoglutarate and in turn to glutamine. Both alanine and glutamine are then carried in the blood to the kidney or the liver where their nitrogen groups are removed and excreted. Increased levels of these two amino acids, especially glutamine may indicate an increased transamination of α -ketoglutarate since α -ketoglutarate is the stimulus for the synthesis of these amino acids (Hunt and Groff, 1990). An increase in transaminated α -ketoglutarate is likely the result of heightened protein degradation due to dietary influences or tissue damage (Vinnars et al., 1990), perhaps the consequence of an acute-phase response due to inflammation.

Alanine also serves as a carrier of carbon from skeletal muscle to liver for gluconeogenesis, a pathway known as the glucose-alanine cycle. During periods of protein degradation, alanine is believed to be synthesized by skeletal muscle since large amounts are released during proteolysis (Felig, 1973; Hellerstein and Munro, 1994).

Once formed, alanine is transported to the liver where it stimulates gluconeogenesis and then is transaminated back to pyruvate with the release of ammonia. Therefore alanine serves a dual function of transporting excess ammonia for disposal and providing substrates for gluconeogenesis.

Glutamate is described as one of the more active amino acids. In muscle, however, its functions are mostly confined to accepting amino groups from oxidized amino acids as it is transaminated into glutamine. Glutamine is known to be important for the disposal of excess ammonia. Glutamate is also synthesized into glutathione in the presence of glycine. Glutathione protects cells from metabolic stress such as peroxides or free radicals, which tend to accumulate under oxidative conditions (Matthews and van Holde, 1990).

Glycine has multiple roles in the body. In muscle, glycine is a precursor for creatine phosphate and glutathione. It also interconverts with serine that is involved with forming phospholipids and pyruvate. Increases in glycine levels within a myofiber may be indicative of excess oxidation processes such as tissue degradation or may be the result of depleted energy stores (Finley et al., 1986; Luo et al., 1996). Furthermore glycine combines with acetate to form the heme precursor essential for the synthesis of myoglobin (Voet and Voet, 1990).

Taurine, 2-aminoethane sulfonic acid, is a β -amino acid or amide with numerous functions in whole body metabolism (see Huxtable, 1992 for a complete review). It is synthesized from cysteine by three, possibly four routes (for detailed description see Wright et al., 1986 or Huxtable, 1992). The particular route of synthesis varies between

species and among tissues, but the literature provides no indication as to which pathway is dominant in skeletal muscle.

Taurine's role in the body is multifaceted. Previous research in our lab (McIntosh et al., 1998a; McIntosh et al., 1998b) and the literature (Huxtable and Bressler, 1973; Wright et al., 1986; Huxtable, 1992) proposes a role for taurine in stabilizing or protecting the sarcolemma from various stresses by mechanisms not yet fully understood. Additionally, Huxtable (1992) describes several other functions for taurine including nonmetabolic (osmoregulation, calcium modulation, phospholipid and protein interactions) and metabolic actions (as a precursor in antioxidation, radioprotection, energy storage, etc.).

This background of energy metabolism demonstrates how the possible changes in $^1\text{H-NMRS}$ -visible metabolites in regenerating skeletal muscle over time can be interpreted with respect to biochemical processes during repair.

Section 3

SKELETAL MUSCLE DEGENERATION AND REGENERATION

3.0 INFLAMMATION

It is well documented that skeletal muscle undergoes cycles of degeneration and regeneration in response to various forms of injury. Such an injury can range from focal damage to whole intact muscle transplantation (experimentally) to disease. The simple act of descending a flight of stairs, specifically the eccentric contractions performed by

such an exercise, can provoke myofiber degeneration in the hamstring muscles of an untrained individual (Bischoff, 1994).

The integrity of the external lamina is important for successful regeneration but not necessary. In some situations, the external lamina persists and only the sarcolemma breaks as in dystrophy. In other situations such as in a crush lesion, fibers stay aligned if not intact. In these two situations the external lamina serves as a framework for new myofibers to rebuild upon. Persistence of the external lamina limits fibrosis and accelerates the reestablishment of fiber continuity across a region of damage. Following extensive physical trauma such as transplantation of minced skeletal muscle grafts where the external lamina is disrupted completely, regeneration still occurs (Carlson, 1970). However in those severe injuries the entire architecture is required to be reformed and the regeneration process is subsequently slower, even though the repair can be just as effective if a blood supply is readily available.

Skeletal muscle degeneration is a function of intrinsic degeneration and cell-mediated fragmentation concomitant with inflammation. The severity of an injury eliciting an inflammatory response governs the time course by which the damage is resolved (Allbrook, 1981). Physical traumas, such as those mentioned above, affect both vascular and cellular elements of skeletal muscle and produce a number of responses occurring simultaneously and in succession, and leading to repair.

The following section reviews skeletal muscle degeneration with respect to the intrinsic phase of degeneration while emphasizing the inflammatory process to explain the manner whereby skeletal muscle resolves impairment. Inflammation is described in

terms of acute (vascular, cellular and acute-phase) and chronic responses which are later integrated with the degenerative processes present in the diseased state.

3.01 Intrinsic Phase

The intrinsic phase of degeneration following sarcolemmal damage with subsequent intracellular calcium influx involves the activation of the complement cascade, calcium-dependent neutral proteases and phospholipases. The elevated intracellular calcium concentration also disrupts microtubule architecture, overloads the sarcoplasmic reticulum's calcium buffering capabilities and inhibits normal mitochondrial activity and energy metabolism (Engel and Biesecker, 1982; Grounds, 1991).

Phospholipase A₂ has been implicated in the formation of several inflammatory mediators such as prostaglandins, leukotrienes, platelet activating factor, and lysophospholipids, e.g. lysophosphatidylcholine, (Lindahl et al., 1995). By cleaving fatty acids from certain membrane phospholipids, e.g. phosphatidylcholine, to arachidonic acid with the subsequent production of prostaglandins, phospholipase A₂ may play an important role in the initiation of inflammation and digestion of dying cells.

Prostaglandins modulate inflammation by inhibiting platelet aggregation, and increasing vascular permeability; lysophospholipids modulate membrane fluidity thereby further increasing calcium influx; and platelet-activating factor increases the adhesiveness of neutrophils for endothelial cells by up-regulating the expression of integrin receptors

on neutrophils thereby promoting extravasation to sites of injury (Abbas et al., 1994).

Activated complement, with subsequent presence of the C5b-9 membrane-attack complex on the surface of the damaged sarcolemma, further contributes to myofiber lysis. Cleavage products of complement such as C5 serve as powerful chemotactic and stimulating factors to inflammatory cells. The C5 leads to the recruitment of inflammatory cells at the site of injury and subsequent removal of necrotic tissues (Grounds, 1991). Essentially extrinsic factors that result in sarcolemmal damage provoke intrinsic cell-mediated necrosis and fragmentation of the injured zone of muscle leading to regeneration. The calcium-induced release of these intrinsic phase mediators at the site of injury initiates cell-signalling cascades hence the cell-mediated phase of inflammation.

3.02 Cell-Mediated Phase

The process of inflammation is the response of vascularized tissues to local injury (Sommers, 1998), signs of which are produced by immunological chemical mediators. Two general types of inflammation exist: 1. an acute inflammatory response of fleeting duration and associated with an acute-phase response; and 2. a chronic inflammatory response of longer duration and self-perpetuating. Imposed trauma to normal skeletal muscle may elicit an acute inflammatory response that is self-limiting. However, if the initial injury does not resolve or is repetitive, the acute-type response may itself become a chronic response which could hinder repair or limit the host's ability to restore normal structure and function.

3.021 Acute Inflammation

An acute inflammatory response (AIR) is our body's reaction to a variety of injurious agents, both extraneous and endogenous. The sequence of events that succeed initiation of an AIR is quite similar for most causative agents. The inflammatory response is described with respect to vascular and cellular responses although each is dependent on the other.

3.021a *Vascular Response*

Generally, initiation of inflammation leads to a transient vasoconstriction of small blood vessels followed by vasodilation of local arterioles and venules (Sommers, 1998; Fantome and Ward, 1994). This results in local congestion which accounts for the redness and warmth at the site of injury. This hyperemic response supercedes an increased capillary permeability whereby fluid leaks into the surrounding tissues to cause swelling. Muscles have been observed to be heavier following injury due to edema (personal observations). As fluid moves out of capillaries into injured tissues, the flow lessens due to local tissue spaces and lymphatics being blocked by fibrinogen clots. Pain associated with injury is the result of inflammatory chemical mediators released at the site of injury. These responses serve to isolate the damage in an attempt to minimize repair time.

The degree of hemodynamic change depends on the severity of damage. A crush

injury used to study synchronous repair in skeletal muscle, elicits an immediate prolonged inflammatory response that lasts several days. Such an injury is associated with damage of local vasculature and nervous tissue in addition to muscle.

The vascular response of an AIR illustrate the classical description of inflammation described by the Roman Physician, Celsius: *rubor* (redness), *calor* (heat), *tumor* (swelling) and *dolor* (pain). A century later the physician, Galen, added *functio laesa* (loss of function) (Sommers, 1998; Fantome and Ward, 1994). These, the cardinal signs of inflammation, are brought about by chemical signals from the interaction of injured tissues and immune cells, known as the cellular response.

3.021b *Cellular Response*

Initiation of an AIR due to trauma is not necessarily the result of one inaugural cellular signal. A substantial injury likely yields events that stimulate a number of effector cells. A crush injury, in particular, challenges vasculature leading to inhibited nutrient and oxygen supply to cells, and disrupted structural integrity of affected tissues with loss of function if the damage is extensive. Such an injury must, at the cellular and molecular level, release a multitude of mediators that signal trouble and stimulate both a local and systemic response simultaneously.

At the site of injury, cells communicate with each other by the release of chemical mediators leading to the onset of inflammation and the acute-phase response. Resident inflammatory cells (tissue macrophages (TM) and mast cells; Nahirney et al., 1997)

possibly activated by the intrinsic degenerative phase, release chemical signals like tumour necrosis factor-alpha (TNF- α), interleukin-1 (IL-1) and interleukin-6 (IL-6) to further activate local tissues and surrounding cells. Vascular endothelial cells (VEC) are one important cell type affected by local phagocytes which in turn release mediators that perpetuate signals received from the activated TM. However the signals VECs receive from TMs are likely secondary to signals produced by the tissue injury. For example, reactive oxygen species are sufficient to stimulate VECs (Natarajan et al., 1998). The TM mediators likely modulate the VEC response which in turn contributes to the infiltration of more leukocytes to the site of injury.

Activated VECs produce vasodilator substances such as prostacyclin and nitric oxide (Abbas et al., 1994). These vasodilators contribute to the increased blood flow to the site of injury. TNF- α from activated TMs increases prostacyclin synthesis and nitric oxide (NO) production when combined with interferon-gamma (IFN- γ) released from activated T-lymphocytes. NO sustains vasodilation thereby heightening blood flow to the damaged area and promoting migration of more inflammatory cells to the site (Ricevuti, 1997).

Normally, the first leukocytes to the injured site are mostly neutrophils with granulocytes, especially mast cells in mice (Nahirney et al., 1997). The blood count of neutrophils increases dramatically during an inflammatory response. Neutrophils engulf foreign and dead particles that are then degraded by enzymes and antibacterial substances produced endogenously in cytoplasmic granules or peroxisomes during the intrinsic phase of degeneration. The digested debris is subsequently presented on the neutrophil's surface

for recognition that activates other immune cells and sustains the inflammatory response. As well mediators released by neutrophils, basophils and mast cells promote chemotaxis, emigration, and diapedesis of other leukocytes such as monocytes. Monocytes leave the vasculature, where they mature and enlarge into long-lived phagocytes. The emigration of these active macrophages further modifies the immune response and removes necrotic tissues in order to resolve the inflammatory process thereby aiding in the reestablishment of normal structure and function for the host.

3.021c *Acute-Phase Response*

Alongside the vascular and cellular inflammatory responses is a set of systemic responses which usually begin within 12 to 24 hours of the initial inflammatory response (Collins, 1999; Sommers, 1998). These responses include changes in plasma protein concentrations, erythrocyte sedimentation rate (ESR), body temperature, increased leukocytosis, skeletal muscle catabolism and a negative nitrogen balance. These changes are related to the release of cytokines by inflammatory cells. $\text{TNF-}\alpha$, IL-1 and IL-6 affect thermoregulatory centers in the hypothalamus thereby increasing body temperature, the most obvious sign of the acute-phase response. IL-1 in association with other cytokines (colony stimulating factors) stimulate stem cells in the bone marrow thus increasing the number of circulating leukocytes. A longer ESR is due to the liver's cytokine-induced production of acute-phase proteins such as fibrinogen (clotting cascade) and C-reactive protein (Sommers, 1998; Fantome and Ward, 1994). The metabolic changes such as

skeletal muscle catabolism contribute amino acids to be used in the immune response and for tissue repair (Sommers, 1998).

The acute-phase response might be thought of as a systemic process that coordinates the inflammatory process with various other ongoing activities in the body to maintain homeostasis and optimize the host's response to injury. Although the acute-phase response is characterized by rapid onset (usually associated with an AIR), it can persist in the chronic inflammatory setting (Abbas et al., 1994).

3.022 Chronic Inflammation

Whereas acute inflammation is self-limiting and short-lived, chronic inflammation is self-perpetuating and long-lived (weeks to years). A chronic inflammatory response (CIR) may result from an unresolved AIR or from a low-grade, persistent insult that fails to elicit an AIR (Collins, 1999). It is characterized by a mononuclear cell infiltrate (macrophages and lymphocytes) without the primary neutrophil and granulocyte influx seen in an AIR. It includes the proliferation of fibroblasts and connective tissues leading to fibrosis thus potentiating the chance of scarring and secondary impairment of function (Sommers, 1998; Collins, 1999). Two important cytokines which lead to initiation and potentiation of a CIR include interferon (IFN)- γ and TNF- α produced by T-lymphocytes and macrophages, respectively.

3.1 THE RESPONSE OF NORMAL SKELETAL MUSCLE TO INJURY

Destruction of a piece of muscle due to a crush injury or impaired blood flow leads to necrosis of all tissue components at the site of injury. Normal skeletal muscle follows the same course of degeneration (intrinsic and cellular-mediated phases) as other tissues although given the size of each myofiber, additional mechanisms are involved to isolate the injury. Associated with inflammation is a process of new sarcolemma development. Papadimitriou et al. (1990) demonstrated a process of sarcolemma formation, concomitant with inflammation and the acute-phase response, that serves to "wall-off" undamaged muscle from injured muscle even within a single myofiber. Sealing the undamaged portion of a myofiber from the damaged region minimizes necrosis and preserves intact myofiber integrity.

The sealing process involves the production of new membrane which contributes to that part of the sarcolemma that separates the viable portion of the myofiber from the injured zone. This process of sealing the sarcoplasm is a function of local cells and the fiber itself, and it is independent of leukocytic infiltrates (Grounds, 1991).

Papadimitriou et al. (1990) have observed that three hours following a crush injury, the damaged zone is demarcated by a ruptured sarcolemma overlying hypercontracted myofibrils. At the time of injury intracellular calcium levels increase dramatically and initiate degeneration as described previously. At the same time blood flow is impaired, which serves to activate VECs leading to NO production and release which is in part responsible for vasodilation and leukocyte infiltration. By three hours post-injury inflammation has been initiated and a few neutrophils appear at the site of injury. After six hours many neutrophils and a few macrophages are present. The

sarcolemma is discontinuous over the damaged myofiber segment and the hyper-contracted myofibrils are separated from the undamaged myofibrils by a clear zone. Mitochondria and several vesicles are present at the periphery of the undamaged zone. These vesicles may release substances that begin to counteract inflammation thus setting the stage for regenerative processes. Twelve hours following the initial injury, phagocytosis of necrotic myofibers and displaced organelles is ongoing and a membrane has formed which isolates the necrotic zone from the structurally intact sarcolemma. By 24 hours the necrotic zone has been successfully "walled-off" from the undamaged zone. Few muscle elements remain in the necrotic zone which, if present, hinder successful regeneration; macrophages predominate.

Phagocytosis is closely followed by the process of angiogenesis; both processes are essential for successful regeneration. Angiogenesis is especially important after severe injury since the central zone of an extensive necrotic zone may become fibrotic if ischemia is prolonged. Low oxygen tension favours the proliferation of fibroblasts (Storch and Talley, 1988; Grounds, 1991). Therefore, the degree of fibrosis following regeneration of injured skeletal muscle may be a useful gauge of successful revascularization. Angiogenesis is stimulated by angiogenic factors, released by ischemic tissue macrophages, which increase endothelial cell proliferation. Basic fibroblast growth factor (bFGF) is one of these angiogenic factors released by macrophages, and it is also released by endothelial cells in an autocrine manner. Following the establishment of phagocytosis and angiogenesis, regeneration can commence.

The success of regeneration varies with the nature and extent of the injury, but in

all situations the regenerative process follows the same basic course. It resembles development but does not recapitulate it. To summarize, the cytological events that lead to successful regeneration include: new sarcolemma formation, cellular infiltration, revascularization, phagocytosis of necrotic debris, proliferation (mitosis) of muscle precursor cells (satellite cells), fusion of daughter cells to form myotubes, myotube elongation, circumferential development and re-innervation (Grounds, 1991).

Once the site of injury is clear of necrotic debris, regeneration begins with the activation of muscle precursor cells (satellite cells) and their subsequent proliferation. Satellite cells, mononucleated cells located between the sarcolemma and the external lamina, are the progenitor cells recruited for skeletal muscle regeneration in response to injury (Caplan et al., 1988). These cells switch from a quiescent state to activated state preceding proliferation. Daughter cells differentiate into myoblasts that can fuse to form immature, centronucleated myotubes. This regenerative process seen within the necrotic zone is also underway at its extremities, and new myotubes grow towards the necrotic zone and elongate inward from the surviving sealed myofibers.

Several reports indicate that satellite cells (SC) have a broad capacity for motility (Konisberg, 1975; Watt et al., 1987; Bischoff, 1994). The quiescent SC is induced by a competence factor to enter the G1 phase of the cell cycle leading to proliferation. The activated SC leaves the surface of the affected myofiber and proliferates, and daughter cells migrate to the site of injury to commence the regenerative process. The result of injury sees the necrotic region being repopulated by SCs from the undamaged region. Although few images have been generated illustrating a SC crossing the external lamina

(Maltin et al., 1983; Anderson et al., 1987), SCs from adjacent muscle may possess the capability of migrating between muscles to an injured region (Bischoff, 1994; Lipton and Schultz, 1979). However, SCs for regenerative processes are usually recruited from the undamaged portion of the same injured myofiber (Bischoff, 1994).

Essential to completion of regeneration is re-innervation. Therefore the formation of synapse and motor endplate for the connection of myofiber and axon is integral in the maturation of newly formed myotubes. Essential to the formation of a functional synapse are surface molecules such as neural cell adhesion molecules (NCAM) and acetylcholine receptors (AChR) which are evenly expressed over the surface of a new myotube. Upon formation of a synapse these surface molecules cluster together and become restricted to the synaptic site. The clustering at the site of the synapse is likely due to other proteins such as agrin and gelasmin (Jay and Barald, 1989b). In fact, the presence of gelasmin positively correlates with successful re-innervation (Jay and Barald, 1989a).

There exist two models by which an axon can make contact with the external lamina (EL) of a new myotube. Both methods are dependent upon the presence or absence of a persisting old EL. In the first scenario, where a myotube does not regenerate within the framework of an old EL, the new myotube is re-innervated "de novo". The formation of such a neuromuscular junction is believed to mostly recapitulate neural-muscle associations in developing muscles, although recent work in our lab shows this is not exactly the case (Kong and Anderson, in preparation). Where the new myotube grows within the confines of the old EL, the axon is attracted to the old synaptic site. Note that the NCAM-AChR clusters in the new myotube are restricted to sites underlying

the agrin-containing synaptic sites of the old EL.

3.2 THE RESPONSE OF DISEASED SKELETAL MUSCLE TO INJURY

A model for skeletal muscle disease is muscular dystrophy. The utmost difference between dystrophic and normal skeletal muscle is the absence of the subsarcolemmal protein, dystrophin, from dystrophic muscle (Bulfield et al., 1984; Emery, 1987; dos Remedios et al., 1990). Although dystrophin's presence is believed to contribute significantly to the integrity of the sarcolemma, it is not necessarily required for successful regeneration (Cullen and Watkins, 1993). No other condition exemplifies this fact more conclusively than the dystrophic mouse (mdx). This murine model of the human muscle disease, Duchenne Muscular Dystrophy (DMD), recovers from dystrophin-associated skeletal muscle degeneration to lead a relatively normal, albeit captive, life with few overt clinical signs of weakness.

The course of dystrophy in the mdx mouse progresses through three phases; predystrophy, active dystrophy and stable dystrophy (Mcintosh, 1998c). The first phase occurs in the first 10 to 15 days of life. Within this time frame, the myofibers in limb muscles appear normal. The active dystrophic phase peaks between 3 and 6 weeks and is characterized by very active degeneration with necrosis of segments of myofibers. Degeneration is followed by regeneration which is evident by the observed centronucleation seen by light microscopy. The active phase is accompanied by muscle weakness, in fact the grip strength of the mdx mouse is substantially less (approximately

60%) than a normal mouse (Weber and Anderson, unpublished results).

At about 8 weeks of age the intensity of the degenerative process decreases substantially although damage and regeneration occur throughout the life of the animal. This is the stable dystrophy phase and it is accompanied by very little accumulation of adipose and connective tissue with no conspicuous myofiber loss. In contrast, DMD muscle does not stabilize after an early peak regeneration, and there is ongoing damage without repair but with profound deposition of fibrotic and adipose tissues. In DMD, this phase accounts for the progressive weakness and disability of the disease.

The question is: why do mdx mice successfully recover from degeneration despite lacking dystrophin whereas DMD patients do not? And what mechanism(s) do muscles in mdx mice possess for successful regeneration which is (are) lacking in DMD patients? Whatever the difference, DMD skeletal muscle must have aberrations, aside from the lack of dystrophin, that render it susceptible to atypical repair and inappropriate immune responses to injury. For example, the inability of neutrophils from DMD patients to properly migrate to sites of injury (Nahirney et al., 1997; Grounds, 1991) may be one of many factors leading to the coupling of an immediate chronic inflammatory response with a detrimental acute-phase-like response. To date most published research describes the immune processes of dystrophy only as secondary observations of regeneration.

Section 4

PROTON NUCLEAR MAGNETIC RESONANCE SPECTROSCOPY

What is nuclear magnetic resonance spectroscopy (NMRS) and why have I used this particular tool to study the mechanisms of skeletal muscle regeneration? Since NMR's theoretical basis (proposed by W. Pauli in 1924) was proven in 1946 by Bloch and Purcell and the first high-resolution NMR spectrometer was designed, NMRS has served as one of the most powerful tools utilized by chemists and biochemists for elucidating chemical structures (Skoog and Leary, 1992). W. Pauli, 1924 proposed that certain atomic nuclei bear spin and magnetic moment, and exposure to a strong magnetic field induces splitting of their energy levels. It was later demonstrated by Bloch (1946) and Purcell (1946), working independently, how atomic nuclei that bear spin and a magnetic moment absorb electromagnetic radiation when in a strong external magnetic field that causes splitting of their energy levels. In the past four decades NMRS has proven to be a valuable tool for studying biological systems and determining specific functions. NMR measures the absorption and release of radio frequency electromagnetic radiation energy by a NMRS-competent nucleus in a magnetic field (Smith and Blanford, 1995).

Before the question "Why use NMRS to study skeletal muscle regeneration?" can be answered it is important to briefly describe some NMR basics so that we might better appreciate the methods and NMR parameters used to acquire the spectra upon which the results of this project are based. The following section presents a general overview of ideas and principles that lead to a basic understanding of NMRS and help answer the important question of why this tool was used.

This section is the compilation of scientific literature and textbooks; where

appropriate, researchers and their work have been cited. Since my knowledge of NMRS is limited to that of a “user”, the material presented in this section is a compilation of my understanding based on the material I have read and that which has been explained to me. Much of this section is difficult to reference without citing every sentence. Many of the ideas presented in this section are those of the authors I have studied and the individuals I have spoken with; I have tried to represent those ideas accurately.

The Magnet: (Martin et al., 1980)

The sensitivity and resolution of NMRS are dependent upon the strength of the magnetic field (Smith and Blanford, 1995). The field generated by the magnet has stringent performance specifications: the field must be homogeneous to a few parts per billion within the sample and it must be stable for the duration of data acquisition (Smith and Blandford, 1995). Furthermore, the field must be reproducible.

Magnets may be permanent, electromagnetic or superconducting. The superconducting magnets, as used for the present study, are the most powerful, capable of generating fields up to 17.6 Tesla (Smith and Blandford, 1995). The high field strengths are the result of the superconducting material (niobium-titanium alloy coil immersed in liquid helium at 4 degrees kelvin, K) carrying a high current with no electric loss or generation of heat in the process (Derome, 1987; Smith and Blanford, 1995).

The Probe and Magnetic Field Stability: (Martin et al., 1980)

The probe is located at the centre of the magnetic field. It consists of a sample cavity within a coil arranged for generating radio frequency pulses for sample excitation and for receiving and detecting the NMR signals. Shim coils present inside the bore of the magnet, surrounding the probe, induce small fields of varying shapes that can be adjusted to maintain the homogeneity and uniformity of the magnetic field over the entire sample (Derome, 1987; Hore, 1995). Homogeneity is necessary to maximize spectral resolution. Resolution is further heightened by spinning the sample pneumatically about its vertical axis thereby averaging inhomogeneities.

Stability of the magnetic field is achieved and maintained by a technique called field frequency locking. It is accomplished with the use of a substance that exhibits a strong NMR signal separate from those of the sample, e.g. deuterium for ^1H -NMRS. This substance can be used physically separate from the sample, an external lock, or it can be dissolved in the sample, an internal lock. The frequency of the lock signal is monitored by the computer and compared to the magnet's field to maintain proportionality between the applied magnetic field and lock frequency (Derome, 1987).

A typical experiment involves a chemically-prepared sample of volume 0.1-10 ml placed in a narrow (5mm in diameter) test tube. The test tube is then pneumatically inserted into the bore of the magnet and analysed under specific parameters set by the operator. Those parameters important for duplication of an experiment include the spectral width, recycle time (relaxation delay + acquisition time), temperature, number of data points, flip angle, and the number of scans used (personal discussion with Dr. B.J. Blackburn, Adjunct Professor, Department of Human Anatomy and Cell Science,

University of Winnipeg). A brief review of NMRS principles will help our comprehension of these parameters and the information ¹H-NMRS has provided for this study.

4.0 SPECTROSCOPY BASICS: (Derome, 1987; Hore, 1995; Skoog and Leary, 1992; Andrew, 1994; Bovey, 1988; Charles, 1996)

Nucléar resonances are due to complex “interactions between the nuclei and electrons of molecules, between nuclei within molecules and between nuclei in neighbouring molecules” (Sir Rex Richards, University of Oxford; Derome, 1987). NMRS exploits these interactions by inducing the splitting and exchange of nuclear energy with an applied electromagnetic field (a radio frequency pulse). The radiofrequency (*rf*) pulse, which is basically a magnetic field oscillating at the Larmor frequency, induces a signal from the sample. That signal is measured by the probe that is in place around the sample and is connected to a radio receiver. The induced emission of the signal (due to a previously applied *rf* pulse) is amplified and displayed as a time-domain signal, the free induction decay (FID). This FID is digitized (analog-to-digital converter) and stored in the magnet’s computer for processing. As described above, the FIDs from numerous successive pulses are added to improve the signal-to-noise ratio. The stored data is converted by Fourier-transformation to a frequency-domain signal and phased which provides the researcher with the typical NMR spectrum of the prepared sample.

4.01 Nuclei and Spin: (Derome, 1987; Hore, 1995; Skoog and Leary, 1992; Andrew, 1994; Bovey, 1988; Charles, 1996)

A number of nuclei possess a magnetic moment, the result of a nucleus bearing charge and spin. The four most extensively studied nuclei with spin quantum numbers of $1/2$ include ^1H , ^{13}C , ^{19}F , and ^{31}P . Each of these nuclei bear spin states of $I=+1/2$ and $I=-1/2$. Due to the interrelationship between nuclear spin and the magnetic moment, each of these four nuclei possess magnetic quantum numbers of $m=+1/2$ and $m=-1/2$.

In an external magnetic field, B_0 , the magnetic moment of a ^1H nucleus orients to one of two possible directions with respect to B_0 , depending upon its magnetic quantum number, parallel ($m=+1/2$, low energy state) or antiparallel ($m=-1/2$, high energy state). Under normal conditions (no B_0) a sample prepared for ^1H -NMRS with an assemblage of protons exhibits no energy difference. In the presence of B_0 , the population of nuclei split, or orient, into high and low energy levels with the low energy level ($m=+1/2$) predominating. NMR absorption is the result of transitions between these two energy levels induced by brief, intense radiofrequency pulses. The success of NMRS is dependent upon the small excess of the $m=+1/2$ energy level protons.

4.02 Nuclear Magnetic Resonance Frequency: (Derome, 1987; Hoult, 1989; Hore, 1995; Skoog and Leary, 1992; Andrew, 1994; Bovey, 1988; Charles, 1996; Yamada and Sugi, 1996)

The resonance frequency of a particular nucleus is determined by a proportionality constant, the gyromagnetic ratio, which is a value characteristic of each nuclear species. The difference between the high and low energy levels, discussed above, is given as:

$$E = h\gamma B_0/2\pi$$

where h is Planck's constant, B_0 is the magnetic field, and γ is the gyromagnetic ratio (Yamada and Sugi, 1996). Transitions between these energy levels may be induced with applied electromagnetic radiation of the appropriate frequency, the resonance frequency, $\nu = E/h = \gamma B_0/2\pi$. So, the protons in $^1\text{H-NMR}$ have a particular resonance frequency in a given magnetic field. The resonance frequency for our purposes was 500MHz at 11.7 Tesla.

4.03 Chemical Shift and Proton J-Coupling: (Derome, 1987; Hore, 1995; Skoog and Leary, 1992; Andrew, 1994; Bovey, 1988; Charles, 1996; Yamada and Sugi, 1996)

The observation of different peaks in a spectrum is due to chemical shift and coupling characteristics. Individual nuclei, e.g. ^1H , in different chemical environments from the same molecule, like taurine, do not necessarily experience the same applied magnetic field (B_0). The strength of the field experienced by a nucleus such as a proton is dependent upon the electronic environment of that nucleus (Derome, 1987; Hore, 1995; Yamada and Sugi, 1996). Different electronic environments cause different apparent field strengths resulting in different resonance frequencies, hence different chemical shifts.

Taurine's multiplet peak is observed as two triplets, one representing by the S-CH₂ moiety and the other by the N-CH₂ moiety. The chemical environment of the protons of the S-CH₂ moiety differ from that of the N-CH₂ moiety. A chemical shift reference compound such as 3-trimethylsilyl propionate (TSP), as is used in aqueous extracts prepared for ¹H-NMRS, possesses highly shielded nuclei. This resonance frequency of TSP's protons is the reference to which all other peaks are compared within a given spectrum. Since the S-CH₂ moiety of taurine has protons with less shielding compared to the protons of the N-CH₂ moiety, it appears furthest from TSP in a spectrum. Therefore, the chemical shift accounts for the two triplets of taurine, but it does not explain the splitting of each triplet. The splitting is due to proton coupling.

The concept of J-coupling describes the interaction between neighbouring proton spins on the same molecule. Simply stated, proton spins indirectly recognize neighbouring spins through bonding electrons. In the case of taurine, each of its NMR-visible nuclei is coupled to two other analogous protons on the adjacent carbon of the CH₂-CH₂- backbone of the molecule. The -CH₂- proton spins see four combinations of m for the adjacent -CH₂- proton spins, 1. (+½, +½); 2. (+½, -½); 3. (-½, +½); 4. (-½, -½). We can see that (2.) and (3.) are equivalent hence taurine appears in ¹H-NMRS spectra as two triplets (intensities in each triplet appear in the ratio 1:2:1) separated because of each moiety's (N-CH₂ and S-CH₂) chemical shift.

4.1 PULSE NMRS TECHNIQUES:

The premise of pulse NMRS is to shorten experiment times relative to conventional NMR techniques, e.g. Continuous Wave NMRS. The value of pulse NMRS is that it measures all frequencies simultaneously, thereby decreasing the total experiment time. It accomplishes this by analysing the response of a sample to a *rf* pulse. The following section reviews the pulse NMR technique as it applies to understanding our study. The pulse, relaxation phenomenon, exponential multiplication and saturation (as it explains peak suppression) are described.

4.11 The Pulse: (Derome, 1987; Hoult, 1989; Hore, 1995; Skoog and Leary, 1992; Andrew, 1994; Bovey, 1988; Charles, 1996; Yamada and Sugi, 1996)

Consider an excess of nuclei, e.g. ^1H , in the lower energy state due to an applied magnetic field, B_0 , along the positive Z-axis. The protons precess randomly about B_0 resulting in a net magnetization vector M (approximately 500 MHz for a group of ^1H nuclei). At equilibrium, M is parallel to B_0 . Application of an *rf* pulse along the X-axis will tilt M away from the positive Z-axis towards the XY plane. The degree of flip (or rotation) from B_0 is dependent upon the *rf* pulse power and its duration. An *rf* pulse of sufficient power will flip M from its equilibrium state (the positive Z-axis parallel to B_0) onto the Y-axis (a 90° pulse). An *rf* pulse of equal power but twice the duration will rotate M onto the negative Z-axis (a 180° pulse).

The *rf* pulse flips M into the XY plane as the nuclei precess about B_0 . This action stimulates the spectrometer's detector coil with a frequency and amplitude equal in

magnitude of the XY component of M . These data are recorded and the signal is traced over time as the spin system relaxes (see below). This signal is known as the free induction decay (FID). Conversion of the FID from the time domain to a frequency domain by Fourier transformation provides the user with a spectrum representative of a given sample.

4.12 Relaxation: (Derome, 1987; Hore, 1995; Skoog and Leary, 1992; Andrew, 1994; Bovey, 1988; Charles, 1996; Yamada and Sugi, 1996)

Following the flip of M into the XY plane, the result of an *rf* pulse, M returns to equilibrium. This is called relaxation, of which two types exist, longitudinal and transverse relaxations.

Longitudinal relaxation corresponds to the recovery of magnetization along the B_0 direction. As “longitudinal” implies, it is the net magnetization component parallel to B_0 that is involved. Under normal circumstances we assume that whenever B_0 is flipped away from the Z-axis it will return there exponentially in time, T_1 .

Transverse relaxation describes the exponential decay of the net magnetization in the XY plane with a time constant, T_2 . The process of transverse relaxation does not affect transitions between energy levels rather it affects phase coherence. Basically, transverse relaxation describes the disappearance of magnetization from the XY plane due to a loss of order. In the absence of any mechanism for transverse relaxation, T_2 theoretically equals T_1 (Derome, 1987). If not for applied magnetic field

inhomogeneities, this situation ($T_1=T_2$) would most frequently be the case for aqueous samples. The transverse relaxation time is very sensitive to and dependent upon the molecular mobility of a sample, and the signal width is inversely proportional to T_2 . A relatively mobile sample, like a PCA extract, has a long T_2 and a narrow signal width.

Relaxation rates can be undesirably accelerated due to the presence of paramagnetic substances, since unpaired electrons in these substances provide an effective stimulus for NMRS transitions between high and low energy levels (Hore, 1995). Removal of paramagnetic ions such as produced by dissolved oxygen, chromium and iron (Fe^{2+}), may improve the resolution of a resultant spectrum.

4.13 Saturation and Peak Suppression: (Derome, 1987)

If transverse relaxation is extremely fast, the net magnetization (M) component in the XY plane following an *rf* pulse, may decay to zero before M reappears along the Z-axis. In this case, the net magnetization is zero (high and low energy states would be equally populated), and the system is said to be saturated. Imposing a second pulse would elicit no signal from the sample. Pre-saturation is a method of eliminating an unwanted peak from the NMRS spectrum. This is frequently applied to the solvent peak of aqueous samples to optimise the experiment. Since the large water peak in aqueous samples covers up the spectra of other important compounds, its suppression reduces the dynamic range of the spectrum (concentrates the finite data points to the peaks of interest rather than wasting them on the solvent peak) (Derome, 1987). This suppression also

occupies less computer space and improves the aesthetics of the spectrum (Yoshizaki et al., 1981; Arus et al., 1984; Derome, 1987). Suppressing a strong peak, such as water, makes neighbouring peaks easier to see and stabilizes the baseline. Ultimately it makes integration much easier.

The process involves setting a weak (or soft) *rf* pulse at the same frequency as the peak to be suppressed. The pulse is applied long enough to diminish the population difference across high and low energy levels. As described above, this saturates the peak and eliminates its signal from the spectrum. The soft *rf* pulse is turned off before application of the strong (or hard) *rf* pulse sequence during which the spectrum is acquired. Terminating the soft pulse early prevents Bloch-Siegert shifts, in which peaks adjacent to the suppressed peak are shifted.

Pre-saturation is the most effective method of peak suppression (for our purpose) because it applies the highest degree of suppression while minimizing distortion to the remaining spectrum.

4.14 Exponential Multiplication: (personal discussion with Terry Wolowiec, NMR technician, Prairie Regional NMR, Department of Chemistry, University of Manitoba, located at IBD, NRC)

Exponential multiplication is a method, in the simplest of terms, of amplifying the signal data found in the bulk of the FID (excludes the tail of the FID) to improve the signal-to-noise ratio (sensitivity) at the cost of resolution, or line widths. Amplification

of the tail of the FID merely increases the noise level (Derome, 1987). EM emphasizes the NMRS signal rather than the baseline; it adds 1 Hz (in our study) to each line to provide a better looking spectrum. Basically it provides more visibility to small peaks in the spectrum; that is, it emphasizes them.

4.2 ADVANCED NMRS TECHNIQUES: 1D-TOCSY: (Kessler et al., 1986; personal discussion with Terry Wolowiec, NMR technician, Prairie Regional NMR, Department of Chemistry, University of Manitoba, located at IBD, NRC)

Physicists and Chemists have both developed numerous methods of structure analysis for the purpose of identifying unknown compounds using NMRS, many of which this author can't even begin to understand. Of the many methods of experimental analysis available, we used one in particular to aid in our identification of one unknown spectral peak. The 1D-TOCSY experiment is a method that exploits coupling properties to provide molecular information about one particular metabolite in a spectrum.

4.3 INSTRUMENTAL SENSITIVITY: (Smith and Blandford, 1995; Yamada and Sugi, 1996; Skoog and Leary, 1992)

The ultimate sensitivity of NMR is reflected in the small amounts of energy that a spin system can absorb. The slight excess of nuclei distributed to the lower energy state (Boltzmann distribution) in our study is indeed small. For 10,000,000 protons in the

antiparallel, high energy state in a 11.73 Tesla field (B_0) at 300K there exists 10,001,840 protons in the parallel, low energy state. The difference is 1840 ppm which represents the number of protons providing information about a sample. Therefore NMRS has a relatively low sensitivity when compared to other detection methods such as immunoassays, gas chromatography and mass spectroscopy (Smith and Blandford, 1995). Due to the relatively low sensitivity of NMRS, it is necessary to average many single measurements to attain a spectrum with a decent signal-to-noise ratio. Since NMRS signals occur in the same place every time and build up more quickly than background noise (Derome, 1987) repetitive measurement is an effective method of improving the instrument's sensitivity. In fact, four repeats of a single measurement will double the NMRS signal relative to background noise (personal discussion with Terry Wolowiec, NMR Technician, Department of Chemistry and Prairie Regional NMR, University of Manitoba). Other techniques such as pre-saturation, PCA extraction and lyophilization of samples also improve NMRS sensitivity.

Despite the low sensitivity NMRS, its value to studying disease processes such as skeletal muscle regeneration, lies in its ability to simultaneously detect a wide range of compounds of biological interest. This provides an NMRS "fingerprint" of a particular tissue based on a specific NMRS-competent nucleus while ignoring physical, chemical or structural properties (Smith and Blandford, 1995). This provides researchers with the ability to readily differentiate "abnormal" from "normal" tissue by novel disease markers without having first-hand knowledge of the marker's identity or function (Smith and Blandford, 1995). This can be quite valuable in a clinical and diagnostic settings where

early diagnosis is prudent. It also fortuitously allows investigators with biology training the means to answer detailed questions concerning the biochemistry of a living system.

Chapter 2 - RESEARCH HYPOTHESES AND SIGNIFICANCE

A. HYPOTHESES

Proton Nuclear Magnetic Resonance Spectroscopy of perchloric acid extracts during skeletal muscle repair in C57 mice can:

1. detect a reproducible time-course of changes during regeneration in peaks of taurine, creatines and carnitine resonances, and
2. determine the time interval when regenerating muscle is optimally discriminated from normal muscle and injured muscle.

B. SIGNIFICANCE

¹H-NMR spectroscopy can detect changes in muscle which correspond to biochemical aspects of muscle repair at particular intervals following injury. Previous results from our lab show it is possible to monitor healthy muscle development and mdx mouse dystrophy with *in vitro* and *in vivo* ¹H-NMR imaging and spectroscopy. This study is designed to advance the ultimate goal of designing a non-invasive clinical test protocol of muscle repair status using ¹H-NMRS resolution of skeletal muscle.

Defining the function of several muscle metabolites and how they interact to

promote regeneration and maintain myofiber integrity will be valuable in many neuromuscular diseases such as Duchenne Muscular Dystrophy, and interventions where treatment is designed to enhance skeletal muscle repair.

Chapter 3 - MATERIALS AND METHODS

3.0 Animals:

C57 (B1/10ScSn) mice were maintained and housed according to the guidelines of the Canadian Council of Animal Care at the University of Manitoba Animal Care Facility. Mice were provided access to food and water 24 hours a day and maintained on a light to dark cycle of 10:14 hours. Animals and samples were handled and treated the same except as related to particular muscle crush surgeries as described below.

The C57 mice were received by litter at six weeks of age and each mouse was randomly assigned to one of seven possible recovery groups: 0 day, 1 day, 2 day, 4 day, 7 day, 9 day or 14 day. An equal male to female animal ratio was maintained for each group. Once all mice were received and distributed to the recovery groups each group contained no less than 9 mice for a total of at least 63 mice per stage. For the actual final numbers of mice used in each group, refer to table 4.1 (a-c).

3.1 MUSCLE CRUSH SURGERY AND SKELETAL MUSCLE RECOVERY

3.11 Crush Surgery

Mice were anaesthetized by intraperitoneal injection with 0.02-0.04 cc of 1:1, rompun-ketalean anaesthetic (Ketamine, 40mg/kg b.w., [115.4mg/ml]; Xylazine,

2.2mg/kg b.w., [20mg/ml]) before both hindlimbs were prepared for crush surgery. The tibialis anterior (TA) muscle of the right leg and the gastrocnemius (GAS) muscle of the left hindlimb were crush injured.

The skin overlying the right TA muscle was cleaned and shaved with a sterile, single edge razor blade. A skin incision measuring 1 centimeter in length was made on the anterolateral aspect of the right hindlimb to expose the deep fascia that ensheaths the right TA muscle. The deep fascia was incised with surgical microscissors and the right TA was subsequently separated and slightly lifted away from the tibia, underlying extensor digitorum longus and the adjacent peroneal muscles. This provided access so a controlled crush injury could be delivered to the right TA muscle using a Steven's "microhemostat" for three seconds at the first closure step (see figure 3.1). The precise site of the crush was located by measuring one centimetre proximal to the calcaneus tarsal bone. The crush site was tagged for future visual reference, with a non-absorbable sterile surgical suture (Ethicon, cuticular, black braided silk, 6-0, 681 G). Sutures were positioned, one proximal and one distal to the crush injury, so as to tag a region three times the width of the crush produced by Steven's Microhemostats (see figure 3.2). The left GAS muscle was also crush injured in the same manner as described for the right TA muscle.

3.12 Sample Collection

All mice were sacrificed by cervical dislocation under ether anaesthesia after 0, 1,

2, 4, 7, 9, or 14 days depending on to which recovery group they were initially assigned. For example, the 14 day recovery group mice were sacrificed 14 days after delivery of the initial crush injury. Immediately following cervical dislocation three separate TA muscle samples were dissected and recovered. The uncrushed left TA muscle served as an internal control for the right crushed TA muscle. A second internal control was recovered from the crushed injured right TA muscle such that the tagged crush injured region was recovered and stored separate from the proximal and distal uncrushed regions of the right TA muscle. Therefore three TA muscle samples were ultimately collected (see figure 3.3): 1. a crushed sample; 2. an uncrushed sample from the same muscle as (1); and 3. an uncrushed intact internal control, contralateral to (1).

Three GAS muscle samples were collected in the same manner as described for the TA muscle samples. The GAS muscle samples were included because there was concern as to whether the TA muscle samples would be large enough for accurate ¹H-NMRS. When it became clear that the crush injured and control TA muscle samples were sufficiently large enough to proceed with our study the GAS muscle samples were no longer considered for study. However to ensure that each mouse was handled equally the left GAS muscle was crush injured for every mouse.

All dissected muscle samples were placed in previously-weighed and coded cryogenic vials, weighed again with the dissected sample, then flash frozen in liquid nitrogen. The frozen muscle samples were stored at -70°C until perchloric acid extraction could be performed in preparation for analysis using proton nuclear magnetic resonance spectroscopy (¹H-NMRS). The entire sample collection process took approximately

fifteen minutes per mouse from start to finish with the muscle dissection itself, including weighing and freezing, averaging four to five minutes. Minimizing the sample recovery time was suspected to be important for minimizing post-mortem effects on lactate concentrations.

For each mouse the TA and GAS muscle samples were recovered in the following order without exception: 1. uncrushed right GAS; 2. crushed left GAS; 3. uncrushed left GAS; 4. uncrushed left TA; 5. crushed right TA; 6. uncrushed right TA; 7. diaphragm; and 8. heart.

[diaphragm and heart samples were collected for future studies.]

3.2 SAMPLE PREPARATION

3.21 Perchloric Acid Extraction: (Peeling et al., 1989; Bell et al., 1994; Blackburn et al., 1995)

For each stage of the following perchloric acid (PCA) protocol, muscle samples, instruments, reagents, and working surfaces were maintained below 0°C. Refrigeration and chilling over ice were included to prevent the potential thermal degradation of amino acids and proteins.

On the first day of the PCA extraction protocol, each muscle sample was first diced on a glass plate on ice using a sterilized, single-edge razor blade. The minced

muscle was subsequently transferred to a previously-weighed and labelled 50ml centrifuge tube (Falcon Blue Max, polypropylene, VWR Canlab Inc.) with 1ml of cold 0.3M PCA per 100mg of tissue. A minimum of 1ml 0.3M PCA was added to those samples weighing less than 100mg.

The samples, with an appropriate amount of 0.3M PCA, were homogenized (POLYTRON, Kinematica, Aggregate, Switzerland) for one minute. Between samples, the homogenizing probe was rinsed sequentially with the probe "on", in double distilled water (ddH₂O) and 70% ethanol, followed by two more rinses of ddH₂O. Instruments and working surfaces were also cleaned between samples. After homogenization, the suspension was centrifuged at 6000 rpm for 20 minutes at -1°C. The clear supernatant was transferred to a clean, labelled 50ml centrifuge tube and refrigerated. 1ml of PCA was added to the precipitated pellet which was again homogenized and centrifuged using the same conditions as described above. The second supernatant was pooled with the first and neutralized to approximate pH 7.0 ± 0.2 with 1.5M potassium hydroxide (KOH). The neutralized supernatant was frozen at -70°C for one hour and lyophilized to dryness (freeze-dried) overnight (10 to 12 hours).

On the second day of the PCA extraction protocol, the freeze-dried sample residue was dissolved in 1ml of deuterated water (D₂O) and brought to pH 7.25 ± 0.05 with 1% sodium deuterioxide (NaOD) and 1% deuterium chloride (DCl). Care was taken not to contaminate the samples with water, e.g. when rinsing the pH probe. The pH was recorded and the samples centrifuged at 6000 rpm for 20 minutes at -1°C. The resultant supernatant was collected in new labelled centrifuge tubes and again frozen at -70°C.

Again the frozen samples were lyophilized to dryness overnight. The freeze-dried sample residue was stored at room temperature in a clean, dark cupboard until preparation for ^1H -NMR spectroscopy.

3.3 ^1H -NMR SPECTROSCOPY

On the third day of the PCA extraction protocol, the freeze-dried sample residue was gently vortexed in 0.60ml of cold 1.5mM D_2O /TSP until the white powder (dried extract) dissolved. The quantity of TSP (sodium 3-trimethylsilyl propionate) added was known and remained consistent for all extracts (0.3125ml of 0.75% TSP/ D_2O per 10ml of D_2O). The solution was transferred to a clean 5mm NMR glass tube (Wilmad Glass Co. Inc., Buena, NJ.) using a 146 mm Wheaton Pasteur Pipette, and chilled in the refrigerator overnight. The following day approximately 10 to 15 pellets of Sodium-Chelex 100 (Biorad, Richmond, CA., analytical grade, 50-100 mesh) were added to each sample. The samples were analyzed at the Prairie Regional NMR Centre housed at the Institute of Biodiagnostics, National Research Council of Canada (IBD, NRC).

One-dimensional ^1H -NMRS spectra were acquired with a Bruker AMX-500 spectrometer (Rheinstetten, Germany and Wissembourg, France) operating at 500.139MHz with presaturation of the water signal. D_2O was used as the internal lock compound. The following analysis parameters were chosen to maximize the signal-to-noise ratio with the shortest experiment time. A total of 160 signal averages were summed for each spectrum. The spectra were acquired with an acquisition time of 1.3599

seconds, a relaxation delay of 5.0000 seconds and 55° radiofrequency (rf) pulse angle (flip angle). The spectral width was 6024.096Hz with 16,384 data points used for acquisition. Measurements were made at 300K (298K). For all spectra, exponential multiplication was 1Hz. As for water suppression (presaturation) the pulse sequence decreased the water signal intensity by a factor of approximately 30. The radiofrequency was set on resonance with the water peak at 500.139MHz for 5.0000 seconds (during the relaxation delay) then turned off prior to initializing the hard pulse for exciting the whole sample. FIDs were Fourier-transformed and the spectra were stored on magnetic tape.

Chemical shifts are given in parts-per-million (ppm) relative to TSP (0.00ppm). Peak assignments to the major metabolites of interest (tertiary-butanol, lactate, alanine, acetate, creatine, choline, taurine, and glycine amongst others) were based upon previous studies in the literature (Bock, 1994; Chang et al., 1995; Desmoulin et al., 1990; Fan et al., 1986; Lynch et al., 1994; Yoshizaki et al., 1981; Sze and Jardetsky, 1990; Sze and Jardetsky, 1994). Selected unknown or ambiguous peaks were confirmed with pure compounds and by adding small amounts of pure compounds to additional muscle samples prior to extraction.

3.4 PURE COMPOUNDS

1. **Tertiary Butyl Alcohol** (2-methyl-2-propanol, $(\text{CH}_3)_3\text{COH}$), Aldrich, approx. 99.0%, A.C.S. reagent, 36,053-8; prepared and analyzed as a pure compound in D_2O .
2. **Mevalonic Acid (MA)**, DL-Mevalonic acid Lactone (DL- β -hydroxy- β -methyl- δ -

valerolactone), Sigma, approx. 97%, FW = 130.1, M-4667.

3. **Hydroxy-3-Methylglutaryl Coenzyme A (HMG-CoA)**, DL-3-hydroxy-3-methylglutaryl coenzyme A, sodium salt, Sigma, approx. 93% (Na = 4mol/mol, H₂O = 5mol/mol), FW = 911.7, H-6132.
4. **Taurine** (C₂H₇NO₃S), 2-aminoethanesulfonic acid, Sigma, synthetic, approx. 99%, FW = 125.1, T-7146.

[**Note:** MA, HMG-CoA and Taurine were added to TA muscle samples prior to the extraction process. The resultant extract spectra were acquired as per all previous extracts.]

3.5 ONE-DIMENSIONAL TOTAL CORRELATION SPECTROSCOPY (1D-TOCSY) PARAMETERS

The 1D-TOCSY, ¹H-NMRS experiment was acquired on the same magnet with similar parameters as for the one-dimensional spectra described above. The spectra were acquired with a Gaussian-shaped pulse, gauss 1024, for 40msec duration at 62.50dB to excite the peak of interest. The mlev spin lock power level was 13dB and the mixing time was 102.776msec. The spectra were further acquired with a total of 10,240 scans summed for each spectrum. The acquisition time was 2.0317sec with a relaxation delay of 3.0000sec. The spectral width was 8064.516Hz with 32,768 data points. Measurements were made at 300K, and 1Hz of exponential multiplication was applied to

the FID before Fourier transformation.

[Note: MIXING TIME = $[(\{P6 * 64\} + P5) * L1] + (2 * P17) = [\{(31.50\text{usec} * 64) + 21.00\text{usec}\} * 48] + (2 * 2,500.00\text{usec}) = 97,776.00\text{usec} + 5,000.00\text{usec} = 102.776\text{msec}.$]

3.6 SPECTRAL ANALYSIS

The metabolite peaks were integrated and standardized to TSP using UXNMR software, version 970101.3. Standardized integrals were entered into a spreadsheet (Microsoft Excel, Version 7.0) and further standardized to the original muscle sample weight.

The spectra acquired from 2 day recovery and 4 day recovery crush-injured skeletal muscle samples were averaged at IBD, NRC using GRAMS/32 Version 5 spectroscopic software (Galactic Industries Corporation, Salem, NH, USA) to visualize suspected and unsuspected changes of the metabolite peaks. Within GRAMS/32 the "AVERAGE.AB" program was used to mathematically average all crushed, 2 day recovery and 4 day recovery spectra into a single spectrum. The same method was used on all the corresponding control spectra. The three resultant spectra were plotted for comparison. Each spectrum used in the averaging procedure was first standardized to TSP.

3.7 STATISTICAL ANALYSIS

Integrals of selected NMRS-visible metabolites were compared between recovery times (0, 1, 2, 4, 7, 9, 14 days) and treatment groups (crush-injured TA muscle samples; sample 1, vs. control TA muscle samples; sample 3) with two-way analysis of variance (ANOVA) without repeated measures using a probability of $p < 0.05$ to define significance (Corel Quattro-Pro 8). Those metabolites that showed significant differences with ANOVA were further tested for specific differences between recovery days and treatment groups with a multiple comparison test, the Duncan's new multiple range test (software provided by Dr. Elliott Scott, Department of Oral Biology, University of Manitoba). All graphic representations of metabolite changes over the recovery period were prepared with Microsoft Excel 7.0.

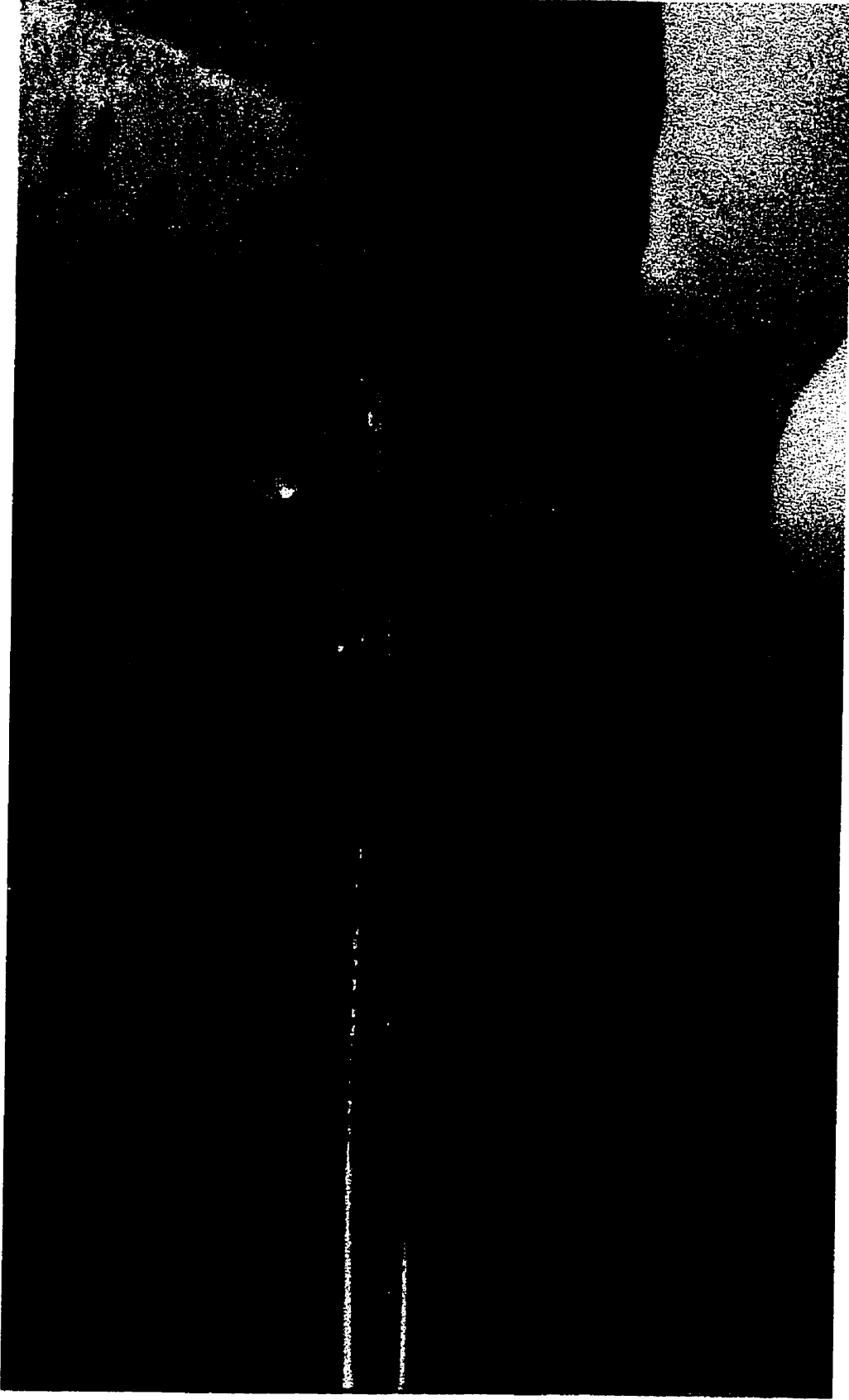


Figure 3.1 This image demonstrates the crush-injury applied to the tibialis anterior muscle of a 6-8 week old mouse with Steven's "microhemostats" to the first closure step, 1cm proximal to the calcaneus bone of the right hindlimb.



Figure 3.2 This image illustrates the appearance and location of the crush-injury to the right tibialis anterior muscle of a 6-8 week old mouse. The center of the crush-injury lies 1cm proximal to the calcaneus bone and is tagged with non-absorbable, 6-0 sutures proximal and distal to the crush site. The overlying skin was subsequently closed with the same suture material.

Right Tibialis Anterior

Left Tibialis Anterior

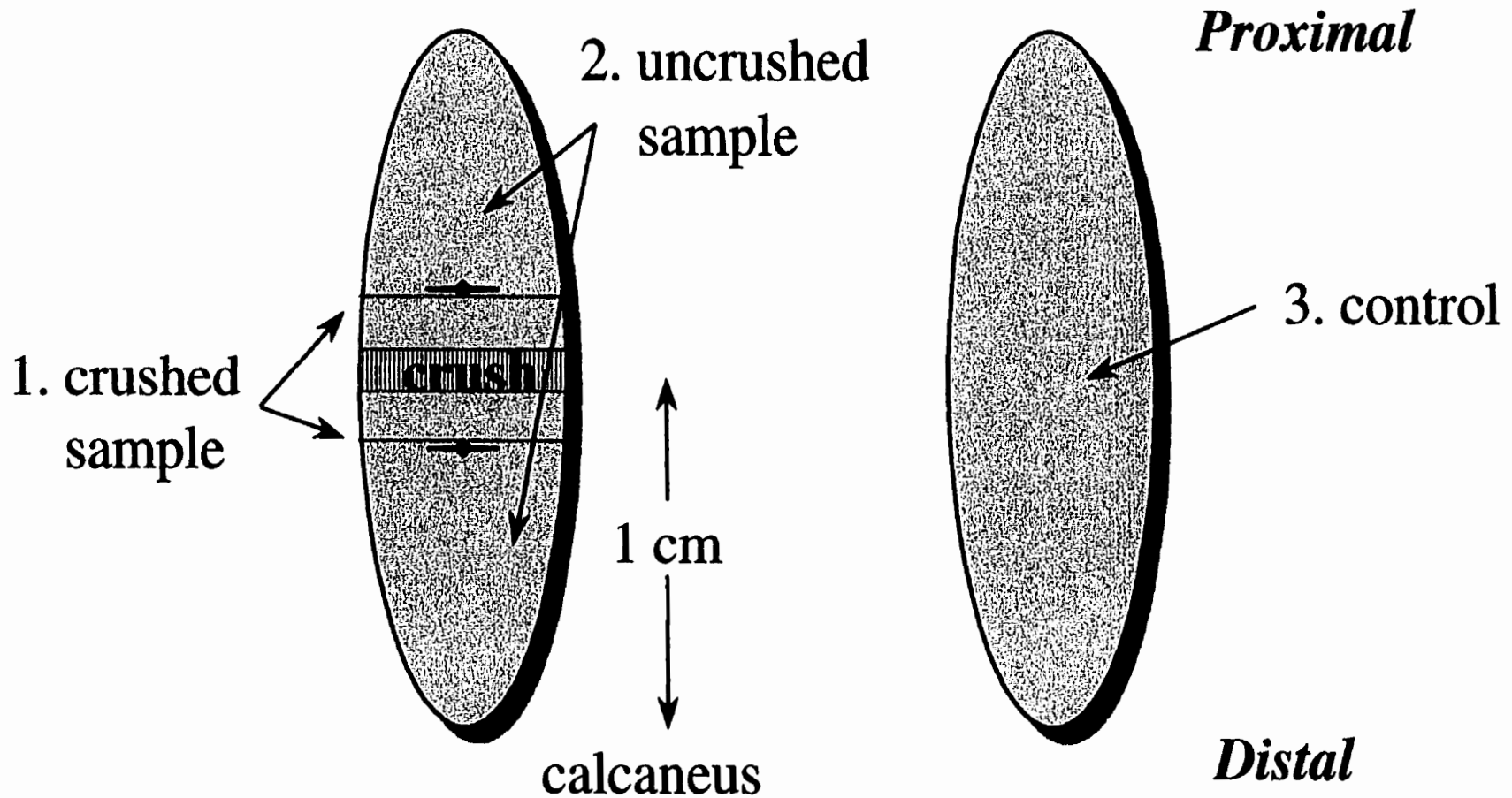


Figure 3.3 This figure illustrates the three separate tibialis anterior muscle samples collected from each mouse. 1. A crushed sample, 2. An uncrushed internal control from the same muscle as (1) and 3. Uncrushed intact internal control, contralateral to (1). The crush injury was applied 1 cm proximal to the calcaneus bone of the right hindlimb.

CHAPTER 4 - RESULTS

4.1 SPECTRAL ACQUISITION

Before explaining our experimental results the validity of our data will be addressed. Theoretically, the N-CH₂ and S-CH₂ moieties of taurine are spectroscopically identical (a 1:1 ratio), therefore charts produced from integration for each taurine peak plotted over the recovery period should be identical. The changes of taurine shown in figures 4.7E and 4.7F display experimental accuracy since the two graphs are similar for the duration of the recovery period. When data from control muscle for taurine are combined (figure 4.9A), similarities between the two taurine moieties are seen, such that they almost overlap each other. The N-CH₂ (3.26 ppm) mean areas were slightly greater since this peak exhibited varying degrees of chemical shift due to the fluctuating unbuffered pH of our skeletal muscle extracts. The variable pH caused the N-CH₂ moiety to overlap adjacent peaks like carnitine and choline in a given spectrum which was reflected in the integrated mean area. However as figure 4.9A illustrates, the two taurine peaks exhibited similar changes over the time course of repair, and values for the two integrals nearly overlaid each other. This indicated accurate integration methods, which were further supported by comparing the lactate peaks at 1.32 and 4.11 ppm. The two spectral peaks of lactate theoretically occur in a 3:1 ratio (lactate1.32 : lactate4.11) however the lactate peak at 1.32 ppm was slightly greater than expected (figure 4.9B). This was likely the result of a small unknown metabolite peak hidden by the lactate1.32

peak. Despite the slightly higher moiety ratio, the two lactate peaks (like the two taurine peaks) followed similar changes over the time course of repair.

Additional checks of the stringency of the $^1\text{H-NMRS}$ experimental method included determination of accurate shimming and saturation practices before integrating the spectra. This was confirmed by a small water peak for each sample analyzed and correct splitting of the lactate peak at 1.32 ppm. If the splitting was greater than 50% and the water peak was relatively small compared to TSP, the experiment was considered successful and the spectrum was integrated. Otherwise the sample was re-analyzed and a new spectrum was acquired.

4.2 EXPERIMENTAL RESULTS

Our experimental results are presented in two sections. The first section (A) considers identification of a previously unknown peak at 1.25 ppm from the $^1\text{H-NMRS}$ spectra. The second section (B) considers significant metabolite differences and trends between control, damaged, and regenerating skeletal muscle.

4.2A AN UNKNOWN METABOLITE PEAK AT 1.25 ppm

Several methods were utilized to identify a metabolite resonating at 1.25 ppm. These included averaged spectra, 1D-TOCSY, pure t-butanol in D_2O , and spiked pure samples of mevalonic acid (MA) and hydroxymethylglutaryl-CoA (HMG-CoA).

4.2A1 Averaged Spectra

Although previous studies in our lab dictated which skeletal muscle metabolite peaks would be integrated, averaging 2 day recovery spectra (2dCr) and 4 day recovery spectra (4dCr) from crush-injured muscle samples (sample 1), and 2 day recovery and 4 day recovery control spectra (control) indicated an additional metabolite peak for integration. The averaged spectra showed unexpected pattern differences for two skeletal muscle metabolites (see figure 4.1) at 1.25 and 1.92 ppm. Metabolites, like taurine, creatine and lactate had peak intensities for 2dCr and 4dCr less than the corresponding control peak intensity ($2dCr < 4dCr < control$). Acetate (at 1.92 ppm) had peak intensities for 2dCr and 4dCr greater than the control peak intensity ($4dCr > 2dCr > control$). The unknown peak at 1.25 ppm from 4dCr was greater than the control which was greater than the unknown peak from 2dCr ($4dCr > control > 2dCr$).

4.2A2 1D-TOCSY

The first step towards identifying the unknown peak at 1.25 ppm was a 1D-TOCSY, 1H -NMRS experiment designed to exploit other nuclear information at different resonances in our spectra that might be related (coupled) to the peak at 1.25 ppm (see figure 4.2). The resulting spectrum of the 1D-TOCSY experiment showed relatively small neighbouring proton resonances at 3.04 ppm and 3.42 ppm with an inordinately large water peak at 4.75 ppm. The lactate peaks at 1.32 and 4.11 ppm also appeared in

the 1D-TOCSY spectrum.

4.2A3 Pure t-Butanol in D₂O

A pure sample of t-butanol in D₂O produced a peak that resonated with the same frequency as the unknown peak from our muscle sample extracts at 1.25 ppm (see figure 4.3).

4.2A4 Skeletal Muscle Extracts Spiked with Mevalonic Acid and 3-Hydroxy-3-Methylglutaryl-Coenzyme A

Two tibialis anterior muscle samples from C57 mice were spiked with mevalonic acid (MA) and 3-hydroxy-3-methylglutaryl coenzyme A (HMG-CoA). The resultant spectra showed numerous peaks. MA displayed a large resonance at 1.25 ppm (a singlet peak) as well as resonances at 1.38 ppm (singlet), 1.84 ppm (triplet), 2.37 ppm (triplet), 2.70 ppm (quartet) and 3.74 ppm (triplet) (see figure 4.4). HMG-CoA also produced a peak at 1.25 ppm (singlet) with many additional small resonances which were not easily differentiated. For both MA and HMG-CoA, the 1.25 ppm peaks were significantly larger than neighbouring peaks in their spectra. TSP-standardized integrals for the 1.25 ppm peaks from MA and HMG-CoA were approximately 1.5 times greater than the next highest peak in the spiked spectra, and 32 times greater than TSP. The 1.25 ppm resonance observed in our muscle sample spectra was about 100 times smaller than that

observed for the MA and HMG-CoA spiked samples and 33 times smaller than TSP.

4.2A5 Contamination

To rule out the possibility that the 1.25 ppm resonance was due to a contaminant of the PCA extraction process, several samples were prepared to analyze the reagents used in the extraction process and the NMR tube-cleaning procedures (see figure 4.5). Each sample provided no evidence of contaminants since only TSP and water resonances were visible in the resultant spectra. When the contaminant spectra were magnified beyond a typical intensity, resonances were observed at 3.360 ppm, 2.129 ppm and 1.919 ppm which were too small to have more than negligible effects on our muscle sample spectra.

4.2B SIGNIFICANT METABOLITE CONCENTRATIONS AND CHANGES

The skeletal muscle metabolites studied and their ¹H-NMRS peaks were lactate (a CH₃ doublet peak at 1.32 ppm and a CH quartet at 4.11 ppm), creatine (N-CH₃ singlet, 3.04 ppm and N-CH₂ singlet, 3.94 ppm), taurine (N-CH₂ triplet, 3.26 ppm and S-CH₂ triplet, 3.41 ppm), alanine (β-CH₂ doublet, 1.47 ppm), glycine (α-CH singlet, 3.56 ppm), acetate (α-CH₃ singlet, 1.92 ppm), the unknown ([CH₃]₇ singlet, 1.25 ppm), choline ([CH₃]₃ N⁺ singlet of choline and phosphocholine, 3.21 ppm), succinate (CH₂ singlet, 2.41 ppm), carnitine ([CH₃]₃ N⁺ singlet, 3.23 ppm) and glutamate (γ-CH₂ triplet, 2.34

ppm) (see figure 4.6). The known concentration of TSP and muscle sample weight were used to standardize the integrals of each muscle metabolites. The differences between crush-injured and control skeletal muscle at each recovery stage were determined by statistical analysis of ¹H-NMRS data.

Standardized integrals were first compared between recovery times (RT; 0-14 days) and treatment groups (Tx; crushed vs control) for each metabolite studied. Two-Way Analysis of Variance (ANOVA) demonstrated significant differences between RT and Tx groups for lactate, creatine, taurine, the unknown, choline, carnitine and glutamate. These results indicated that injured muscle could be differentiated from control muscle. The ANOVA test was followed by the Duncan's New Multiple Range post-hoc statistical method which tested for specific differences between: 1. damaged muscle (crush-injured muscle on day 0) and control muscle, 2. regenerating muscle (crush-injured muscle between days 1 to 14) and control muscle, 3. damaged muscle and regenerating muscle and 4. within the control group itself. These data are summarized in figure 4.7 (A-N), figure 4.8 (day 0 to day 14) and table 4.1. See appendix B for specific statistical details (ANOVA tables, metabolite integral means and standard deviations).

The uncrushed Tx group (sample 2) was not included for statistical analysis (see discussion).

4.2B1 Comparison of Damaged Muscle to Control Muscle

Our results showed significantly lower concentrations for creatine^{3.04},

creatine^{3.94}, taurine^{3.26} and taurine^{3.41} between damaged muscle and control muscle on day 0 of recovery. All other metabolites studied remained statistically unchanged between damaged and control muscle samples on recovery day 0.

4.2B2 Comparison of Regenerating Muscle to Control Muscle

Differences between regenerating muscle and control muscle are presented in terms of phasic or progressive metabolite changes. By way of definition, the term “phasic” refers to a short term shift in metabolite concentration, while the term “progressive” describes a gradual increase or decrease in the concentration of a metabolite over the RT.

Progressive metabolites included lactate^{1.32}, lactate^{4.11}, creatine^{3.04}, creatine^{3.94}, taurine^{3.26} and taurine^{3.41}. The concentrations of these metabolites were below control concentrations immediately following the crush injury and returned towards control levels in a step-wise fashion over the time course of repair. Lactate (1.32 and 4.11) concentrations for regenerating muscle samples were less than the corresponding control concentrations between recovery days 1 to 7. Creatine (3.04 and 3.94) and taurine (3.26 and 3.41) concentrations in regenerating muscle samples were less than the corresponding control concentrations for the duration of the recovery period except on recovery day 9 when taurine showed no difference.

Choline^{2.31}, carnitine^{2.36} and glutamate^{2.34} had phasic differences that distinguished regenerating muscle from control muscle. Choline and carnitine

concentrations from regenerating muscle samples were less than their corresponding control concentrations on recovery day 1 and recovery day 2. The concentration of glutamate was greater in regenerating muscle samples on recovery days 4, 7 and 9 compared to the corresponding control concentration on the same day.

4.2B3 Comparison of Damaged Muscle to Regenerating Muscle

By comparing damaged muscle to regenerating muscle, two trends were observed; skeletal muscle metabolite concentrations in crush-injured muscle samples either increased following the crush injury or decreased. On recovery day 1 the concentration of lactate 1.32 was greater than its concentration on day 0. Creatine (3.04 and 3.94) concentrations were significantly greater on recovery day 14 as were the taurine concentrations when compared to recovery day 0. Taurine 3.26 was also increased on recovery days 4 and 9 compared to day 0 concentrations. On recovery day 4 the unknown metabolite concentration was increased as was the glutamate concentration and choline and carnitine concentrations were higher by recovery day 4 compared to their concentrations on day 1 and day 2. On recovery day 9, choline, carnitine and glutamate concentrations were still higher than earlier concentrations. By recovery day 14 the glutamate concentration was still increased related to its concentration on recovery day 0.

4.2B4 Comparison of Control Muscle Samples

The metabolite concentrations from the control muscle samples did not change significantly over the time course of repair except lactate 1.32 and taurine 3.26 on the recovery days 7 and 14, respectively.

4.3 CHEMICAL SHIFT OF TAURINE

As mentioned in section 4.1 (spectral acquisition), the taurine resonances displayed chemical shift changes for some of our prepared skeletal muscle samples. Eleven randomly selected spectra showed how the S-CH₂ and N-CH₂ moieties of taurine moved away from their expected chemical shifts (3.41 and 3.26 ppm, respectively). The S-CH₂ fraction shifted towards N-CH₂ as far to the right as 3.29 ppm and the N-CH₂ fraction shifted within the range of 3.27 to 3.21 ppm. These shifts made it difficult, sometimes impossible, to integrate the choline and carnitine resonances that remained stationary at 3.21 and 3.26 ppm, respectively. This explains the small *n* observed for these two metabolites (appendix B, table B1-3). Figure 4.10 illustrates the variable chemical shifts exhibited by the taurine resonances among the eleven chosen spectra.

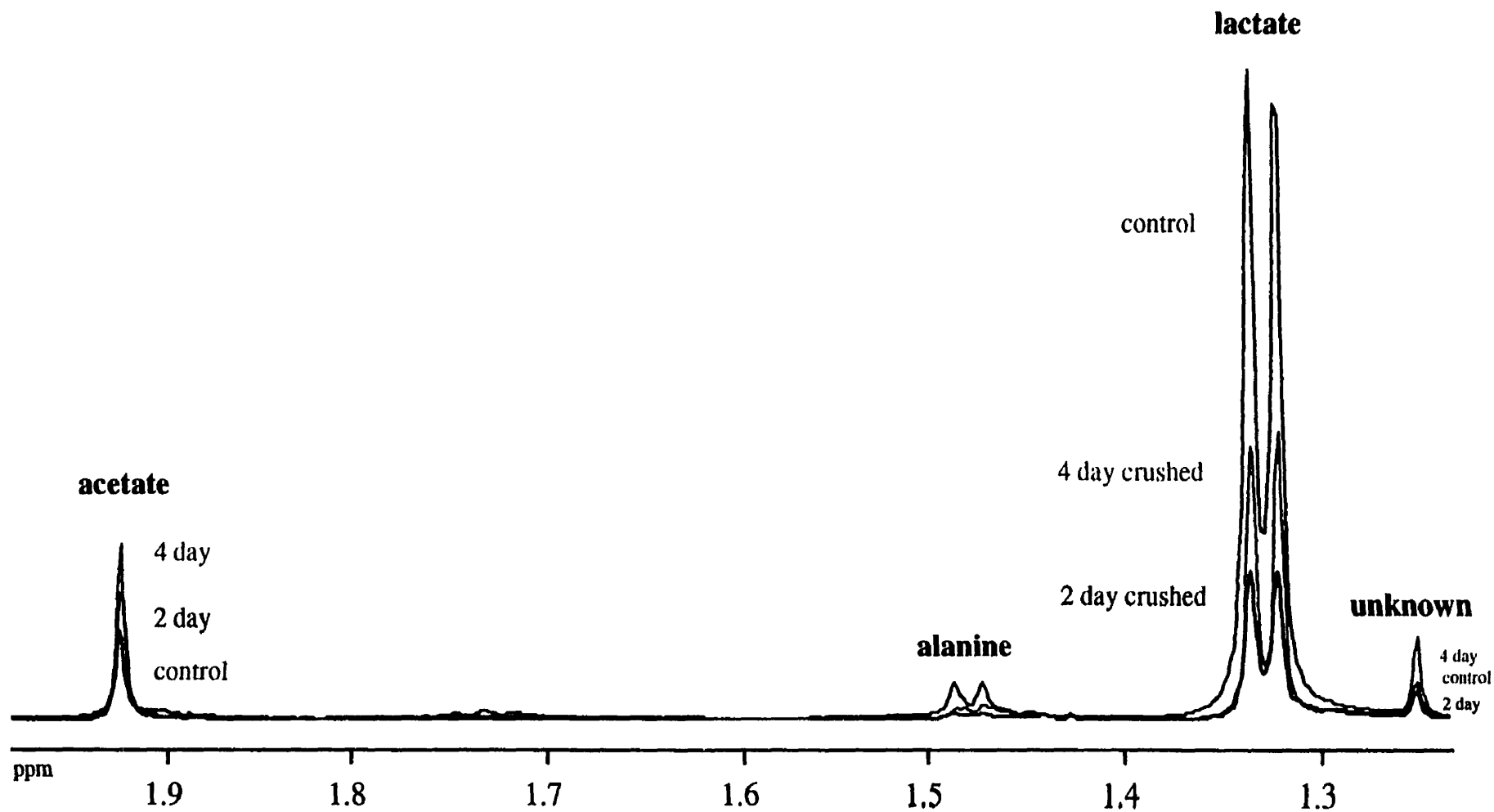


Figure 4.1 Averaged $^1\text{H-NMR}$ spectra of 2 day recovery and 4 day recovery perchloric acid extracts from crush-injured right tibialis anterior muscle samples compared to control muscle sample spectra.

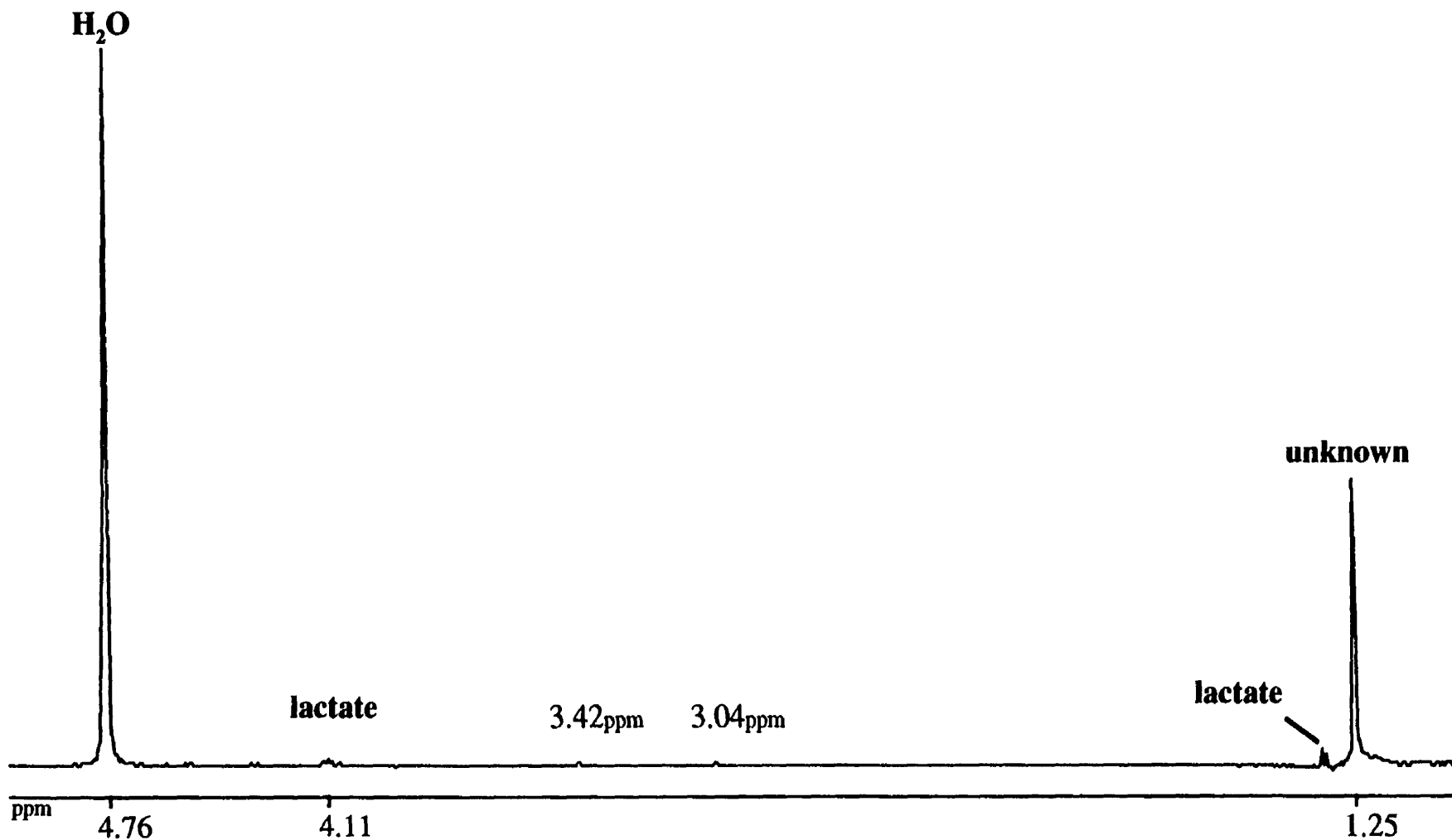


Figure 4.2 The spectrum from the 1D-TOCSY experiment with a mixing time of 100 milliseconds at 300K. Acquired from a crush-injured skeletal muscle extract (sample 1) to exploit information in the spectrum related to the unknown resonance at 1.25ppm.

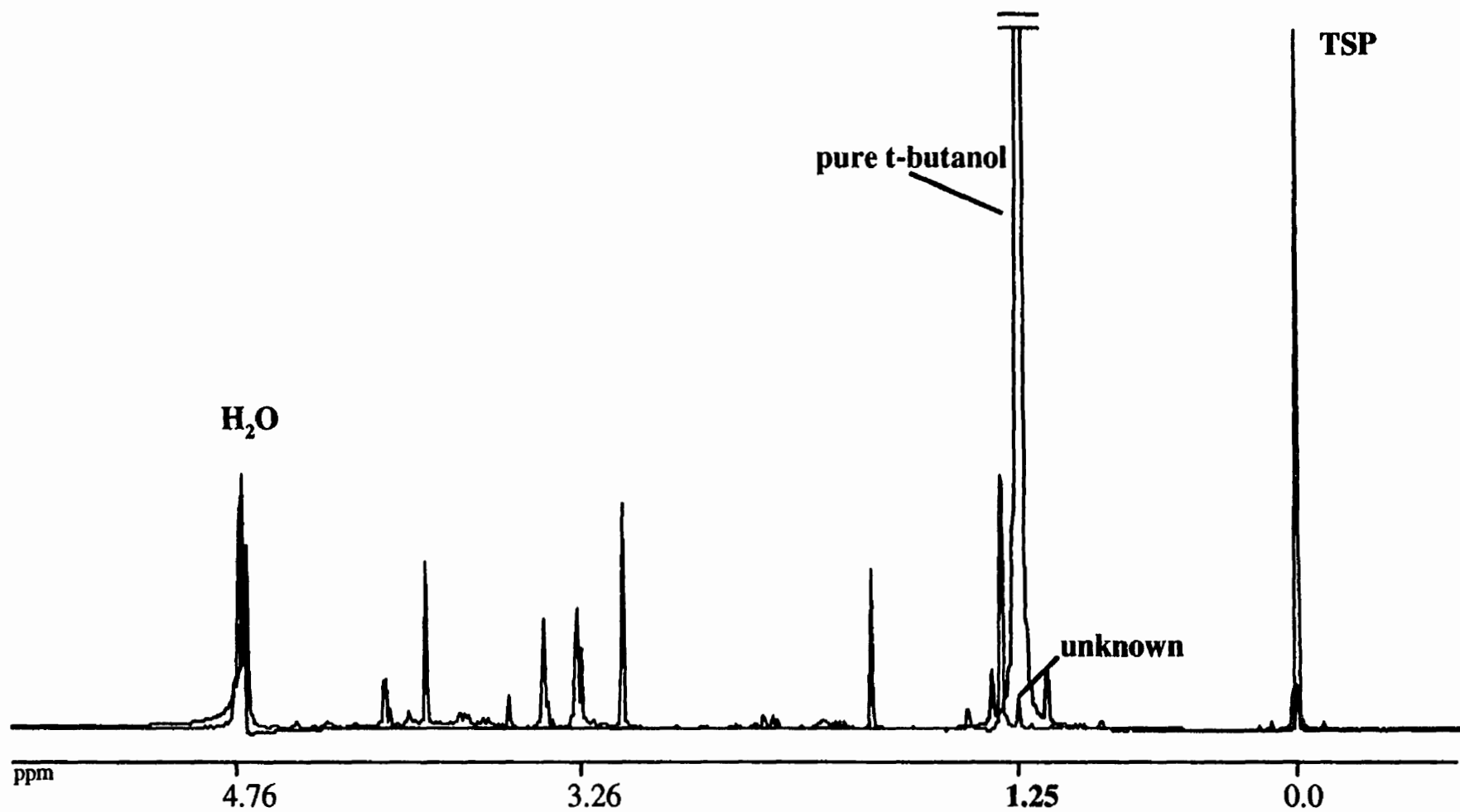


Figure 4.3 This figure illustrates overlap between the 1.25ppm peak from a pure sample of tertiary butyl alcohol (t-butanol) and the unknown peak at 1.25ppm in a crush-injured skeletal muscle sample. Each one-dimensional ¹H-NMR spectrum was acquired at 300K with a Bruker AMX-500 spectrometer operating at 500MHz.

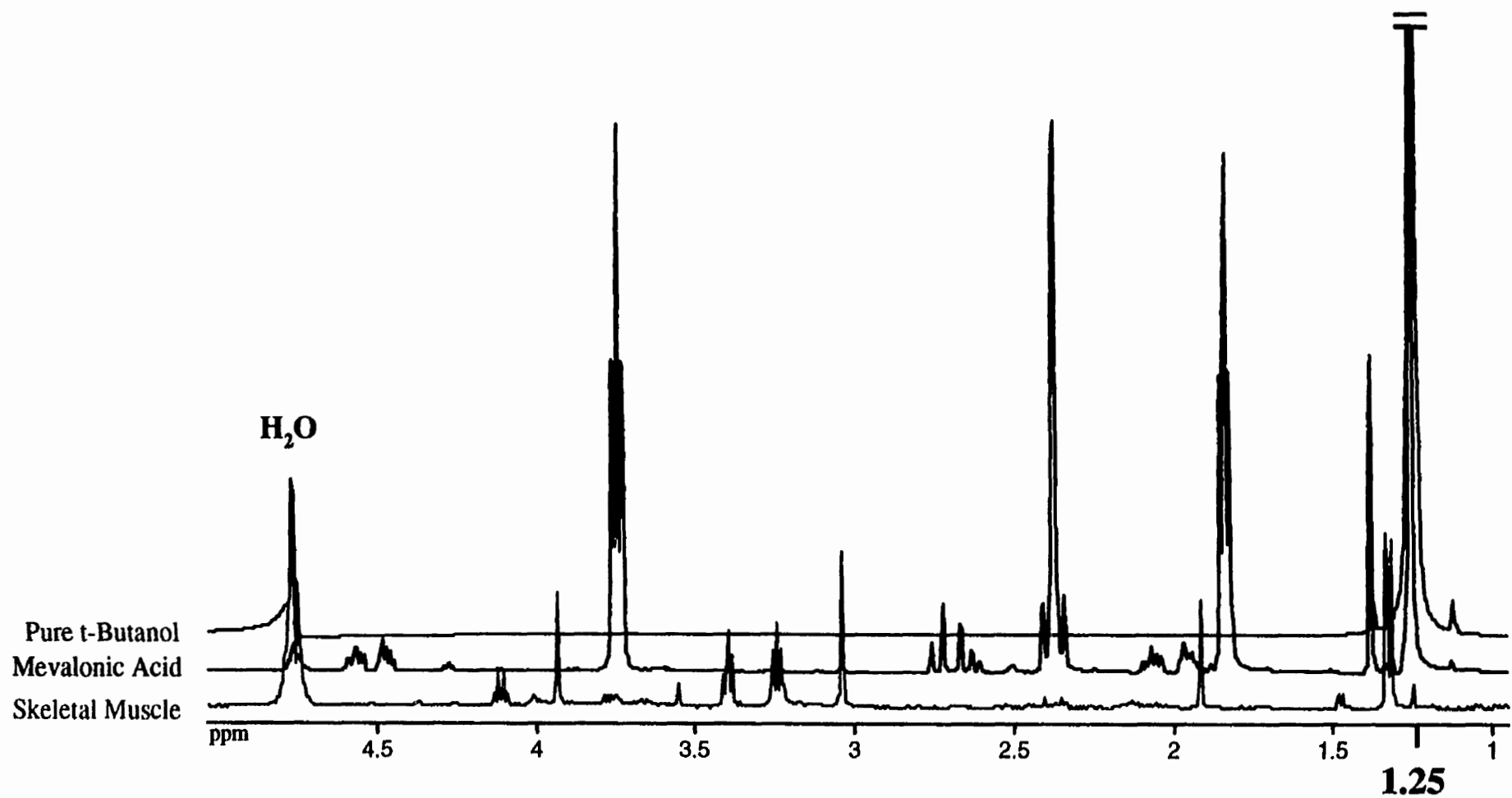


Figure 4.4 Samples of tibialis anterior muscle were spiked with mevalonic acid and 3-hydroxy-3-methylglutaryl coenzyme A. The spectrum from the mevalonic acid-spiked sample is overlaid with the spectrum from a crush-injured skeletal muscle extract and the pure tertiary butyl alcohol spectrum to show similarities at 1.25ppm. Each spectrum was acquired at 300K on a Bruker AMX-500 spectrometer operating at 500 MHz.

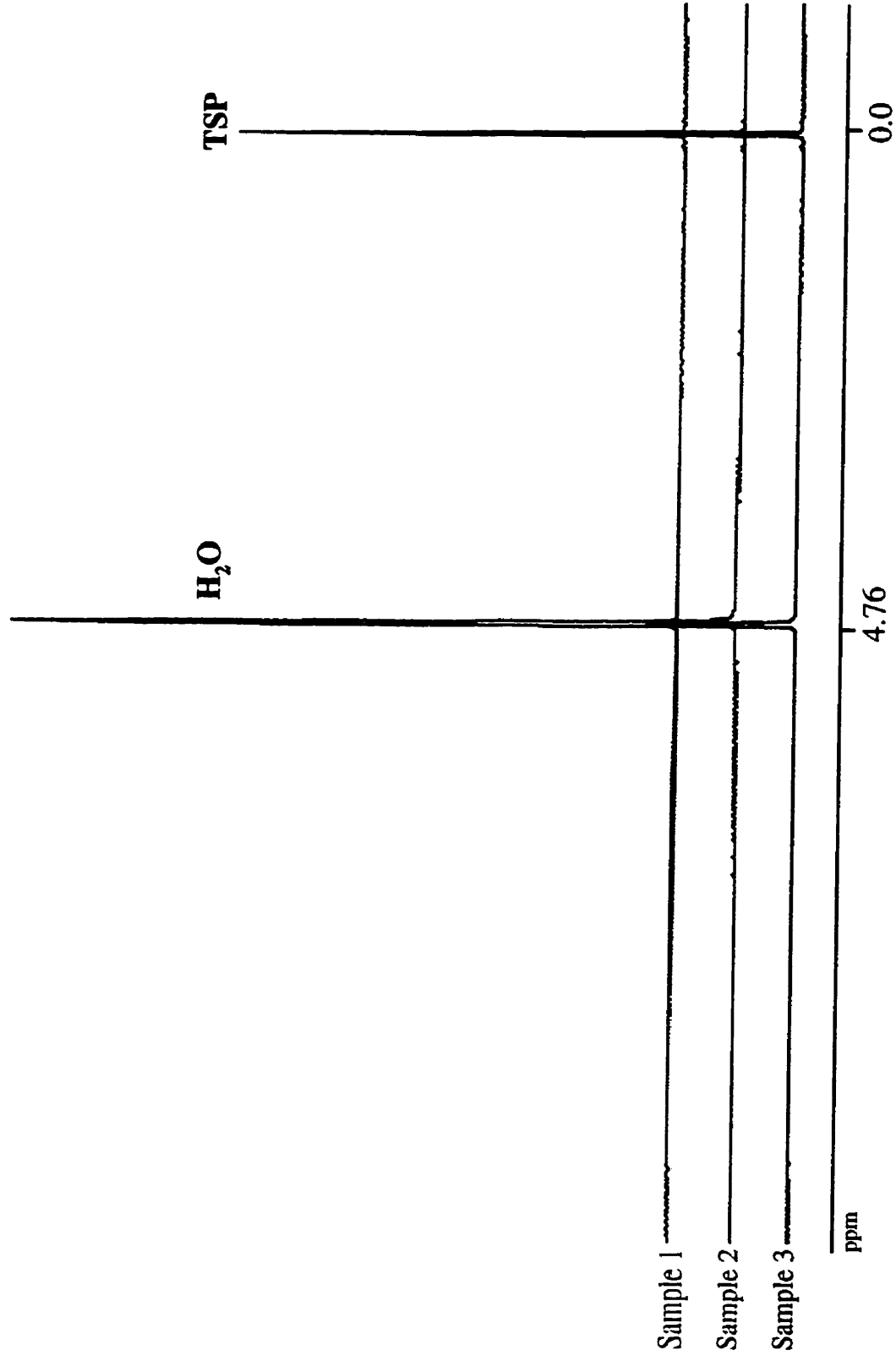


Figure 4.5 Three one-dimensional ¹H-NMR spectra from individually prepared samples tested the possibility of a contaminant at 1.25ppm due to the perchloric acid extraction process and/or cleaning practices. These spectra illustrate no contaminant at 1.25ppm. Sample1 tested the purity of the D2O/TSP standard, sample 2 tested the stringency of our NMR-tube cleaning practices and sample3 tested the purity of the chelating agent added to each muscle extract. Each spectrum was acquired at 300K on a Bruker AMX-500 spectrometer operating at 500MHz.

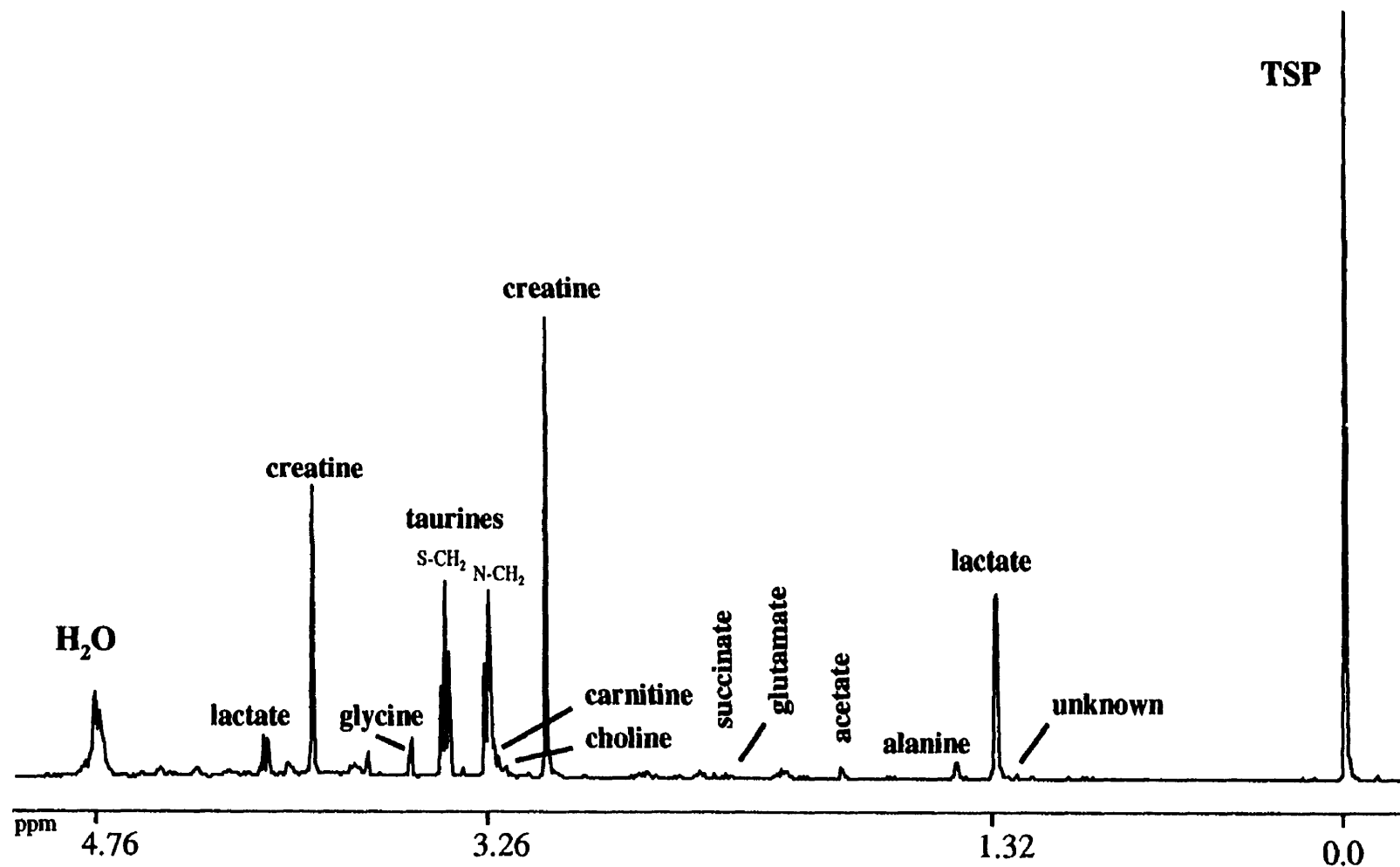


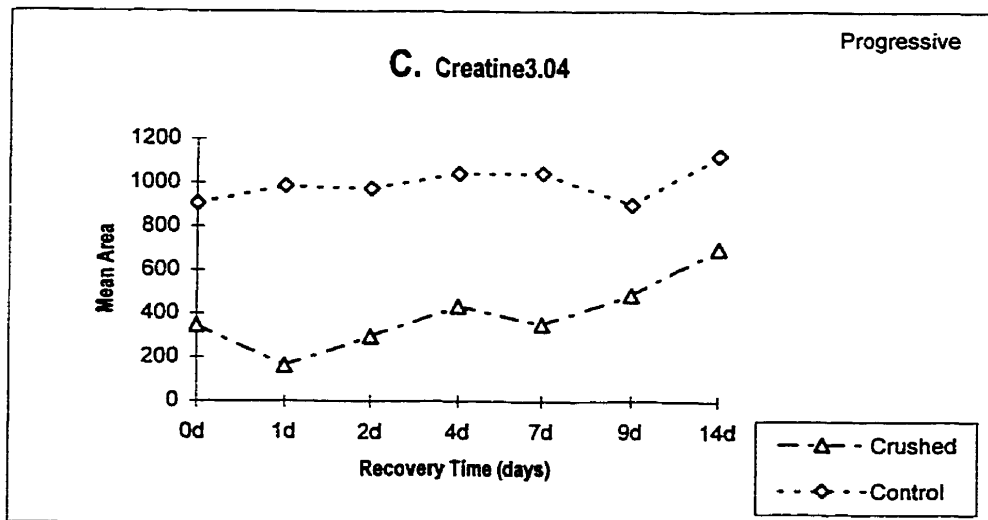
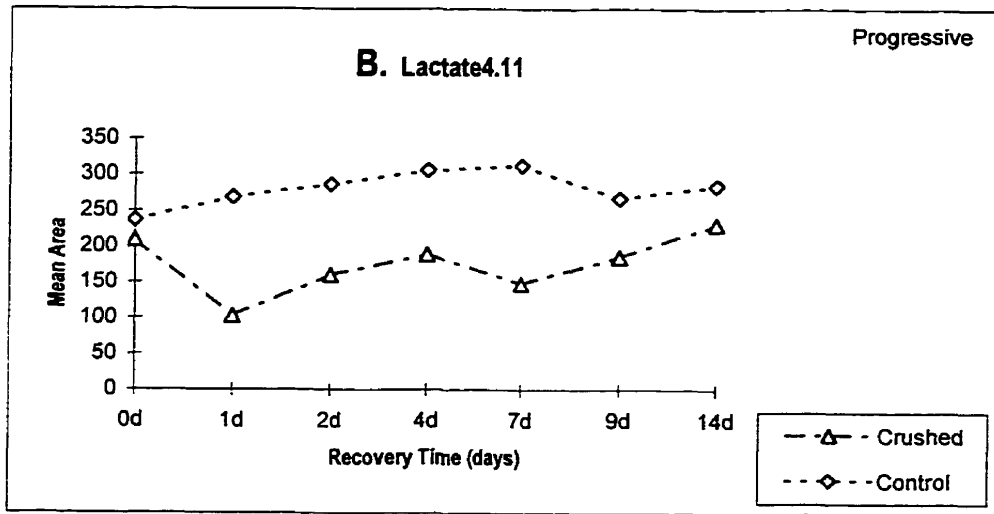
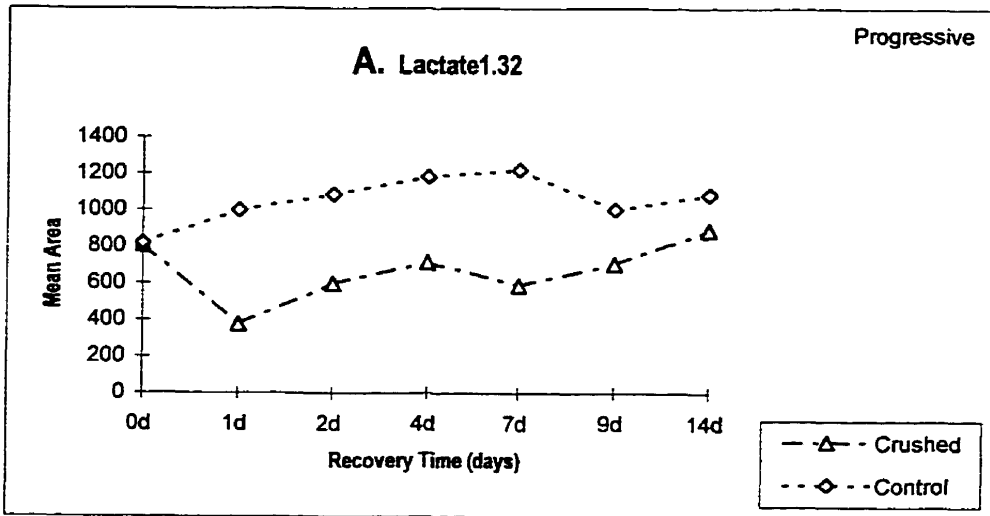
Figure 4.6 A representative one-dimensional ¹H-NMR spectrum of a perchloric acid extract from control tibialis anterior muscle acquired at 300K on a Bruker AMX-500 spectrometer operating at 500 MHz. Integrated peaks are indicated.

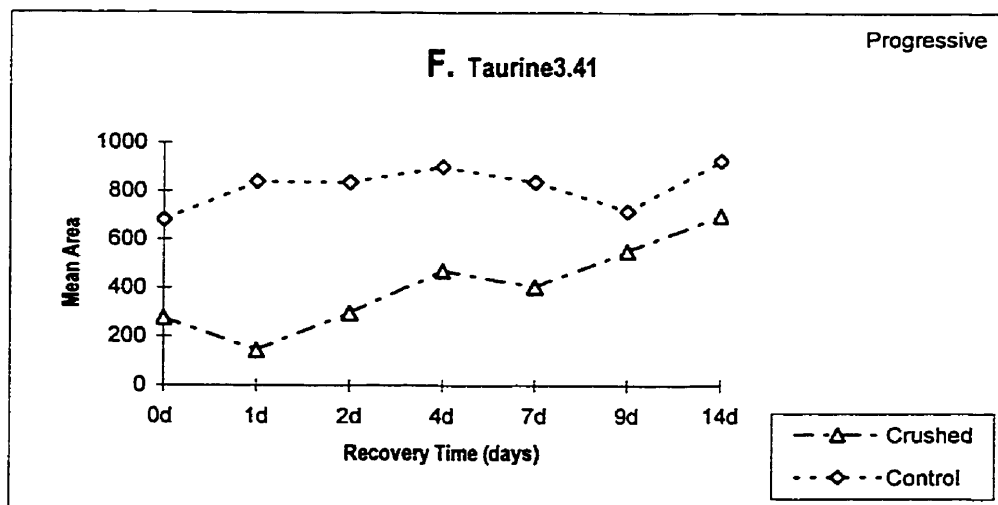
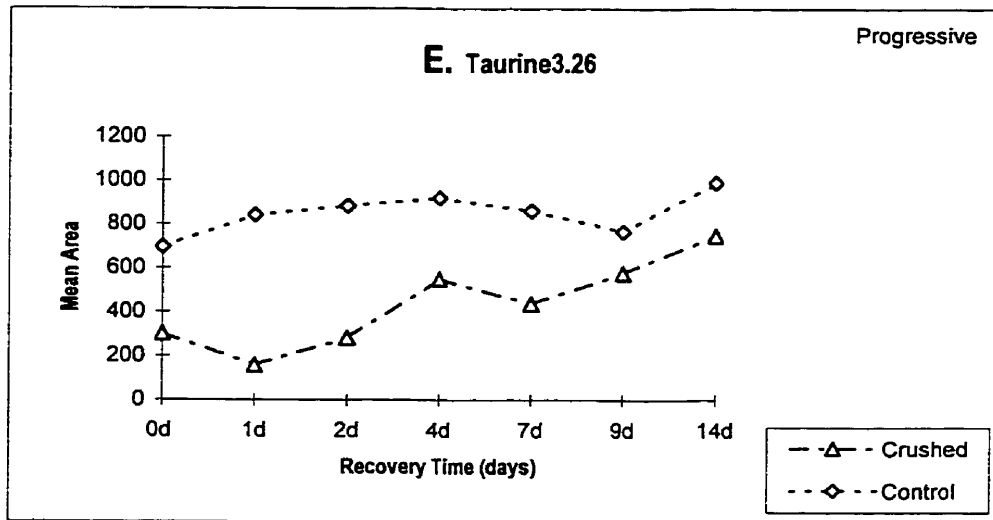
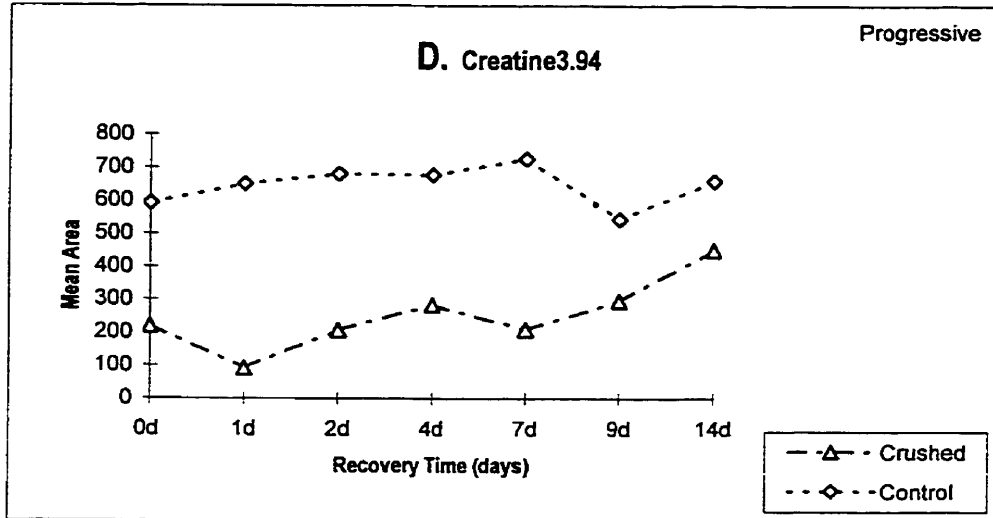
TABLE 4.1 Summary of Duncan's New Multiple Range Test

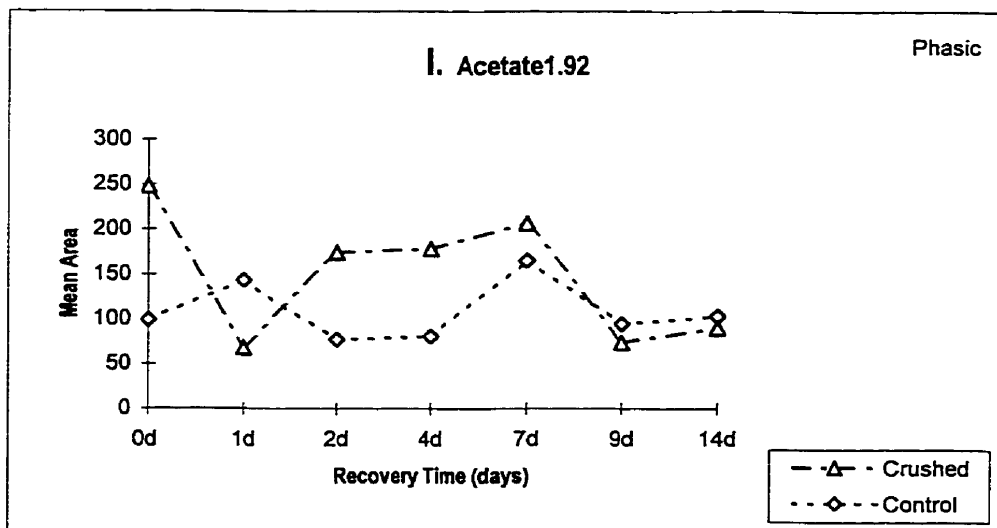
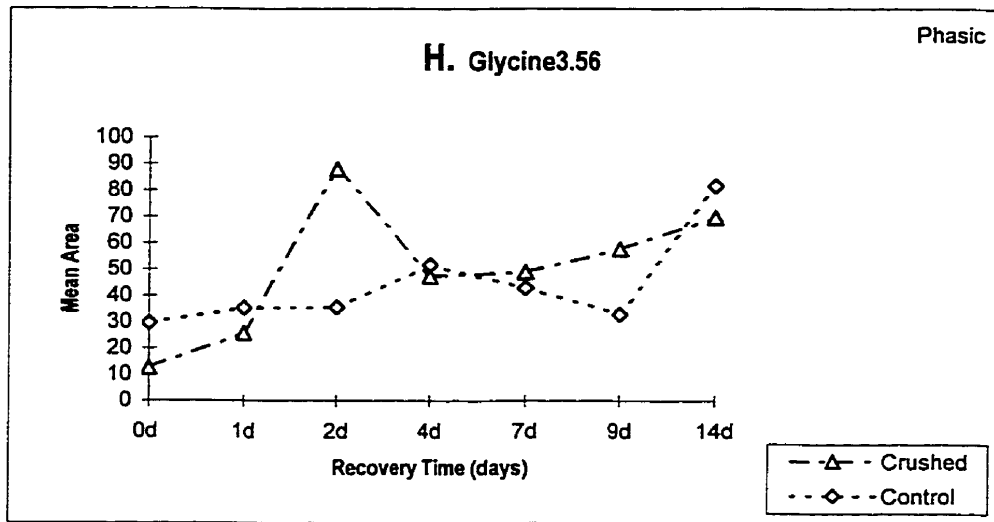
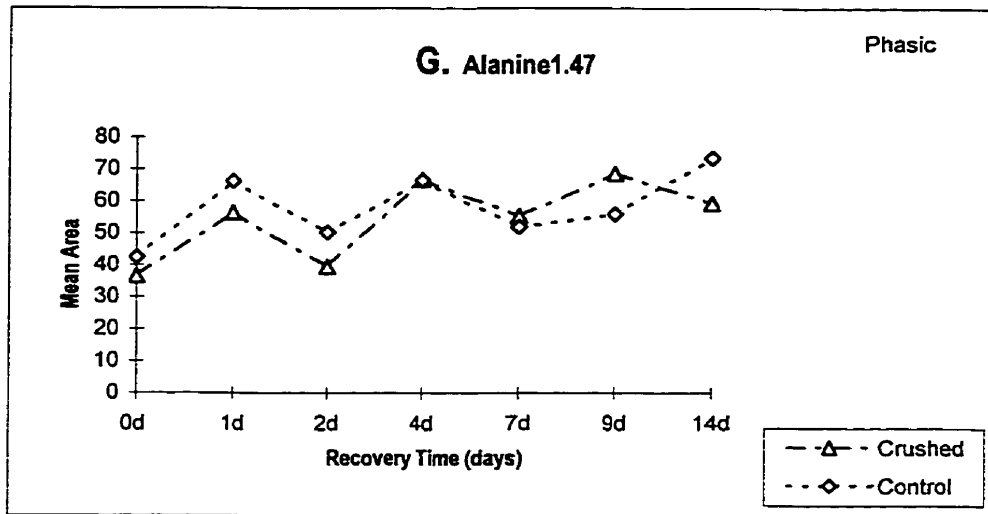
The statistically significant differences of crush injured muscle from control muscle at the same recovery time are indicated by an asterisk for each metabolite. Differences between crush injured muscle groups at two different recovery times are indicated by a "Cr" followed by a recovery day (Cr4 for different from day 4). Differences between control muscle groups at two different recovery times are indicated by a "C" followed by a recovery day (C4, for different from control day 4). In all cases significant results in ANOVAs preceded the Duncan's post-hoc tests which are reported in Appendix B. Those metabolites that showed significant differences with ANOVA are shaded.

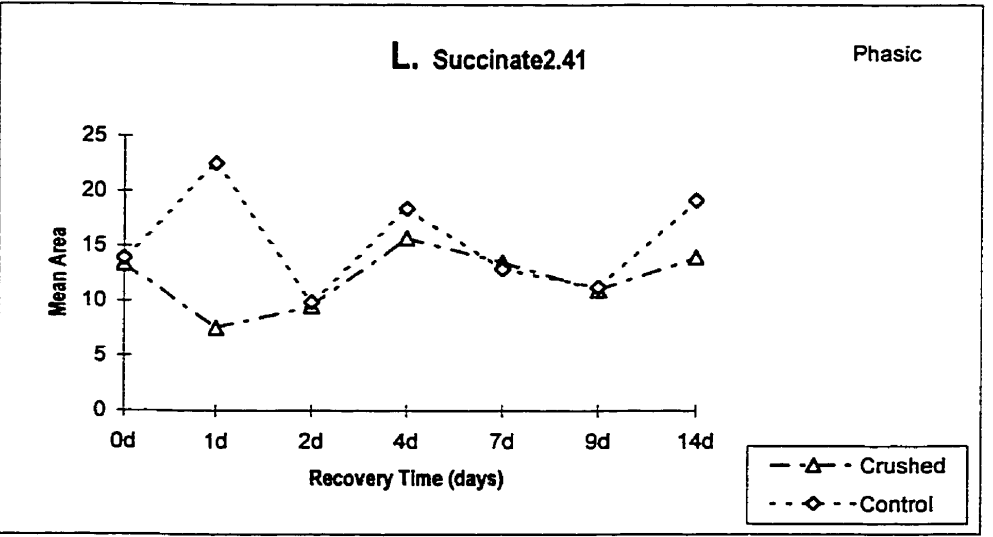
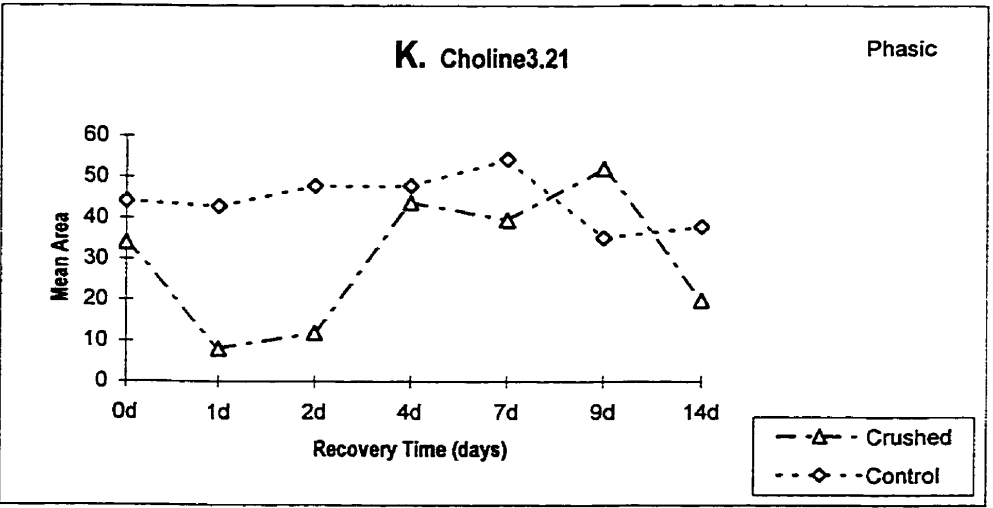
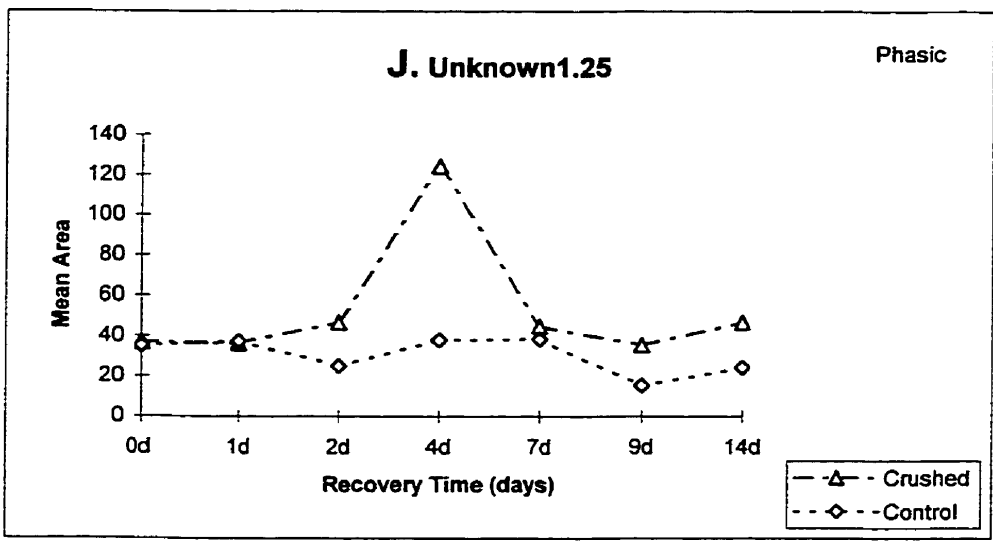
Metabolite	CONTROL MUSCLE							CRUSHED MUSCLE						
	0 day	1 day	2 day	4 day	7 day	9 day	14 day	0 day	1 day	2 day	4 day	7 day	9 day	14 day
lactate1.32							C0							
creatine1.11														
alanine3.03														Cr0
creatine3.43														Cr0
taurine3.26							C0				Cr0		Cr0	Cr0
taurine3.41													Cr0	Cr0
alanine1.47														
glycine3.56														
acetate1.92														
Unknown1.25												Cr0	Cr1	Cr1
choline3.21												Cr1	Cr1	Cr1
succinate2.41														
carmitine3.23												Cr0	Cr0	Cr0
glutamate2.34												Cr0	Cr0	Cr0

Figure 4.7(A-N) The integrated mean area for each skeletal muscle metabolite studied is measured against the crush injury recovery time (0-14 days). Crush-injured muscle samples are compared to control muscle samples to illustrate differences between damaged muscle (at recovery day 0) and control muscle, regenerating muscle (recovery day 1-recovery day 14) and control muscle, and damaged muscle and regenerating muscle. Significantly different means areas are summarized in table 4.1. Standard deviations are included in appendix B.









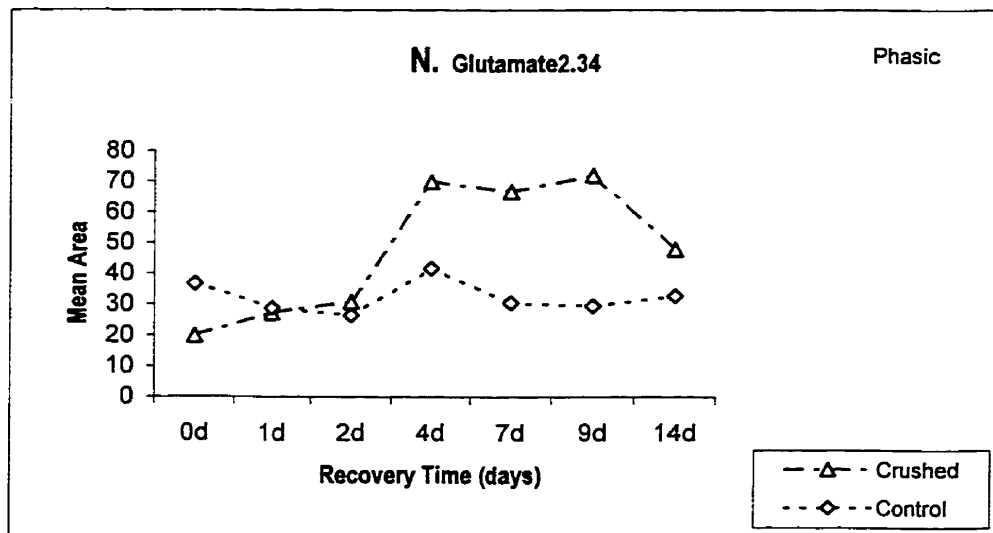
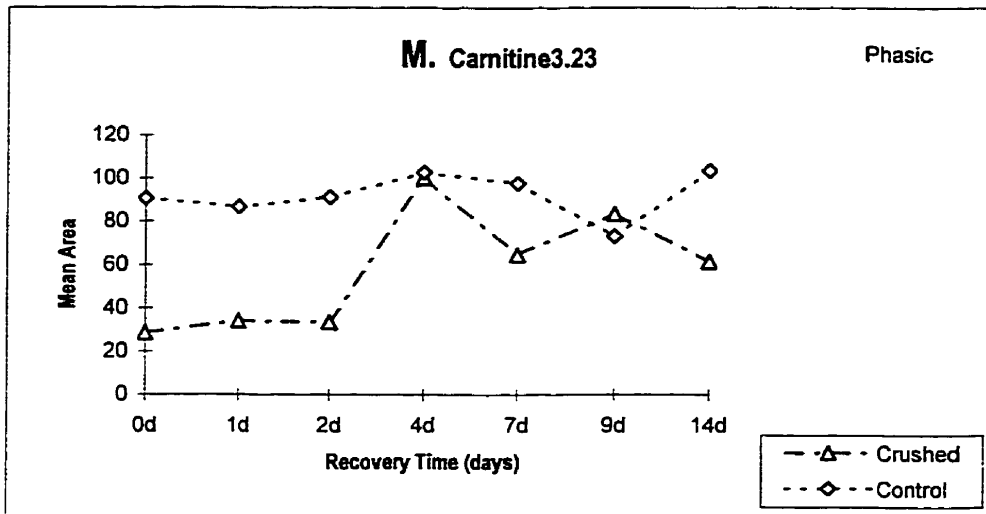
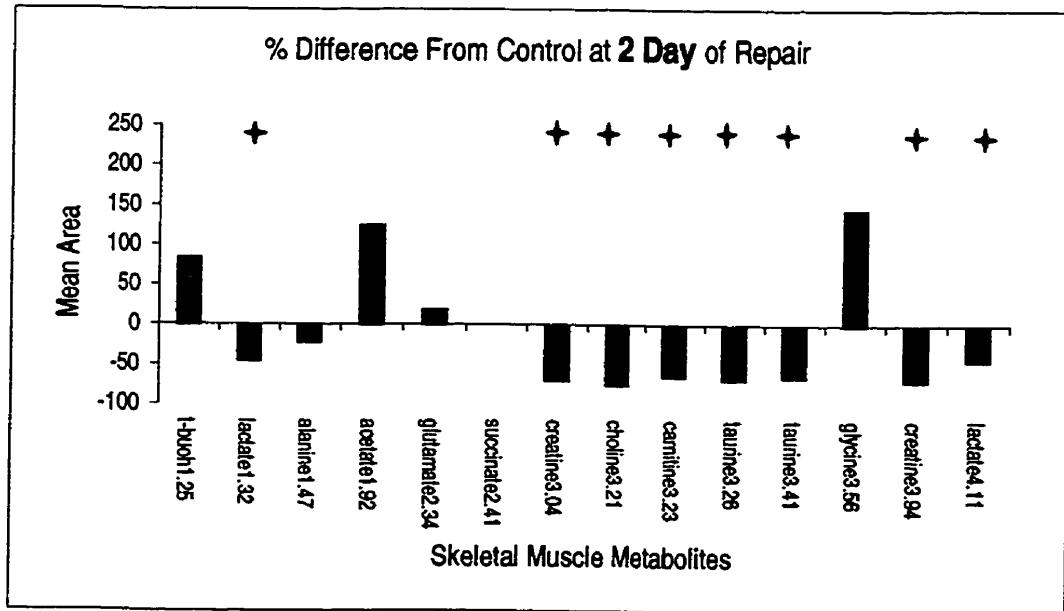
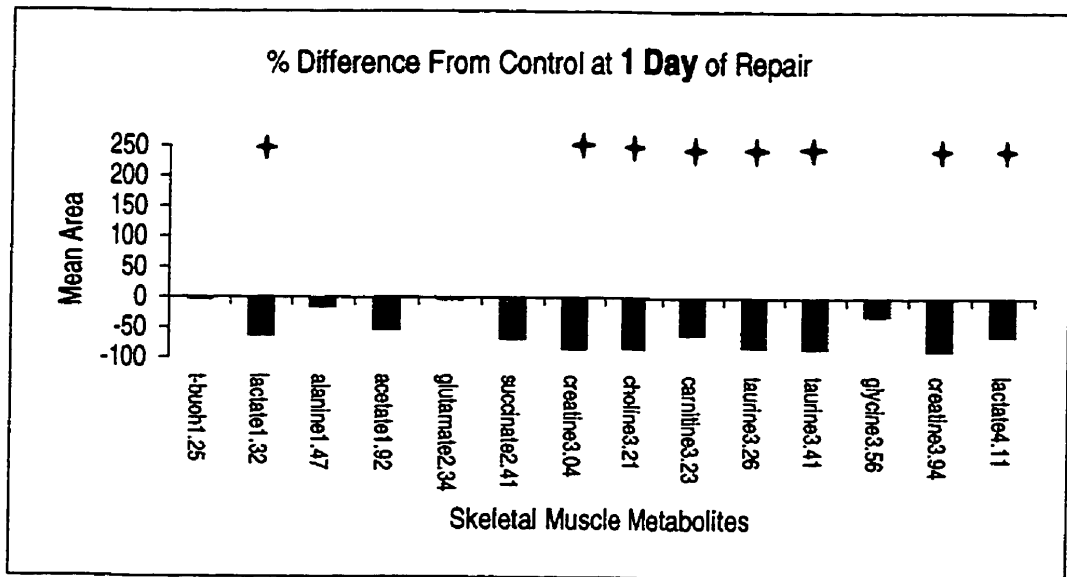
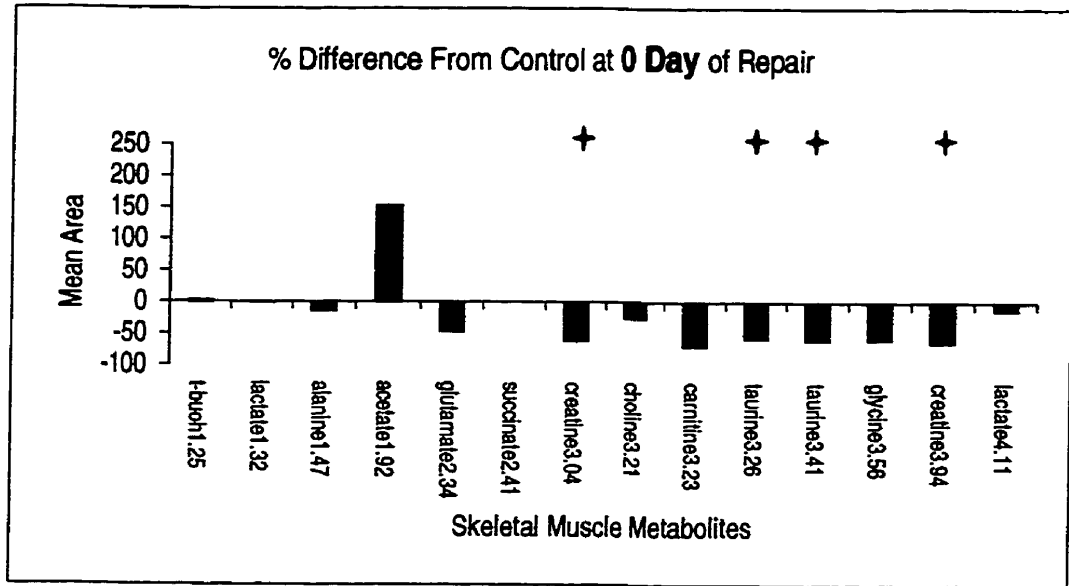
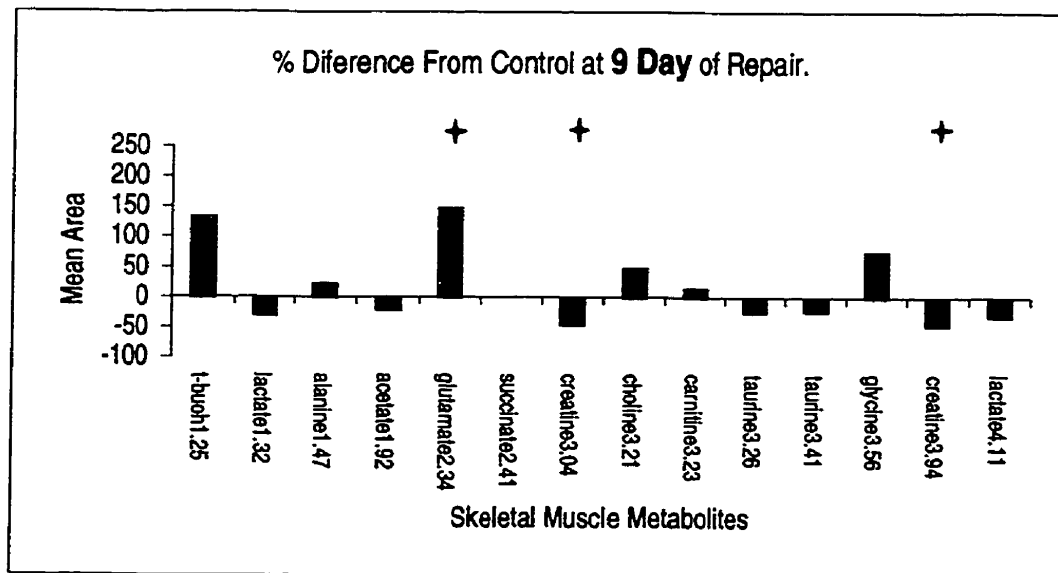
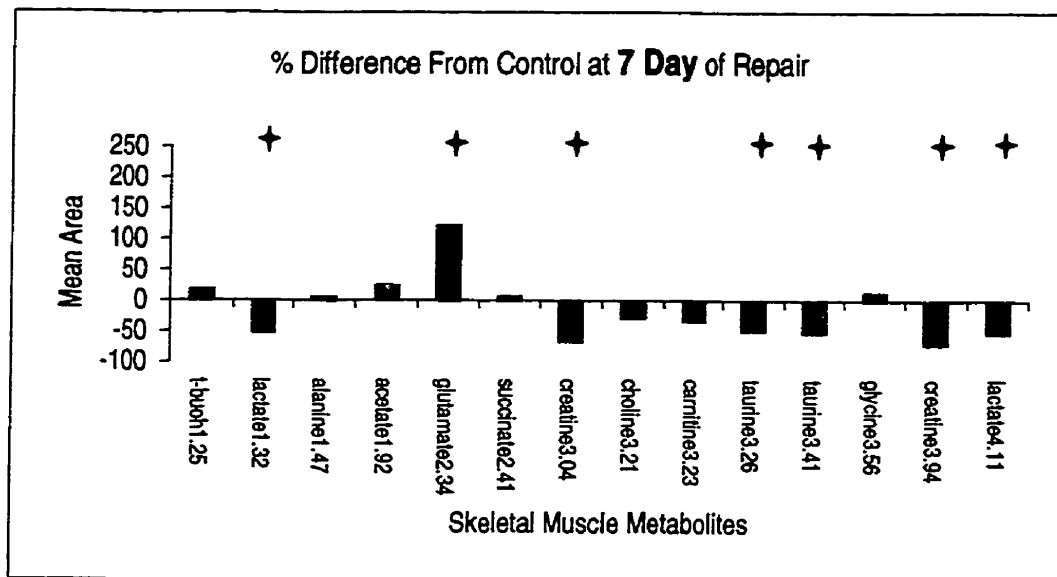
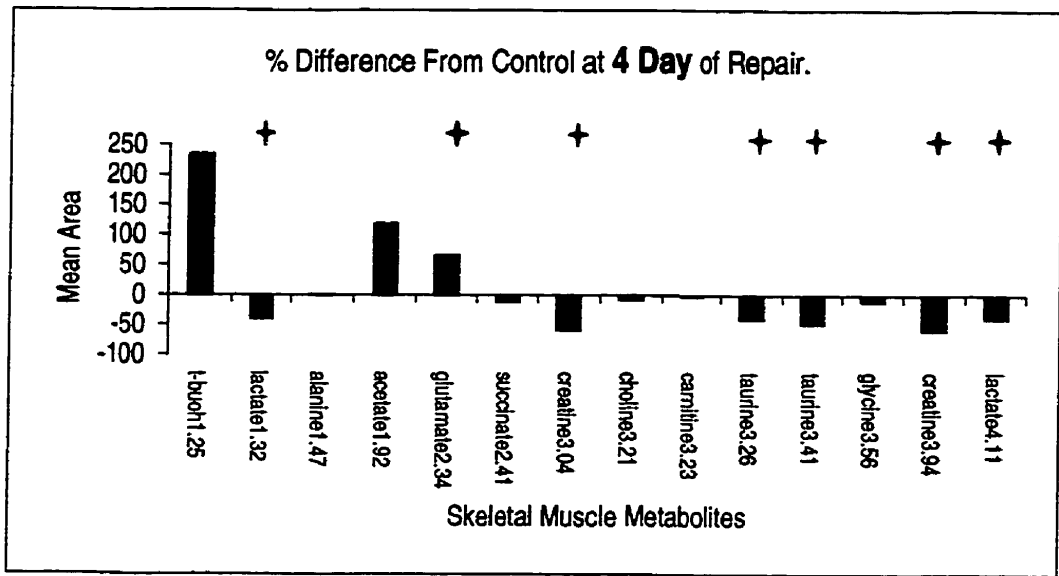
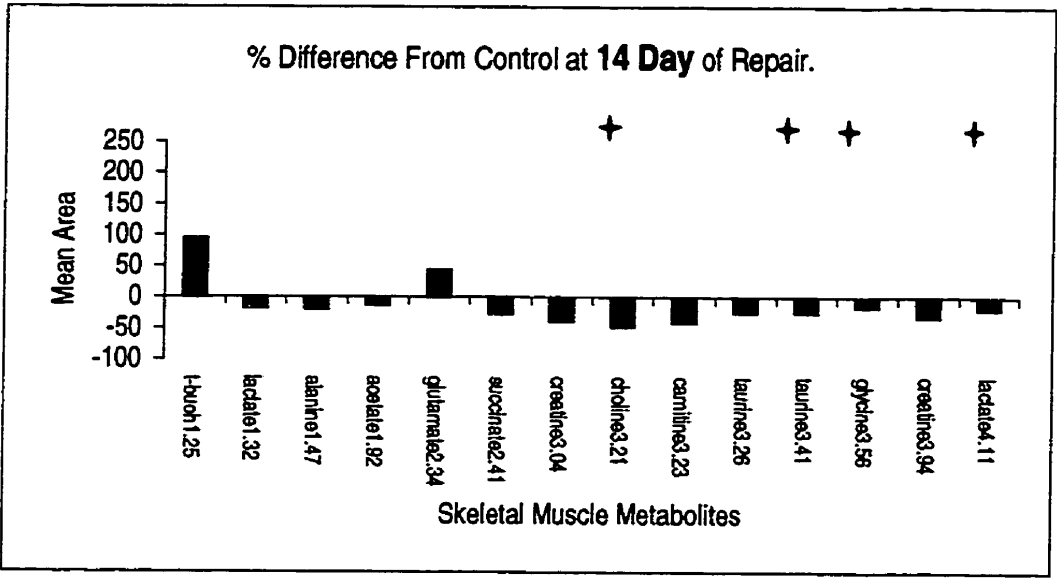


Figure 4.8 (0 day -14 day) Crush-injured skeletal muscle sample data expressed as the percent difference from control muscle samples over the time course of repair (0 day to 14 day) for each metabolite studied. This figure illustrates metabolites changes for each recovery day. Statistically significant differences are indicated by an asterisk.







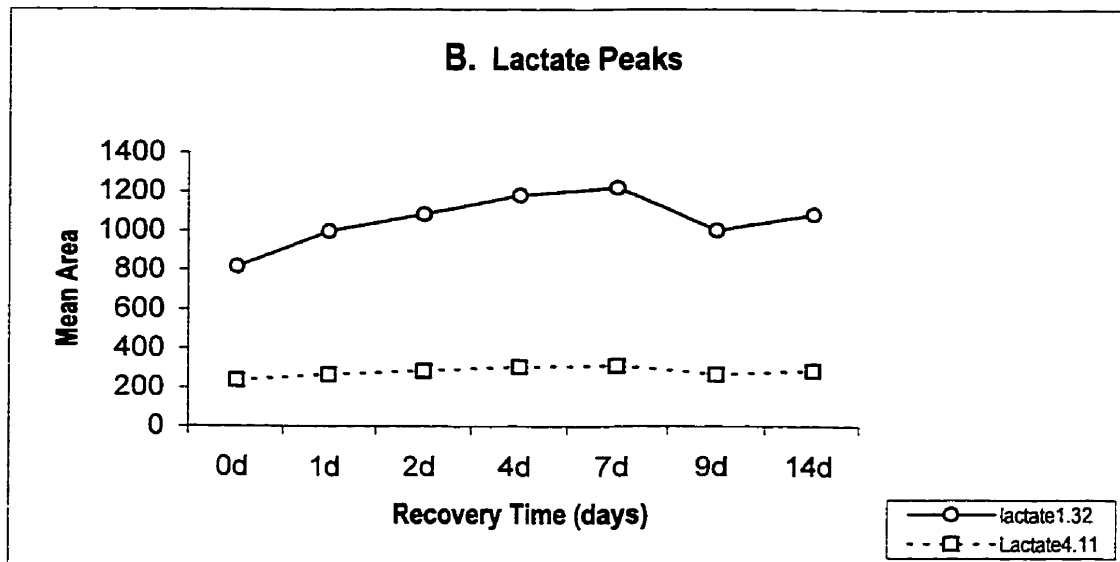
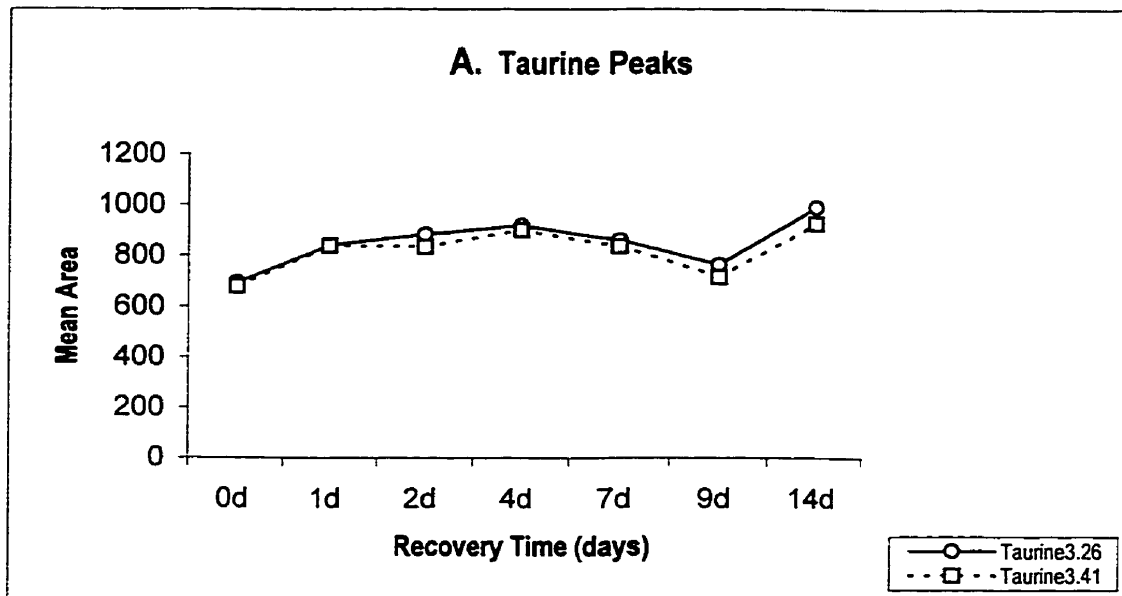


Figure 4.9 This figure illustrates the changes observed between integrated mean peak areas for the skeletal muscle metabolites taurine and lactate over the time course of repair (0-14 days). Taurine3.26 and taurine3.41 are overlaid to demonstrate moiety ratios (A). Lactate1.32 and lactate4.11 are grouped for the same purpose (B).

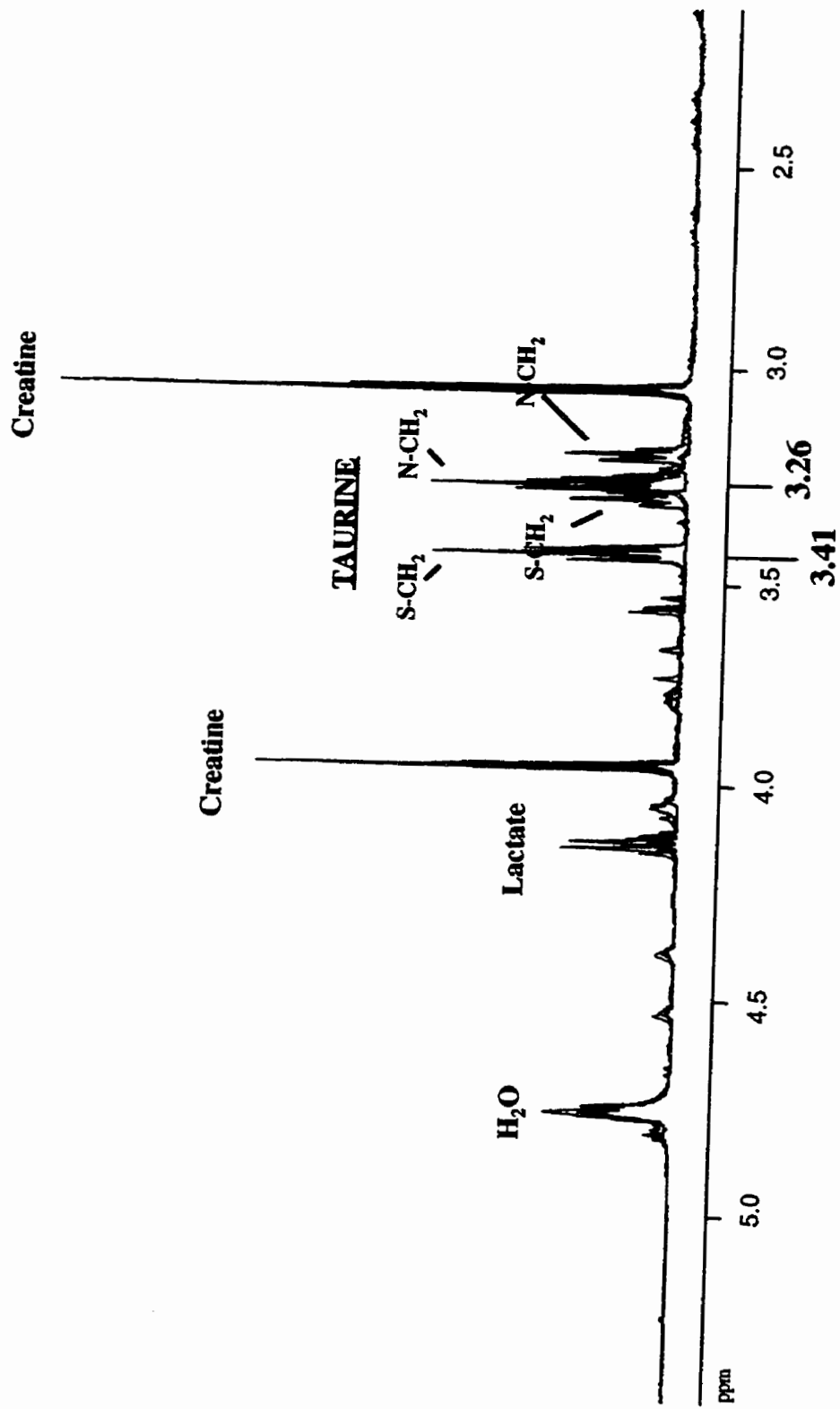


Figure 4.10 One-dimensional ¹H-NMR spectra from crush-injured skeletal muscle extracts demonstrating the variable chemical shift of taurine. Spectrum 1 (orange) and spectrum 2 (green) overlie each other at 3.26 and 3.41 ppm whereas spectrum 3 (Blue) has shifted to the right covering both the carnitine and choline peaks at 3.23 and 3.21 ppm, respectively. Taurine's pH sensitive shift made it difficult to integrate the carnitine and choline resonances and impossible to average the taurine peaks.

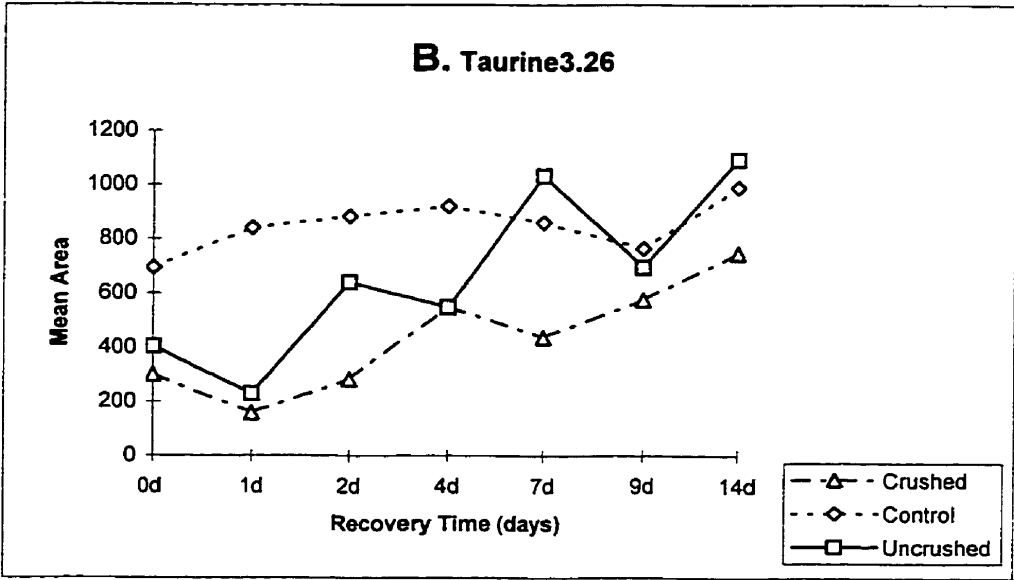
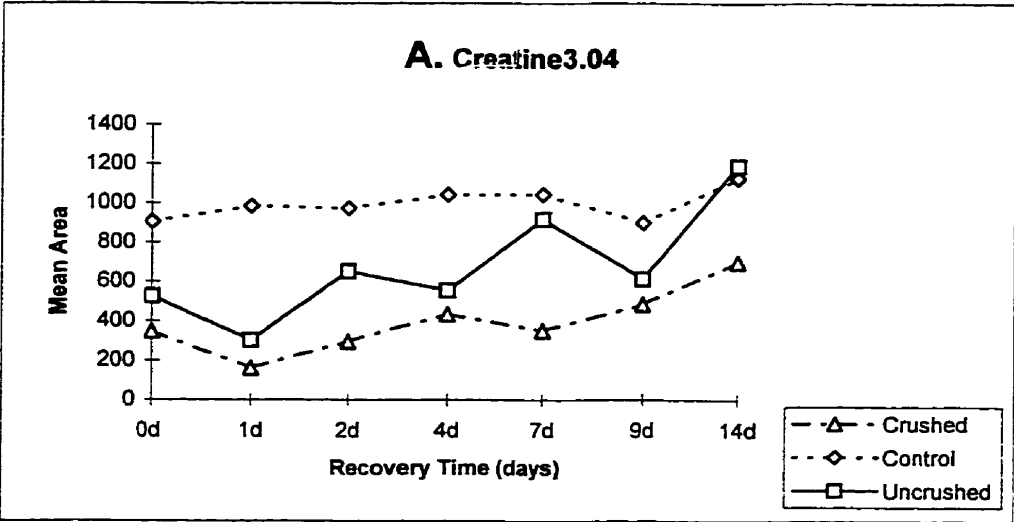


Figure 4.11 Uncrushed muscle sample data reflect both control muscle and regenerating muscle phenotypes. This figure compares uncrushed muscle with crushed and control muscle samples over the time course of repair. The changes with repair for creatine and taurine are used to make this comparison.

CHAPTER 5 - DISCUSSION

The dynamic data gathered with $^1\text{H-NMRS}$ from skeletal muscle is not easily understood, and a superimposed pathological condition such as a crush injury further complicates analysis and interpretation. However the applied crush injury used in this study is a much less extreme method to study synchronous repair in skeletal muscle than the graft procedure described by Carlson (1970). It has a further advantage in that it permits the study of all sequential cellular events of regeneration (McComas, 1996). A crush injury to a particular muscle alters energy, lipid and protein metabolism as well as eliciting an immune response coincident with the process of skeletal muscle repair. These changes can all be detected with $^1\text{H-NMRS}$.

Studying the time course of skeletal muscle regeneration in the TA muscle from C57 mice using $^1\text{H-NMRS}$ further demonstrates the ability of this tool to trace metabolic activity in biological tissues. Using perchloric acid to extract all water-soluble metabolites from selected muscle samples, this study detected a reproducible time-course of changes during skeletal muscle regeneration and demonstrated time intervals when regenerating muscle can be discriminated optimally from damaged muscle or control muscle.

By tracking NMR-visible metabolites during the regenerative process, we have delineated stages of skeletal muscle repair with progressive and phasic metabolite changes. As well, the ability to simultaneously detect many different compounds of biological interest with $^1\text{H-NMRS}$ revealed a peak of previous unknown origin relevant in

the skeletal muscle repair process.

5.1 A COMPOUND SIMILAR TO TERTIARY BUTYL ALCOHOL

Following consideration of the averaged spectra from recovery day 2 and recovery day 4 muscle extracts, the 1D-TOCSY experiment, pure compounds and muscle samples spiked with mevalonic acid (MA) or 3-hydroxy-3-methylglutaryl coenzyme A (HMG-CoA), it seems likely that the unknown resonance at 1.25ppm is due to a metabolite important to skeletal muscle regeneration.

5.11 Averaged Spectra

Before averaging the 2 day recovery and 4 day recovery spectra it was expected that all metabolite concentrations from crush-injured muscle samples would be less than metabolite concentrations from control muscle samples especially in the early stages of repair (recovery days 0 to 4). This is founded on the idea that a crush injury disrupts the sarcolemma causing intracellular muscle metabolites to leak out of the affected muscle cells (Tatsumi et al., 1998). The initial decrease of metabolite concentrations from crushed muscle extracts was expected to rebuild to control muscle levels over the course of successful repair, e.g. new muscle formation. However, the averaged spectra (figure 4.1) show the peak heights of acetate and the unknown at 1.25 ppm are higher than the control sample peak heights on recovery days 2 and 4, indicating greater quantities of

these metabolites in the early stages of regeneration rather than later.

Since spectral averaging standardized our muscle sample spectra for TSP but not for muscle sample weight, concluding anything from these results would be erroneous. The most that can be taken from the averaged spectra results is that they indicate the resonances at 1.25ppm and 1.92ppm might be important metabolites related to the early stages of skeletal muscle regeneration. The identification of the unknown peak at 1.25ppm was therefore pursued.

5.12 The 1D-TOCSY Experiment

The large water resonance associated with the unknown peak from the 1D-TOCSY experiment (figure 4.2) was thought to signify the presence of a hydroxyl group in the molecular structure of the unknown compound at 1.25ppm. The possible presence of a hydroxyl group in the unknown compound, the chemical shift of the unknown peak and spectrometric identification tables (Silverstein et al., 1974) indicate the muscle sample peak at 1.25ppm may represent the methyl groups of a t-butanol-type compound, e.g. a tricarboxylic acid like mevalonic acid (MA) or HMG-CoA.

The two small peaks at 3.04ppm and 3.42ppm may be due to coupled protons within the t-butanol-type compound or the lactate 1.32 peak covering a smaller metabolite resonance, e.g. threonine (γ -CH₂) at 1.33ppm (Sze and Jardetsky, 1994). In our attempt to isolate the 1D-TOCSY acquisition to the unknown 1.25ppm peak, the pulse sequence also excited the protons of lactate at 1.32ppm which explains the presence of the 1.32ppm

and 4.11 ppm lactate peaks present in the 1D-TOCSY spectrum. As described in section 4.1 of the results, figure 4.9 B shows an increased moiety ratio for the lactate resonances despite their having similar changes over the time course of repair. This might be due to a small unknown metabolite peak hidden by the lactate 1.32 resonance which may be coupled to the small resonances at 3.04 ppm and 3.42 ppm.

5.13 Tertiary Butyl Alcohol, Mevalonic Acid and 3-Hydroxy-3-Methylglutaryl Coenzyme A

The pure sample of tertiary butyl alcohol and the skeletal muscle samples containing standards of (spiked) with MA and HMG-CoA each produced a resonance at 1.25 ppm, but this alone does not confirm the identification of the unknown muscle peak. Theoretically, it is not possible to confirm the identification of an unknown peak in a spectrum without matching chemical shifts and splitting patterns between unknown and pure compounds. However our experiments do narrow the range of possibilities. If in fact the unknown peak is due to a metabolite like MA, the presence of the unknown peak in our muscle sample spectra may be a marker for cholesterol biosynthesis, and therefore of skeletal muscle membrane regeneration (see section 5.5). Based on integral values and the small concentration of the unknown metabolite, the coupled resonances of MA (other than the 1.25 ppm peak) (figure 4.4) would likely not be observed in a skeletal muscle sample spectrum. As well, a larger sample size, e.g. more muscle, may not assist identification of the 1.25 ppm peak especially if its presence is in response to skeletal

muscle regeneration. By collecting just the crush site (sample 1) for this study we may have made the unknown metabolite more evident especially if its presence is restricted to the crush injury region.

5.2 CONTROL SKELETAL MUSCLE SAMPLES

Before formulating conclusions from comparisons between treatment groups it is important to know if our control muscle samples reflect typical skeletal muscle. The control muscle samples should be distinct from damaged and regenerating muscle samples and consistent with standard knowledge of skeletal muscle metabolism.

The general stability of metabolite concentrations observed for control muscle samples over the time course of repair corresponds with the concept of skeletal muscle being a tightly regulated tissue type under ordinary conditions. Muscle metabolites extracted from the control muscle samples were expected to not differ significantly during the recovery of the crush-injured muscles (TA and GAS).

Both lactate^{4.11} and taurine^{3.26} concentrations were significantly greater in control muscle samples on recovery days 7 and 14, respectively (table 4.1). All other muscle metabolites studied were not significantly different within the control group over the time course of repair. This indicates a largely stable homeostatic state for the control TA muscle samples. Therefore, systemic changes due to the crush surgery to the right TA and left GAS did not significantly affect the majority of the NMR-visible metabolites we were studying.

The changes observed for lactate^{1.32} and taurine^{3.26} may have been due to an increased energy demand put on the left hindlimb as it compensated for the loss of function of the injured right TA muscle. The increased concentration of lactate may be due to a high energy demand and insufficient oxygen supply to the compensating TA muscle. The increased concentration of taurine may reflect the function of this metabolite as a sarcolemmal stabilizer (see section 5.4). The lactate and taurine changes observed for control muscle samples suggest that many muscles will act as a source for muscle metabolites, similar to muscle serving as an energy source during systemic conditions, e.g. starvation, diabetes and trauma.

The relative stability of metabolites extracted from the control muscle samples ensured that the internal control was appropriate and could be compared to crush-injured muscle samples with confidence. The following sections discuss changes in crush-injured muscle samples compared to control muscle samples. Muscle metabolites are discussed with respect to sarcolemmal stabilization and cholesterol biosynthesis as they pertain to skeletal muscle regeneration.

5.3 CRUSH-INJURED SKELETAL MUSCLE SAMPLES

Metabolite differences observed within the crush site of the crush-injured skeletal muscle samples include changes that differentiated crush-injured muscle from control muscle and changes in crushed muscle over the time course of repair. The experimental results are discussed relative to the typical events that succeed a skeletal muscle crush

injury which include post-crush inflammation, new membrane formation, muscle precursor cell activation and proliferation, myotube formation and growth leading to complete regeneration of the injured muscle (see chapter 1, section 3 for details).

5.31 Comparison of Damaged Muscle to Control Muscle

The decreased concentration of creatine and taurine on recovery day 0 (table 4.1 and figure 4.8) were expected in part due to the crush injury. The crush injury disrupted the sarcolemma and caused muscle segment necrosis leading to an efflux of cytosolic and structural muscle metabolites from affected myofibers, therefore creatine and taurine concentrations were expected to decrease immediately following the crush injury. After the initial drop on recovery day 0, creatine and taurine concentrations were expected to increase and return to control levels as the damaged muscle repaired (McIntosh et al., 1998a; McIntosh et al., 1998c) and normal function returned to the right TA muscle.

5.32 Comparison of Regenerating Muscle to Control Muscle

In regenerating muscle, the concentrations of progressive metabolites (lactate, creatine and taurine) remained significantly less than control muscle samples until recovery day 9. The increased lactate and taurine concentrations on recovery day 9 may reflect a partial return of muscle function. At this point during the muscle repair process most structural elements that were damaged by crush injury have been repaired. By five

to nine days post-injury myogenesis (myotube formation) is complete, although muscle precursors may still divide and continue fusing to already-formed myotubes for some days further (Grounds and McGeachie, 1989; Bischoff, 1994). However the low creatine concentration in regenerating muscle compared to control muscle over the time course of repair and the decrease in taurine on recovery day 14 indicate that metabolism in the repairing TA muscle had not yet returned to normal. If the time course of our experiment had been extended to 21 recovery days when skeletal muscle repair and maturation is complete (Mastaglia and Walton, 1982; Mitchell et al., 1992; Gillet et al., 1995), the muscle sample spectra and metabolite concentrations would likely have reflected more typical skeletal muscle metabolism, although a signature of healthy regenerated muscle would also be expected (McIntosh et al., 1998d).

By recovery day 4, the concentrations of metabolites like the unknown, choline and carnitine had increased compared to the corresponding control muscle samples. The increasing concentration of the unknown metabolite is suspected to be a marker of sarcolemmal regeneration. If the unknown peak represents MA (mevalonic acid), the increase on the fourth day of recovery may reflect upregulated cholesterol biosynthesis (see section 5.5). This would make sense teleologically since new membranes are required for all dividing cells and for new myotubes forming during muscle repair up to day five.

The decrease in choline concentration on recovery days 1 and 2 may be due to an increase in the rate of formation of phospholipids used for new membrane synthesis. Phospholipid and cholesterol synthesis are concomitant with the formation of new muscle

membranes (Alberts et al., 1994) which may explain the increase of choline and the unknown metabolite concentrations after recovery day 2. The increase in choline and that unknown on recovery day 4 may follow upon the process of membrane sealing within the necrotic zone of the crush-injured TA muscle (Papadimitriou et al., 1990). The decrease in carnitine on recovery days 1 and 2 coincident with the decreased choline concentration is likely not related to phospholipid biosynthesis. The decreased carnitine concentrations were not substantial enough to affect intracellular fatty acid transport and phospholipid synthesis since only 2% of the total metabolic pool of carnitine is required (Carter et al., 1995). These conclusions must be made with caution especially since the samples sizes (*n*) for carnitine and choline were very small (see section 4.3, and appendix B, table B-1, B-2).

The increased glutamate concentration from crushed muscle samples between recovery days 7 and 14 may reflect a return to healthy limb function in that the dispensable (non-essential) amino acid pool was used to reestablish typical concentrations. Increased concentrations of glutamate may facilitate the acceptance by glutamine of ammonium ions produced from protein catabolism in the early stages skeletal muscle regeneration. Glutamate and ammonium ions form glutamine which is a benign vehicle for carrying toxic ammonia to the liver or the kidney for excretion (Voet and Voet, 1990; Hunt and Groff, 1990). Glutamine also functions as a nitrogen donor for the formation of purines and pyrimidines (Hunt and Groff, 1990). Purine and pyrimidine synthesis is expected with the formation of new muscle, however the contribution of glutamate in this capacity is likely required before recovery day 7.

5.4 TAURINE AND STABILITY OF THE SARCOLEMMA

Previous research in our lab has explored the significance of a high intracellular taurine concentration for skeletal muscle. Although taurine has been described in the literature as a multifaceted sulfonic amino acid (Huxtable, 1992) and McIntosh (1998c) provided evidence supporting the role of taurine in maintaining the integrity of skeletal muscle membranes. Using mostly *ex vivo* ¹H-NMRS, McIntosh (1998c) differentiated: 1. normal and mdx hindlimb muscle, 2. three distinct stages of murine muscular dystrophy (predystrophy, active dystrophy and stable dystrophy), 3. specific spectral fingerprints for different muscle types (tibialis anterior vs. diaphragm), 4. glucocorticoid treatment effects in mdx mice and 5. distinct stages of regeneration in crush-injured mdx muscle (uncrushed vs. 4 day recovery). Many of the differences observed by McIntosh (1998c) were related to changes in taurine with time and muscle type. Our study concentrated on the characterization of synchronous repair over a longer recovery time period while paying close attention to taurine as a membrane stabilizer, and used only perchloric acid extracts over a very detailed time course of study.

If taurine is a sarcolemmal stabilizer, it is expected that taurine concentrations will rise and fall with muscle health. The taurine concentration in healthy muscle (as in our control muscle samples) should remain high and constant whereas damaged muscle (as in our crush-injured right TA muscle) should exhibit a fall in taurine concentration before returning to healthy concentrations when muscle repair is complete.

The increased taurine^{3.26} concentration in our recovery day 14 control muscle

samples (see table 4.1 and figure 4.7E) may have been a prophylactic response to the crush injured right TA muscle. The rise in taurine may be a response to the increased use of the left leg (and the left TA) as a result of loss of function to the right TA.

Alternatively a systemic inflammatory response may have stimulated taurine synthesis in muscles adjacent and contralateral to the crush-injured muscle. Increased taurine concentrations by both scenarios may provide protection to vulnerable membranes due to a heightened level of physical stress, thereby requiring a greater degree of sarcolemmal stability. Measuring taurine concentrations in ipsilateral and contralateral extensor digitorum longus muscles after the crush injury may have helped determine if the taurine changes were indicative of systemic changes. The increased taurine levels from zero to 14 days observed for the control muscle samples appear to be in agreement with the role of taurine as a sarcolemmal stabilizer.

The taurine concentration showed progressive increases over the time course of repair such that it was significantly greater in recovery day 14 crushed muscle samples compared to recovery day 0 muscle samples. This indicates that taurine concentration in crush-injured muscle increased with repair; healthier muscle showed greater concentrations of taurine. As I have stated previously, as a sarcolemmal stabilizer taurine concentration would be expected to increase as damaged skeletal muscle repaired (Huxtable, 1992; McIntosh et al., 1998c). The increased taurine concentration in our crushed muscle samples on recovery day 14 support the notion that taurine increases with repair and stabilizes newly formed muscle membranes.

5.5 CHOLESTEROL BIOSYNTHESIS AND NEW MEMBRANE FORMATION

One important difference between this study and previous studies in our lab concerns the unknown metabolite with a peak at 1.25 ppm that previously went unnoticed. Averaging spectra and researching pure metabolites and potential impurities revealed the importance of this peak as a new finding and ruled out the possibility of muscle sample contamination.

Cederbaum et al. (1983) describe t-butanol as a scavenger of the highly reactive hydroxy radical reduced from hydrogen peroxide. In this role, the unknown peak may be a cleavage product that is advantageous in skeletal muscle regeneration by controlling inflammation-induced damage brought about by the phagocytic action of neutrophils during removal of necrotic debris from the crush site (Ricevuti, 1997). Less autolysis at a site of injury could speed the repair process and lead to an earlier return of normal muscle function.

In addition, the reduction of HMG-CoA to MA by HMG-CoA reductase represents the rate-limiting step in cholesterol biosynthesis (Goldstein and Brown, 1990). The unknown metabolite may represent MA and as such be a molecular marker for the process of membrane sealing in damaged myofibers. The generation of new membrane and its constituents requires cholesterol and would be at the maximum rate at recovery day 4 (Papadimitriou et al., 1990).

Furthermore, the farnesylpyrophosphate and geranylgeranylpyrophosphate metabolites of MA are required for cell cycling activity (Brown and Goldstein, 1980;

Siperstein, 1984; Vogt et al., 1996). Inhibition of HMG-CoA reductase has been shown to reduce cell proliferation of cultured myoblasts (van Vliet et al., 1996). This indicates that the unknown metabolite may also be a marker for muscle precursor cell activation although its peak activity would be expected earlier than recovery day 4.

We believe the unknown metabolite with a ¹H-NMRS peak at 1.25ppm is relevant to the processes of inflammation and membrane formation although its change on recovery day 4 does not exactly coincide with the time course of muscle fiber sealing described in chapter 1, section 3.1 (Papadimitriou et al., 1990). The unknown metabolite data combined with observations for choline on recovery days 1 and 2 suggests that membrane regeneration in our experiment did not commence until 24-48 hours after the crush injury. However, new membrane formation is also required after membrane sealing is finished. Following the process of membrane sealing and phagocytosis of necrotic debris, muscle precursor cells (and other cells) proliferate and will begin to repair the necrotic zone caused by the crush injury (Grounds, 1991). Muscle precursor cell (mpc) proliferation requires the formation of new muscle membranes and therefore, subsequently new cholesterol synthesis. Both mpc proliferation and sarcolemmal repair may therefore require (in synchrony) large amounts of MA and its derivatives and that process may be marked by ¹H-NMRS and the unknown metabolite with a peak at 1.25ppm.

5.6 ACETATE AND EXPERIMENTAL PRECISION

Close inspection of our data reveals integral mean values with large standard deviations (appendix B, table B-1,2,3). Low muscle sample weight and natural variability between mice may account for the low degree of precision within our data. However, the feature of our data that likely had the greatest affect on precision was the experimental design. The time course of repair was planned as “recovery days” when “recovery hours” would have been better, especially in the early stages of regeneration when many metabolic changes can be observed within a span of 30 minutes. Significant metabolite changes may have been hidden because of the design of our experiment.

Those metabolites most affected were the unknown metabolite and acetate since they had standard deviations that usually exceeded their respective mean concentration (appendix B, table B-1). Figure 4.8 shows an immediate increase for acetate on recovery day 0 while all other metabolite concentrations dropped below or remained unchanged from control levels. The apparent rise in acetate concentration on recovery day 0 may indicate a metabolic process present in crush-injured muscle extracts that acts to increase the acetate concentration while the other metabolite concentrations decrease. However, the change in acetate concentration on recovery day 0 was not statistically significant. If it were a significant increase (after a repeat experiment) two separate or combined mechanisms may explain the observation.

The first, discussed earlier, involves sarcolemmal disruption and leakage of metabolites out of cells (Tatsumi et al., 1998). The second mechanism may involve post-crush injury and a stress-induced cortisol release from adrenocortical cells in response to the crush injury. The increased glucocorticoid release may account for a potential

increase in acetate concentration on recovery day 0 due to enhanced fatty acid catabolism.

The explanation follows.

Cortisol, the principle glucocorticoid, is secreted from the adrenal cortex in response to most types of trauma, infection, intense heat or cold, forceful restraint and surgery (Guyton and Hall, 1996). This particular glucocorticoid is a powerful anti-inflammatory agent (Collins, 1999) and exhibits profound effects on protein and lipid metabolism. It decreases the quantity of protein in most tissues, thereby making amino acids available in body fluids for gluconeogenesis, and catabolizes fatty acids to acetate for the same purpose (Guyton and Hall, 1996). This may explain the high acetate levels observed in our crush-injured muscle samples on recovery day 0.

A breached sarcolemma and necrosis contribute, in part, to the decline of lactate, creatine and taurine, however the most significant cause for this decline is most likely the post-crush release of cortisol. Since Vinnars et al. (1975) first described low glutamine levels in skeletal muscle after trauma, many investigators have demonstrated the relationship between elevated plasma concentrations of stress hormones (cortisol and adrenaline) and muscle protein catabolism. Studies of the concentration and configuration of ribosomes in skeletal muscle by Wernerman et al. (1989) demonstrated that muscle protein synthesis declined after trauma. Finley et al. (1986) showed increased muscle proteolysis and rapid loss of muscle mass in trauma patients. Therefore the general decline of muscle metabolites on recovery day 0 until recovery day 1 may reflect skeletal muscle proteolysis, inhibited protein synthesis and leakage of existing intracellular muscle metabolites into the extracellular compartment due to sarcolemmal

degeneration.

5.7 UNCRUSHED SKELETAL MUSCLE SAMPLES

Interpretation of the uncrushed muscle sample (sample 2) data is very difficult. This is due to the fact that the formation of new muscle is known to occur in regions outside the crush zone (McIntosh et al., 1994; McIntosh and Anderson, 1995). The data acquired from this region (sample 2) illustrates overlap between crushed and control muscle samples. Discriminating between new and old muscle would be very difficult if not impossible given only the $^1\text{H-NMR}$ spectra and integrated mean areas. For most metabolites studied extracts of uncrushed muscle (sample 2), the changes over the time course of repair appeared to lie between control and the changes in crushed muscle. This pattern supports the notion that the data for uncrushed muscle samples reflect the contents that includes both control muscle and regenerating muscle phenotypes (figure 4.11).

The second important feature of the uncrushed muscle data is that it was acquired from relatively small muscle samples, frequently less than the crushed muscle samples. The crushed muscle sample remained consistent during sample recovery; the crush site recovered was always three times the size of the actual crush injury (see figure 3.3). Therefore in smaller animals (with smaller muscles) the uncrushed region was frequently minimal.

5.8 CONCLUSIONS

The time course of skeletal muscle degeneration and regeneration in C57 mice follows a well-characterized time sequence (see chapter 1, section 3). Following muscle injury, membrane sealing of the necrotic zone is complete by 24 hours (Papadimitriou et al., 1990) and it is closely followed by muscle precursor cell replication which commences between 24 and 30 hours (Bischoff, 1986; Grounds and McGeachie, 1989). By five days post-injury myogenesis is achieved (Grounds, 1991) and by 14 to 21 days post-injury skeletal muscle regeneration is complete (Mastaglia et al., 1982; Mitchell et al., 1992; Gillet et al., 1995). Our data parallels this known time course of repair.

The muscle sample extracts prepared for ¹H-NMRS produced detailed metabolic information related to the process of skeletal muscle regeneration. ¹H-NMRS clearly discriminated injured muscle from healthy muscle with respect to progressive and phasic metabolite changes over a specific time course of repair. Low concentrations of lactate, taurine and creatine from injured muscles on recovery day 0 progressively increased to control muscle levels over the time course of repair. Phasic metabolites like acetate, choline, carnitine, the unknown (1.25ppm) and glutamate changed at specific time intervals during the repair process. In general, progressive metabolites discriminated injured muscle from healthy muscle, while phasic metabolites delineated the recovery period into four regeneration stages: 0 day (acetate): inflammation; 1-2 day (choline and carnitine): membrane synthesis; 4 day (the unknown metabolite): membrane synthesis and completion of inflammation; and 4-9 day (glutamate): onset of restored

muscle function.

Therefore we can accept our hypothesis since $^1\text{H-NMRS}$ of perchloric acid extracts during skeletal muscle repair in C57 mice detected a reproducible time-course of changes during regeneration of taurine, creatines and carnitine resonances (among others), and determined a time interval when regenerating muscle was optimally discriminated from damaged muscle and control muscle.

5.9 SIGNIFICANCE

This study advances the ultimate goal of designing a non-invasive clinical test protocol of muscle repair status using $^1\text{H-NMRS}$ resolution of skeletal muscle and specific marker metabolites indicative of repairing muscle.

FUTURE RESEARCH

The next step in characterizing skeletal muscle regeneration will involve coupling our C57 data with data acquired in the same manner from the mdx mouse. Regeneration data from the mdx mouse will help further our understanding of the precise events of repair during dystrophy. It will be interesting to observe the sequelae that follow crush injury in mdx mice and what happens with metabolites like taurine, the unknown (1.25ppm), acetate and glutamate. The dystrophic animal model may provide further insight into the function of these metabolites during skeletal muscle regeneration and help us confirm an appropriate marker metabolite or an mdx group of metabolites that can track regeneration *in vivo*.

Taurine is suspected of maintaining membrane stabilization but the precise mechanism by which this occurs is not currently understood. Following control and crush-injured mdx mice with ¹H-NMRS *in vitro* may reveal that taurine concentrations are higher in mdx mice compared to C57 mice prior to an imposed crush injury and return to pre-crush levels quicker. High taurine levels in mdx mice throughout a time course of repair may reflect the function of taurine in membrane stabilization. However if taurine leaks from dystrophic myofibers quicker than it is synthesized then taurine may be less in uncrushed mdx muscle very early after injury. Low taurine concentrations may exacerbate the dystrophin-deficient, weakened sarcolemma of the muscles in the mdx mouse. Once taurine levels have been determined for different muscle types and species it may serve as a metabolic marker of sarcolemmal health.

The exact function of taurine in wild-type skeletal muscle needs to be determined. What is the difference between membrane-bound and cytosolic taurine? Does taurine associate with dystrophin-associated proteins in the sarcolemma? How does it stabilize the junction between the intracellular cytoskeleton and extracellular matrix? Is it possible that taurine associates with the dystroglycan complex of the sarcolemma thereby facilitating interaction with laminin in the basement membrane?

Metabolites that characterized regeneration in C57 mice should be studied in the mdx mouse. Specifically acetate, choline, carnitine, the unknown, glutamate and the progressive metabolites which appeared to change in sequence over the time course of repair require further investigation. The changes observed in our C57 data may appear sooner in the repair sequence of the mdx mouse since mpc proliferation and then fusion occur about one day sooner in the mdx mouse (McIntosh and Anderson, 1995).

Furthermore it is important to understand why mdx muscle recovers from myofiber necrosis while DMD muscle does not. Perhaps the primary difference is related to inflammatory mechanisms which restrict proper mpc proliferation and fusion. Is it possible that the unknown metabolite is simply an inflammatory by-product for “mopping” up hydroxyl radicals? If so, this peak may be higher in DMD muscle indicative of heightened inflammation or it might be altogether absent in DMD muscle indicative of aberrant inflammatory mechanisms.

REFERENCES:

Abbas AK, Lichtman AH, Pober JS.: Cellular and Molecular Immunology. 2nd edition, *W. B. Saunders Co.*, Philadelphia, Pennsylvania, **1994**.

Alberts B, Bray D, Lewis J, Raff M, Roberts K, Watson JD.: Molecular Biology of the Cell. Third Edition, *Garland Publishing Co.*, New York, New York, **1994**.

Allbrook D.: Skeletal Muscle Regeneration. *Muscle Nerve* 4:234-245, **1981**.

Anderson JE, Ovalle WK, Bressler BH.: Electron Microscopic and Autoradiographic Characterization of Hindlimb Muscle Regeneration in the Mdx Mouse. *Anatom Rec* 219:243-257, **1987**.

Anderson JE, Mitchell CM, McGeachie JK, Grounds MD.: The Time Course of Basic Fibroblast Growth Factor Expression in Crush-Injured Skeletal Muscles of SJL/J and BALB/c Mice. *Exp Cell Res* 216:325-334, **1995**.

Andrew ER.: Introduction to Nuclear Magnetic Resonance. In: NMR in Physiology and Biomedicine. Ed.: Gillies RJ., *Academic Press Inc.*, San Diego, **1994**.

Arus C, Barany M, Westler WM, Markley JL.: 1H-NMR of Intact Muscle at 11T. *Febs Letts* 165(2):231-237, **1984**.

Bähler, Walliman T., Eppenberger HM.: Myofibrillar M-Band Proteins Represent Constituents of Native Thick Filaments, Frayed Filaments, and Bare Zone Assemblages. *J Muscle Res Cell Motil* 6:783-800, **1985**.

Banks WJ.: Applied Veterinary Histology. Third Edition, *Mosby-Year Book Inc.*, St. Louis, Missouri, **1993**.

Bárány M, Venkatasubramanian PN, Mok E, Siegel IM, Abraham E, Wycliffe ND, Mafee NF.: Quantitative and Qualitative Fat Analysis in Human Leg Muscle of Neuromuscular Diseases by 1H Magnetic Resonance Spectroscopy *in vivo*. *Magn Reson Med* 10:210-226, **1989**.

Bell JD, Preece NE, Parkes HG.: NMR Studies of Body Fluids and Tissue Extracts. In: NMR in Physiology and Biomedicine. Ed.: Gillies RJ., *Academic Press Inc.*, San Diego, **1994**.

Bischoff R.: Proliferation of Muscle Satellite Cells on Intact Myofibers in Culture. *Dev Biol* 115:129-139, **1986**.

Bischoff R.: The Satellite Cell and Muscle Regeneration. In: Myology. Engel, Andrew G, Franzini, Armstrong C (editors), 2nd edition, *McGraw-Hill*, New York, New York, 1994.

Blackburn BJ, Modha A, Novak M.: Phosphate Metabolites of *Tenebrio molitor* (Coleoptera: Tenebrionidae) Infected with Metacestodes of *Hymenolepis diminuta*. *J Med Entomol* 32(3):223-128, 1995.

Bloom W, Fawcett DW.: A Textbook of Histology. 10th edition, *W. B. Saunders Co.*, Philadelphia, Pennsylvania, 1975.

Bock JL.: Metabolite Profiling of Amniotic Fluid by Proton Nuclear Magnetic Resonance Spectroscopy: Correlation with Fetal Maturation and Other clinical Variables. *Clin Chem* 40(1):56-61, 1994.

Bongers H, Schick F, Skalej M, Jung WI, Stevens A.: Localized in vivo ¹H Spectroscopy of Human Skeletal Muscle: Normal and Pathological Findings. *Magn Reson Imaging* 10:957-964, 1992.

Bovey FA.: Nuclear Magnetic Resonance Spectroscopy. *Academic Press Inc.*, San Diego, California, 1988.

Breckler J, Lazarides E.: Isolation of a New High Molecular Weight Protein Associated with Desmin and Vimentin Filaments From Avian Embryonic Skeletal Muscle. *J Cell Biol* 92:795-806, 1982.

Brown MS, Goldstein JL.: Multivalent Feedback Regulation of HMG-CoA Reductase, a Control Mechanism Coordinating Isoprenoid Synthesis and Cell Growth. *J Lipid Res* 21:505-517, 1980.

Brown SC, Lucy JA.: Dystrophin as a Mechanical Transducer in Skeletal Muscle. *Bioessays* 15(6):413-419, 1993.

Bulfield G, Siller WG, Wight PA, Moore KJ.: X-Chromosome-Linked Muscular Dystrophy (mdx) in the Mouse. *Proc Natl Acad Sci USA* 81:1189-92, 1984.

Campbell KP.: Three Muscular Dystrophies: Loss of Cytoskeleton - Extracellular Matrix Linkage. *Cell* 80:675-679, 1995.

Campos A, Nunez R, Koenig CS, Carey DJ, Brandon E.: A Lipid-Anchored Heparin Sulfate Proteoglycan is Present in the Surface of Differentiated Skeletal Muscle Cells: Isolation and Characterization. *Eur J Biochem* 216(2):587-595, 1993.

Caplan A, Buckwalter JA, Carlson B, Caterson B, Fischman D.: Skeletal Muscle. In:

Injury and Repair of the Musculoskeletal Soft Tissues. Woo SL-Y, Buckwalter JA (editors), *American Academy of Orthopaedic Surgeons*, Park Ridge, Illinois, 1988.

Carlson BM.: Regeneration of the Rat Gastrocnemius Muscle From Sibling and Non-Sibling Muscles Fragments. *Amer J Anat* 128:21-31, 1970.

Carlsson E, Grove BK, Walliman T, Eppenberger HM, Thornell L-E.: Myofibrillar M-Band Protein in Rat Skeletal Muscles During Development. *Histochemistry* 95:27-35, 1990.

Carter AL, Abney TO, Lapp DF.: Biosynthesis and Metabolism of Carnitine. *J Child Neurol* Nov., 10(suppl. 2):253-257, 1995.

Cederbaum AI, Qureshi A, Cohen G.: Production of Formaldehyde and Acetone by Hydroxyl-Radical Generating Systems During the Metabolism of Tertiary-Butyl Alcohol. *Biochem Pharmacol* 32:3517-3524, 1983.

Chang C, Chen GC, Jang T.: A Critical Assessment of Brain Metabolites: Analysis of Perchloric Acid Extracts Using Proton Magnetic Resonance. *Neurosci Letts* 196:134-136, 1995.

Charles HC.: The Whole Body NMR Spectroscopy Examination: Clinical Applications and Techniques. Ed.: Young IR., Charles HC., *Martin Dunitz Ltd.*, London, England, 1996.

Collins T.: Acute and Chronic Inflammation. In: Robbins Pathologic Basis of Disease. Cotran RS, Kumar V, Collins T (editors), 6th edition, *W.B. Saunders Co.*, Philadelphia, Pennsylvania, 1999.

Craig SW, Pardo JV.: Gamma Actin, Spectrin and Intermediate Filament Proteins Colocalize with Vinculin at Costameres, Myofibril to Sarcolemma Attachment Sites. *Cell Motil* 3:449, 1983.

Cullen MJ, Watkins SC.: Ultrastructure of Muscular Dystrophy: New Aspects. *Micron* 24:287-307, 1993.

Danowski BA., Imanaka-Yoshida K., Sanger JM., Sanger JW.: Costameres are Sites of Force Transmission to the Substratum in Adult Rat Cardiomyocytes. *J Cell Biol* 118:1411, 1992.

Derome AE.: Modern NMR Techniques for Chemistry Research. *Pergamon Press Ltd.*, New York, New York, 1987 (pp. 1-96).

Desmoulin F, Confort-Gouny S, Masson S, Bernard M, Doddrell DM, Cozzone PJ.: Application of Reverse-DEPT Polarization Transfer Pulse Sequence to Study the Metabolism of Carbon-13-Labelled Substrates in Perfused Organs by ¹H-NMR Spectroscopy. *Magn Reson Med* 15(3):456-461, 1990.

Durbeej M, Henry MD, Ferletta M, Campbell KP, Ekblom P.: Distribution of Dystroglycan in Normal Adult Mouse Tissues. *J Histo Cyto* 46(4):449-457, 1998.

dos Remedios, CG, Boey W, Yeoh T, Morgan G, Nicholson G, Maruyama K.: Duchenne Muscular Dystrophy: A Protein Chemist's Perspective of its Diagnosis, the Protein Defect and Associated Change. In: Pathogenesis and Therapy of Duchenne Muscular Dystrophy. Kakulas BA. and Mastaglia FL. (editors), *Raven Press Ltd.*, New York, New York, 1990.

Edwards PÅ.: Regulation of Sterol Biosynthesis and Isoprenylation of Proteins. In: Biochemistry of Lipids, Lipoproteins and Membranes. Vance DE, Vance J (editors), *Elsevier Science Publishers*, New York, New York, 1991.

Emery AEH.: Duchenne Muscular Dystrophy, *Oxford Press*, New York, New York, 1987.

Ervasti JM, Ohlendieck K, Kahl SD, Gover MG, Campbell KP.: Deficiency of a Glycoprotein Component of the Dystrophin Complex in Dystrophic Muscle. *Nature* 345:315-319, 1990.

Engel AG, Biesecker G.: Complement Activation in Muscle Fiber Necrosis: Demonstration of the Membrane Attack Complex of Complement in Necrotic Fibers. *Ann Neurol* 12:289-296, 1982.

Fan TW-M, Higashi RM, Lane AN, Jardetzky O.: Combined Use of ¹H-NMR and GC-MS for Metabolite Monitoring and in vivo ¹H-NMR Assignments. *Biochim Biophys Acta* 882:154-167, 1986.

Fantome JC, Ward PA.: Inflammation. In: Pathology. Rubin E, Farber JL (editors), 2nd edition, *J.B. Lippincott Co.*, Philadelphia, Pennsylvania, 1994.

Faust JR, Trzaskos JM, Gaylor JL.: Cholesterol Biosynthesis. In: Biology of Cholesterol. Yeagle PL (editor). *CRC Press Inc.*, Boca Raton, Florida, 1988.

Felig P.: Progress in Endocrinology and Metabolism: the Glucose-Alanine Cycle. *Metabolism* 22:179-207, 1973.

Finley RJ, Inculet RI, Pace R, Holliday R, Rose C, Duff JH, Groves AC, Woolf LI.:

Major Operative Trauma Increases Peripheral Amino Acid Release During the Steady-State Infusion of Total Parenteral Nutrition. *Surgery* 99(4):491-499, 1986.

Gillet B, Verré-Sébrié C, Lefaucheur JP, Sébille A, Beloeil JC.: Time Course of Muscular Regeneration Assessed by 1H 2D NMR. *Proceedings of SMR* 3:1870, 1995.

Goldstein JL, Brown MS.: Regulation of the Mevalonate Pathway. *Nature (London)* 343:425-430, 1990.

Goldstein MA, Schroeter JP, Michael LH.: Role of the Z Band in the Mechanical Properties of the Heart. *FASEB J* 5:2167-2174, 1991.

Granger BL, Lazarides E.: Desmin and Vimentin Coexist at the Periphery of the Myofibril Z-Disc. *Cell* 18:1053-1063, 1979.

Granger BL., Lazarides E.: Synemin: A New High Molecular Weight Protein Associated with Desmin and Vimentin Filaments in Muscle. *Cell* 22:727-738, 1980.

Grove BK, Kurer V, Lehner C, Doetschman TC, Perriard J-C, Eppenberger HM.: A New 185,000 Dalton Skeletal Muscle Protein Detected by Monoclonal Antibody. *J Cell Biol* 98:518-524, 1984.

Grounds MD.: Towards Understanding Skeletal Muscle Regeneration. *Pathology Research Practice* 187:1-22, 1991.

Grounds MD, McGeachie JK.: A Comparison of Muscle Precursor Replication in Crush-Injured Skeletal Muscle of Swiss and BALBc mice. *Cell Tissue Res* 255:385-391, 1989.

Grounds MD, McGeachie JK.: Skeletal Muscle Regeneration After Crush Injury in Dystrophic mdx Mice: An Autoradiographic Study. *Muscle Nerve* 15:580-586; 1992.

Guyton AC, Hall JE.: Textbook of Medical Physiology. 9th edition, W.B. Saunders Corp., Philadelphia, Pennsylvania, 1996.

Hellerstein MK, Munro HN.: Interaction of Liver, Muscle and Adipose Tissue in the Regulation of Metabolism in Response to Nutritional and Other Factors. In: *The Liver: Biology and Pathobiology*. Arias IM, Boyer IL, Fausto N, Jakoby WB, Schachter DA, Shafritz DA, editors. 3rd edition, *Raven Press Ltd.*, New York, New York, 1994.

Hoffman EP, Brown RH, Kunkel LM.: Dystrophin: The Protein Product of the Duchenne Muscular Dystrophy Locus. *Cell* 51:919-28; Dec. 1987.

Hore PJ.: Nuclear Magnetic Resonance. *Oxford University Press Inc.*, New York, New York, 1995.

Hoult DI.: The Magnetic Resonance Myth of Radio Waves. *Concepts Magn Reson*, 1:1-5 1989.

Hunt SM, Groff JL.: Advanced Nutrition and Human Metabolism. *West Publishing Co.*, St. Paul, Minnesota, 1990.

Huxtable RJ.: Physiological Actions of Taurine. *Physiol Rev* 72(1):101-160, 1992.

Huxtable RJ, Bressler R.: Effect of Taurine on a Muscle Intracellular Membrane. *Biochimica Biophysica Acta* 323:573-583, 1973.

Jay JC, Barald KF.: Maintenance of Neurite contacts at Junctional Regions of Cultured Individual Muscle Fibers From Aged Rats is Correlated with the Presence of a Synapse-Associated Protein, Gelasmin. *Mech Ageing Dev* 49(2):171-197, 1989a.

Jay JC, Barald KF.: Denervated Single Myofibers: Neurite Interactions and Synaptic Molecules. *Muscle Nerve* 12(12):981-992, 1989b.

Kessler H, Oschinat H, Griesinger C, Bermel W.: Transformation of Homonuclear Two-Dimensional NMR Techniques into One-Dimensional Techniques Using Gaussian Pulses. *J Magn Reson* 70:106-133, 1986.

Koenig M, Hoffman EP, Bertelson CJ, Monaco AP, Feener C, Kunkel LM.: Complete Cloning of the Duchenne Muscular Dystrophy (DMD) cDNA and Preliminary Genomic Organization of the DMD Gene in Normal and Affected Individuals. *Cell* 50:509-517, 1987.

Konisberg IR, Lipton BH.: The Regenerative Response of Single Mature Muscle Fibers Isolated in vitro. *Dev Biol* 45:260-, 1975.

Kurth L.: Utilization of Intracellular Acylcarnitine Pools by Mononuclear Phagocytes. *Biochim Biophys Acta* 1201(2):321-327, 1994.

Lazarides E, Granger BL, Gard DL, et al.: Desmin- and Vimentin- Containing Filaments and Their Role in the Assembly of the Z-Disk in Muscle Cells. *Cold Spring Harb Symp Quant Biol* 46:351-378, 1981.

Lindahl M, Backman E, Henriksson KG, Gorospe JR, Hoffman EP.: Phospholipase A2 Activity in Dystrophinopathies. *Neuromuscular Disorders* 5(3):193-199, 1995.

Lipton BH, Schultz E.: Developmental Fate of Skeletal Muscle Satellite Cells. *Science* 205:1292-1294, 1979.

Luo JI, Hammarqvist F, Andersson K, Wernerman J.: Skeletal Muscle Glutathione After Surgical Trauma. *Ann Surg* 223(4):420-427, 1996.

Luther P, Squire J.: Three-Dimensional Structure of the Vertebrate Muscle M-Region. *J Mol Biol* 125:313-324, 1978.

Lynch MJ, Masters J, Pryor JP, Lindon JC, Spraul M, Foxall PJD, Nicholson JK.: Ultra High Field NMR Spectroscopic studies on Human Seminal Fluid, Seminal Vesicle, and Prostatic Secretions. *J Pharmaceutical Biomed Analysis* 12(1):5-19, 1994.

Maltin CA, Harris JB, Cullen MJ.: Regeneration of Mammalian Skeletal Muscle Following the Injection of the Snake-Venom Toxin, Taipoxin. *Cell Tissue Res* 232:565-577, 1983.

Martin ML, Delpuech J, Martin GJ.: Practical Nuclear Magnetic Resonance Spectroscopy. *Heyden and Son Ltd.*, London, England, p. 30-35, 1980.

Mastaglia FL, Walton SJ.: Skeletal Muscle Pathology. *Churchill Livingstone*, New York, New York, 1982.

Matthews CK, van Holde KE.: Biochemistry. *Benjamin/Cummings Publishing Co.*, Redwood City, California, 1990.

Matsumara K, Campbell KP.: Dystrophin-Glycoprotein Complex: Its Role in the Molecular Pathogenesis of Muscular Dystrophies. *Muscle Nerve* 17:2-15, 1994.

McComas AJ.: Skeletal Muscle: Form and Function. *Human Kinetics*, Champaign, Illinois, 1996.

McIntosh LM, Pernitsky AP, Anderson JE.: The Effects of Altered Metabolism (Hypothyroidism) on Muscle Repair in the *mdx* Dystrophic Mouse. *Muscle Nerve* 17:444-453, 1994.

McIntosh LM, Anderson JE.: Hypothyroidism Prolongs and Increases *mdx* Muscle Precursor Proliferation and Delays Myotube Formation in Normal and Dystrophic Limb Muscle. *Biochem Cell Biol* 73:181-190, 1995.

McIntosh LM, Garrett KL, Megeney L, Rudnicki MA, Anderson JE.: Regeneration and Myogenic Cell Proliferation Correlate with Taurine Levels in Dystrophin- and Myo-D Deficient Muscles. *Anatom Rec* 252:311-325, 1998a.

McIntosh LM, Baker RE, Anderson JE.: Magnetic Resonance Imaging of Regenerating and Dystrophic Mouse Muscle. *Biochem Cell Biol* 76:1-10, **1998b.**

McIntosh LM.: A Proton Magnetic Resonance Study of Muscle Growth, Dystrophy, Repair and Drug Treatments in Control and Mdx Mice. PhD Thesis, University of Manitoba, **1998c.**

McIntosh LM, Granberg K-E, Briere KM, Anderson JE.: Nuclear Magnetic Resonance Spectroscopy Study of Muscle Growth, mdx Dystrophy and Glucocorticoid Treatments: Correlation with Repair. *NMR Biomed* 11(1):1-10, **1998d**

Mitchell CA, McGeachie JK, Grounds MD.: Cellular Differences in the Regeneration of Murine Skeletal muscle: A Quantitative Histological Study in SJL/J and BALBc Mice. *Cell Tissue Res* 269:159, **1992.**

Moreno A, Arús C.: Quantitative and Qualitative Characterization of ¹H-NMR Spectra of Colon Tumours, Normal Mucosa and Their Perchloric Acid Extracts: Decreased Levels of Myo-Inositol in Tumours Can be Detected in Intact Biopsies. *NMR Biomed* 8:33-45, **1996.**

Nahirney PC, Dow PR, Ovalle WK.: Quantitative Morphology of Mast Cells in Skeletal Muscle of Normal and Genetically Dystrophic Mice. *Anatom Rec* 247:341-349, **1997.**

Natarajan V, Scribner WM, Al-Hassani M, Vepa S.: Reactive Oxygen Species Signaling Through Regulation of Protein Tyrosine Phosphorylation in Endothelial Cells. *Environ Health Perspect* 106(5, suppl.):1205-1212, **1998.**

Ohlendieck K, Matsumara K, Ionasesan VV, et al.: Duchenne Muscular Dystrophy: Deficiency of Dystrophin-Associated Proteins in the Sarcolemma. *Neurology* 43:795-800; **1993.**

Ozawa E, Noguchi S, Mizuno Y, Hagiwara Y, Yoshida M.: From Dystrophinopathy to Sarcoglycanopathy: Evolution of a Concept of Muscular Dystrophy. *Muscle Nerve* April, 21(4):421-438, **1998.**

Papadimitriou JM, Robertson TA, Mitchell CA, Grounds MD.: The Process of New Plasmalemma Formation in Focally Injured Skeletal Muscle Fibers. *J Struct Biol* 103(2):124-134, **1990.**

Peeling J, Wong D, Sutherland GR.: Nuclear Magnetic Resonance Study of Regional Metabolism After Forebrain Ischemia in Rats. *Stroke* 20(5):633-640, **1989.**

Petrof BJ, Stedman HH, Shrager JB, Eby J, Sweeney HL, Kelly AM.: Adaptive

Alterations in Myosin Heavy Chain Expression and Contractile Function in the Dystrophic (mdx) Mouse Diaphragm. *Am J Physiol* 265:C834-C841, 1993.

Price MG., Gomer RH.: Skelemin, a Cytoskeletal M-Disc Periphery Protein, Contains Motifs of Adhesion Recognition and Intermediate Proteins. *J Biol Chem* 286:21800-21810, 1993.

Ricevuti G.: Host Tissue Damage by Phagocytes. *Ann NY Acad Sci* 832:426-448, 1997.

Silverstein RM, Bassler GC, Morrill TC.: Spectrometric Identification of Organic Compounds. 3rd edition, *John Wiley and Sons*, New York, New York, 1974.

Siperstein MD.: Role of Cholesterologenesis and Isoprenoid Synthesis in DNA Replication and Cell Growth. *J Lipid Res* 25:1462-1468, 1984.

Skoog DA, Leary JJ.: Principles of Instrumental Analysis. *Saunders College Publishing*, Orlando, Florida, 1992.

Smith ICP, Blandford DE.: Nuclear Magnetic Resonance Spectroscopy. *Analytical Chem* June 15, 67(12):509R-518R, 1995.

Sommers C.: Immunity and Inflammation. In: Pathophysiology: Concepts of Altered Health States. Porth CM (editor), 5th edition, *J.B. Lippincott Co.*, Philadelphia, Pennsylvania, 1998.

Strehler E, Carlsson E, Eppenberger HM, Thornell L-E.: Ultrastructural Localization of M-Band Proteins in Chicken Breast Muscle as Revealed by Combined Immunocytochemistry and Ultramicrotomy. *J Mol Biol* 166:141-158, 1983.

Storch TG, Talley GD.: Oxygen Concentration Regulates the Proliferative Response of Human Fibroblasts to Serum and Growth Factors. *Exp Cell Res* 175:317-325, 1988.

Stromer MH.: Immunocytochemistry of the Muscle Cell Cytoskeleton. *Microscopy Research and Technique* 31:95-105, 1995.

Sze DY, Jardetzky O.: Determination of Metabolite and Nucleotide Concentrations in Proliferating Lymphocytes by ¹H-NMR of Acid Extracts. *Biochim Biophys Acta* 1054:181-197, 1990.

Sze DY, Jardetzky O.: High-Resolution Proton NMR Studies of Lymphocyte Extracts. *Immunomethods* 4:113-126, 1994.

Tachi N, Ohya K, Chiba S, Matsuo M, Patria SY, Matsumara K.: Deficiency of

Syntrophin, Dystroglycan and Merosin in a Female Infant with a Congenital Muscular Dystrophy Phenotype Lacking Cysteine-Rich and C-Terminal Domains of Dystrophin. *Neurology* 49:579-583, 1997.

Tatsumi R, Anderson JE, Nevoret CJ, Halevy O, Allen RE.: HGF/SF is Present in Normal Adult Skeletal Muscle and is Capable of Activating Satellite Cells. *Dev Biol* 194(1):114-128, 1998.

Taylor RG, Geesink GH, Thompson VF, Koohmaraie M, Goll DE.: Is Z-Disk Degradation Responsible for Postmortem Tenderization? *J Ani Sci* 73(5):1351-1367, 1995.

Tokuyasu KT, Dutton AH, Singer SJ.: Immunoelectron Microscopic Studies of Desmin (Skeletin) Localization and Intermediate Filament Organization in Chicken Skeletal Muscle. *J Cell Biol* 96:562-570, 1983.

van Vliet AK, Negre-Aminou P, van Thiel GCF, Bolhuis PA, Cohen LH.: Action of Lovastatin, Simvastatin and Pravastatin on Sterol Synthesis and Their Antiproliferative Effect in Cultured Myoblasts from Human Striated Muscle. *Biochem Pharmacol* 52:1387-1392, 1996.

Vinnars E, Hammarqvist F, von der Decken, Wernerman J.: Role of Glutamine and its Analogs in Posttraumatic muscle Protein and Amino Acid Metabolism. *J Parenteral Enteral Nutr* 14:125S-129S, 1990.

Vinnars E, Bergstrom J, Furst P.: Influence of the Postoperative State on the Intracellular Free Amino Acids in Human Muscle Tissue. *Ann Surg* 182:665-671, 1975.

Voet D, Voet JG.: Biochemistry. John and Wiley and Sons Inc., New York, New York, 1990.

Vogt A, Qian Y, McGuire TF, Hamilton AD, Sebt SM.: Protein Geranylgeranylation, not Farnesylation, is Required for the G1 to S Phase Transition in Mouse Fibroblasts. *Oncogene* 13:1991-1999, 1996.

Watt DJ, Morgan JE, Clifford MA, Partridge TA.: The Movement of Muscle Precursor Cells Between Adjacent Regenerating Muscles in the Mouse. *Anat Embryol (Berl)* 175:527, 1987.

Walliman T, Doetschman TC, Eppenberger HM.: Novel Staining Patterns of Skeletal Muscle M-Lines Upon Incubation with Antibody Against MM-Creatine Kinase. *J Cell Biol* 96:1772-1779, 1983.

Wang K, Ramirez-Mitchell R.: A Network of Transverse and Longitudinal Filaments is Associated with Sarcomeres of Adult Vertebrate Skeletal Muscle. *J Cell Biol* 96:562-570, 1983.

Watermann-Stroerer CM.: The Cytoskeleton of Skeletal Muscle: is it affected by exercise? A Brief Review. *Med Sci Sports Exer* 23(11):1240-1249, 1991.

Wernerman J, Botta D, Hammarqvist F, Thunell S, von der Decken A, Vinnars E.: Stress Hormones Given to Healthy Volunteers Alter the Concentration and Configuration of Ribosomes in Skeletal Muscle, Reflecting Changes in Protein Synthesis. *Clin Sci* 77:611-616, 1989.

Wright CE, Tallan HH, Lin YY, Gaul GE.: Biological Update. *Ann Rev Biochem* 55:427-453, 1986.

Yamada T, Sugi H.: Nuclear Magnetic Resonance Spectroscopy of Skeletal Muscle and Muscle Proteins. *Japan J Physiol* 46(3):201-213, 1996.

Yoshida M, Ozawa E.: Glycoprotein Complex Anchoring Dystrophin to Sarcolemma. *J Biochem* 108:748-752, 1990.

Yoshida M., Suzuki A., Yamamoto H., Noguchi S., Mizuno Y., Ozawa E.: Dissociation of the Complex of Dystrophin and its Associated Proteins into Several Unique Groups by N-Octyl β -D-Glucoside. *Eur J Biochem* 222:1055-1061, 1994.

Yoshizaki K, Yoshiteru S, Nishikawa H.: High-Resolution Proton Magnetic Resonance Spectra of Muscle. *Biochimica Biophysica Acta* 678:283-291, 1981.

APPENDIX A

¹H-NMRS YIELD OF TAURINE

For accurate interpretation of spectral data it is important to know how much of a metabolite present in a tissue will be extracted with the perchloric acid extraction procedure. This is as important as reproducible handling of all tissues and samples during recovery, extraction and spectral acquisition. Two trials were run to determine the percentage of metabolites that could be extracted from a tissue, and to calibrate the taurine yields. The first trial involved adding a known amount of synthetic taurine, HMG-CoA and MA to a TA muscle sample before extracting the sample with perchloric acid for ¹H-NMRS. The second trial involved dissolving a known amount of synthetic taurine in 600 μ l of 1.5mM D₂O/TSP and acquiring a spectra using ¹H-NMRS. Spectra from each trial were integrated and the concentrations determined.

Trial 1 involved a known amount of taurine and MA were added to a minced TA muscle sample before extracting with perchloric acid. The extracts were prepared for ¹H-NMRS and analyzed as per all previous extracts. The concentration added to each muscle sample is given in table A-1 ([initial]) and the concentration determined from integrating each spectrum is also given. The yields for taurine should have been approximately 95% of the initial concentration. Our results were much less than the expected. It is believed that the inaccuracies were due to measurement error.

Trial 2 (table A-2) was performed to determine if a known concentration of taurine could be determined from its spectrum. For this procedure the initial concentrations were determined for measurements from two different scales. The concentrations determined from each sample's spectrum revealed inaccurate scale measurements.

Attempting to determine the $^1\text{H-NMRS}$ yield we discovered the difficulty in doing so with inaccurate weight measurements. To properly determine the yield of $^1\text{H-NMRS}$ of any metabolite the sensitivity of NMR should be respected. This means sensitive, calibrated weight scales are imperative. If our weights were more precise likely our results would have reflected this. When taurine 2 and 3 samples were measured on the Sartorius scale (trial 2) the yield was approximately 6% greater than what was initially added but still closest than all other measurements. A small part of this might be due to integration error but the greatest error is seen in the sample weights.

Figures A-1 through A-3 show MA, and taurine samples from each trial. The integrals of peaks used to calculate the samples concentration are indicated.

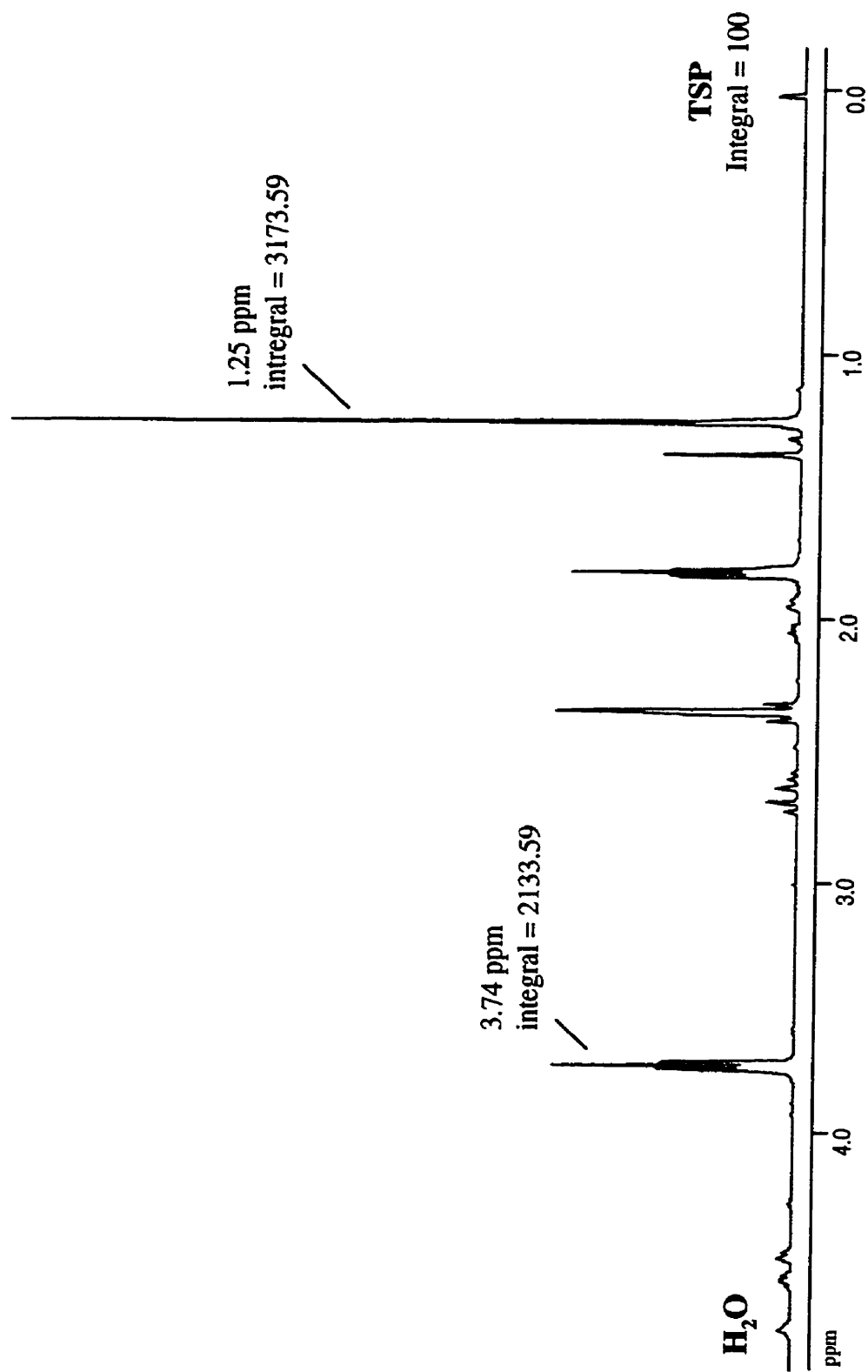


Figure A-1 A muscle sample spiked with mevalonic acid showing integrated peak areas used for calculating the concentration.

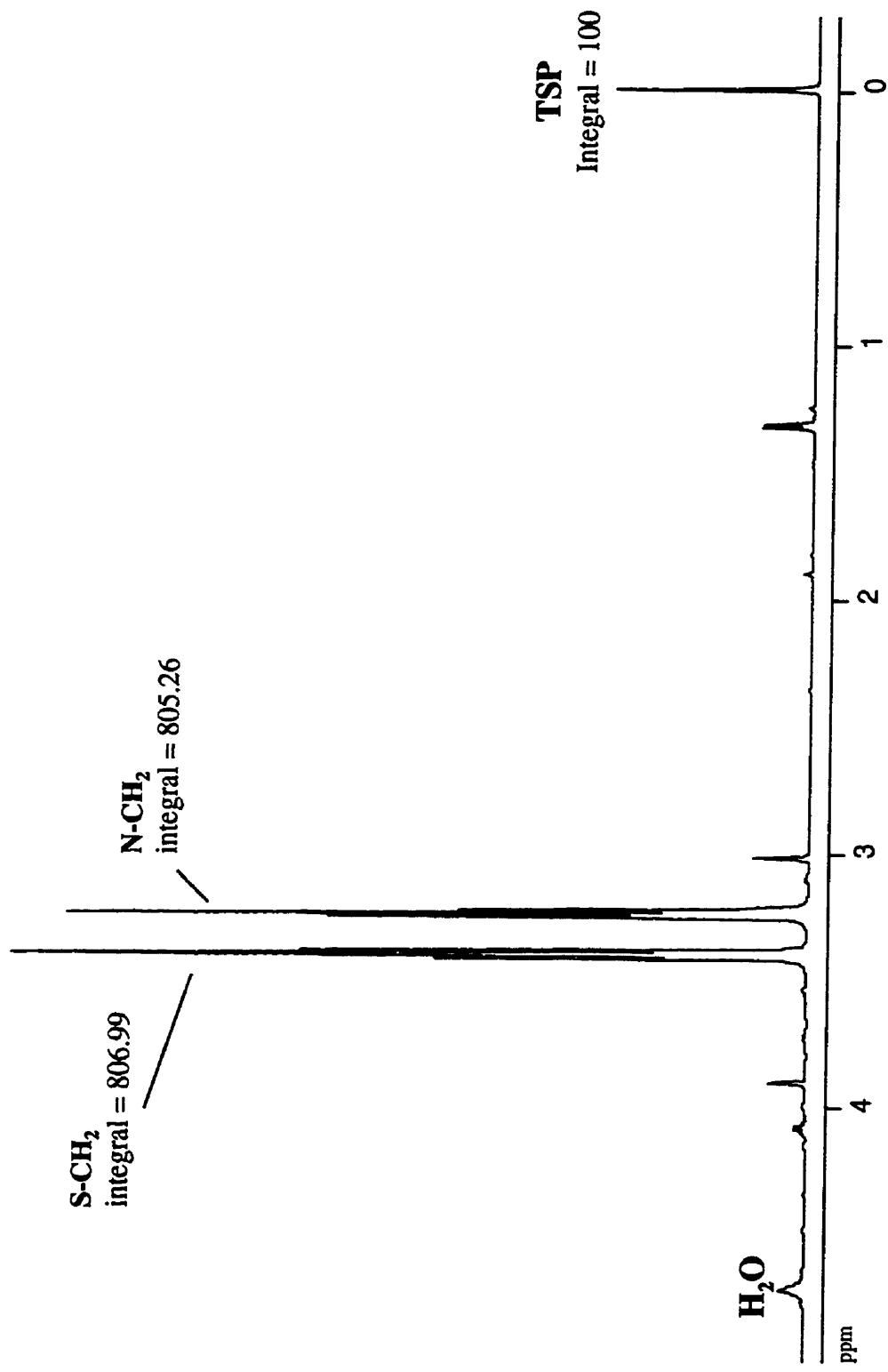


Figure A-2 A muscle sample spiked with taurine for trial 2 showing integrated peak areas used in calculating the concentration.

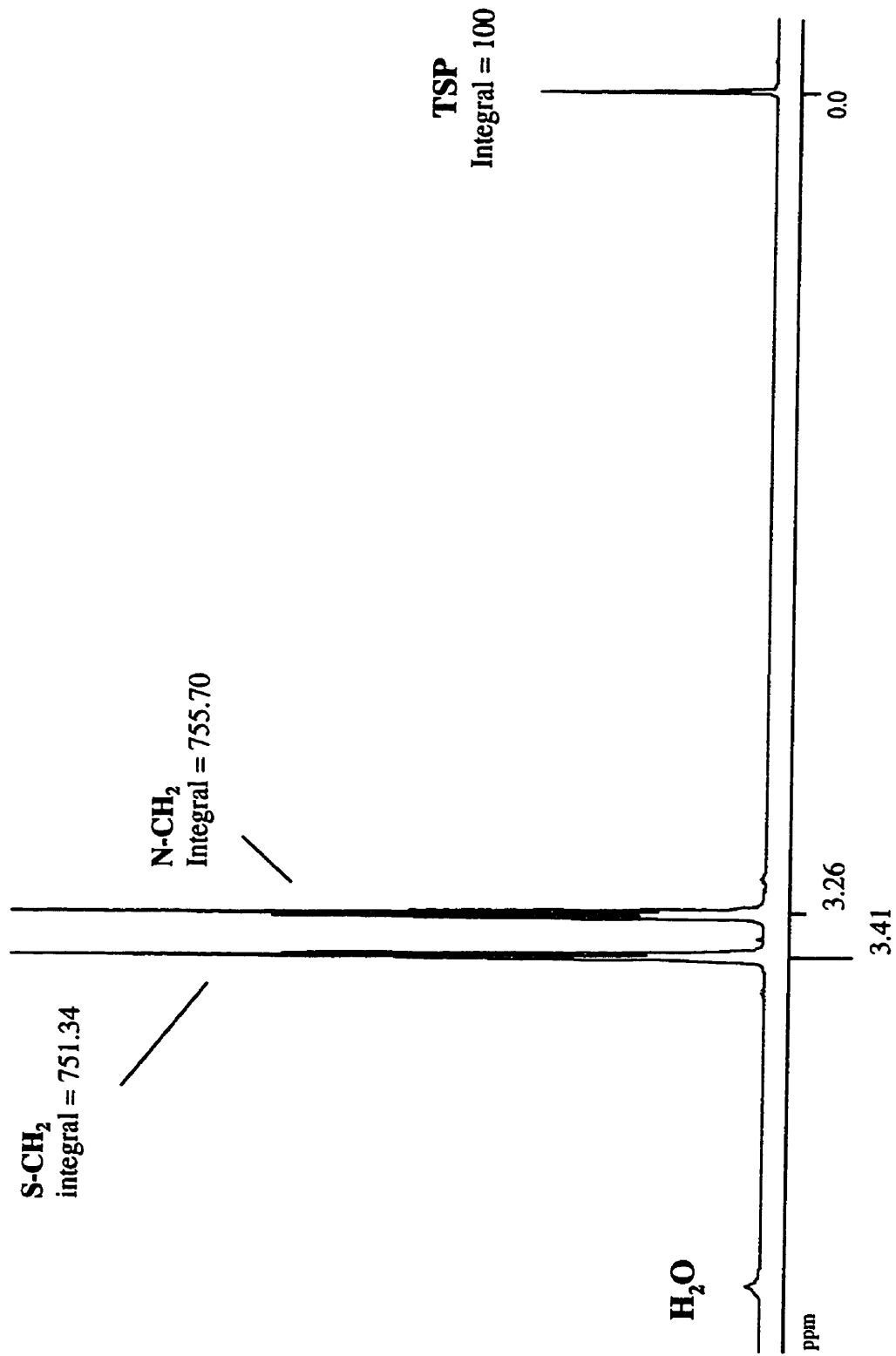


Figure A-3 A pure sample of laurine from trial 2 showing integrated peak areas used for calculating the concentration.

Table A-1

Trial 1: Extracted Samples From Male, C57 Mice (23 days of Age).
Extracts Were Subsequently Added to 0.6mL of 1.5mM TSP/D2O
and Processed Using ¹H-NMR Spectroscopy. AND scale was used.

	vial wt. (g)	Sample + Vial (g)	Sample (g)	Compound wt. (g)
MA-sample	2.032	2.054	0.022	0.019
MA-control	2.03	2.058	0.028	
<i>FW = 130.1</i>				
HMG-CoA-sample	1.98	2.01	0.03	0.003
HMG-CoA -control	2.009	2.027	0.018	
<i>FW = 911.7</i>				
Taurine-1**	1.993	2.035	0.042*	0.009
Taurine-2	2.008	2.047	0.039*	0.006

* Right and Left TA Muscle Samples were Combined.

** Formula Weight (FW) for Taurine = 125.1

From Spectra:

	Integral	Concentration (umol/mg)	
		[initial]:	[¹ H-NMRS]:
MA-sample			
1.26 ppm (3 1H)	3173.59	6.64	3.847
3.74 ppm (2 1H)	2133.59	6.64	3.879
Taurine-1			
N-CH2 (2 1H)	256.62	1.71	0.244
S-CH2 (2 1H)	254.15	1.71	0.242
Taurine-2			
N-CH2 (2 1H)	805.26	1.23	0.826
S-CH2 (2 1H)	806.99	1.23	0.828

Table A-2

Trial 2: A Known Quantity of 99% Pure Synthetic Taurine was Added to 0.6mL of 1.5mM TSP/D2O. Samples Weights Were Measured on Two Different Scales

Scale 1 - Sartorius:

	NMR tube wt. (g)	With Sample (g)	Sample wt. (g)
Taurine 1	2.45755	2.46085	0.0033
Taurine 2	2.4453	2.45025	0.00495
Taurine 3	2.4467	2.45025	0.00355

Scale 2 - AND:

	Vial wt. (g)	With Sample (g)	Sample wt. (g)
Taurine 1	2.458	2.462	0.004
Taurine 2	2.448	2.451	0.003
Taurine 3	2.449	2.452	0.003

From Spectra:

	Integral	Concentration (umol/ml)		
		[initial]: scale 1	[initial]: scale 2	[1H-NMRS]:
Taurine 1				
N-CH2 (2 1H)	855.66	43.965	53.291	57.044
S-CH2 (2 1H)	850.78	43.965	53.291	56.719
Taurine 2				
N-CH2 (2 1H)	999.69	65.947	39.965	66.646
S-CH2 (2 1H)	991.47	65.947	39.965	66.098
Taurine 3				
N-CH2 (2 1H)	755.7	47.295	39.965	50.38
S-CH2 (2 1H)	751.34	47.295	39.965	50.089

APPENDIX B - STATISTICS

Table B-1: Standardized Mean Area for Crushed Perchloric Acid Skeletal Muscle Extracts From C57 Mice Including Standard Deviation, Group Size and Age at Time of Muscle Sample Recovery.

Crushed Skeletal Muscle Extract Data

	0 day (n)	1day (n)	2 day (n)	4 day (n)	7 day (n)	9 day (n)	14 day (n)	N
unknown1.25	36.92 (9)	36.31 (6)	46.67 (8)	124.31 (6)	44.78 (5)	35.40 (7)	46.58 (9)	50
st dev	59.08	29.93	10.24	176.9	3.19	27.26	15.89	
lactate1.32	807.57 (9)	373.86 (8)	594.89 (9)	713.38 (7)	587.27 (5)	704.82 (7)	887.88 (10)	55
st dev	515.57	172.59	215.17	291.26	115.93	215.33	205.73	
alanine1.47	36.55 (8)	56.41 (8)	39.46 (9)	66.74 (7)	55.31 (5)	68.73 (7)	59.26 (10)	54
st dev	16.77	27.92	11.22	15.51	15.23	10.07	9.5	
acetate1.92	248.03 (9)	76.23 (9)	174.57 (9)	178.26 (7)	206.93 (5)	73.77 (7)	89.89 (10)	56
st dev	256.37	109.23	226.27	130.56	215.16	35.69	111.95	
glutamate2.34	19.88 (7)	27.17 (6)	30.70 (9)	69.95 (7)	66.74 (5)	71.96 (7)	47.83 (10)	51
st dev	10.86	7.23	13.09	13.11	13.11	13.32	15.31	
succinate2.41	13.35 (7)	7.50 (6)	9.49 (9)	15.74 (6)	13.53 (5)	10.99 (6)	13.97 (10)	49
st dev	12.64	8.23	15.09	7.04	10.97	10.97	14.83	
creatine3.04	346.98 (9)	160.51 (8)	296.77 (9)	434.25 (7)	351.38 (5)	484.81 (7)	699.08 (10)	55
st dev	203.57	103.71	193.83	291.15	110	201.74	145.72	
choline3.21	33.96 (3)	7.92 (4)	11.83 (6)	43.74 (4)	39.44 (4)	52.00 (3)	19.82 (4)	28
st dev	11.89	4.39	3.63	23.09	13.91	12.36	7.11	
carnitine3.23	28.53 (4)	34.10 (4)	33.39 (4)	100.24 (4)	64.69 (4)	83.52 (5)	61.39 (4)	29
st dev	13.72	17.16	22.11	43.36	15.91	36	15.01	
taurine3.26	300.40 (6)	158.16 (8)	282.36 (9)	549.59 (7)	437.75 (5)	575.71 (7)	746.90 (10)	52
st dev	168.35	102.34	139.07	333.72	137.20	173.22	187.8	
taurine3.41	276.37 (7)	143.95 (8)	296.97 (9)	472.02 (7)	404.82 (5)	552.98 (7)	699.14 (10)	53
st dev	137.19	87.75	126.23	291.23	132.86	151.03	130.52	
glycine3.56	12.49 (5)	29.46 (7)	113.15 (7)	47.39 (6)	48.92 (5)	57.74 (7)	69.65 (10)	50
st dev	10.1	13.21	207.03	30.34	21.66	18.25	16.76	
creatine3.94	219.79 (9)	91.09 (8)	206.81 (9)	283.83 (7)	208.66 (5)	296.68 (7)	449.96 (10)	55
st dev	116.11	75.96	112.11	149.84	91.16	113.26	126.84	
lactate4.11	208.92 (9)	103.06 (8)	160.33 (9)	188.40 (7)	147.83 (5)	185.18 (7)	230.75 (10)	55
st dev	159.76	45.62	64.92	64.58	26.9	37.71	48.37	
Sample weight (g)	0.023	0.025	0.022	0.028	0.023	0.026	0.023	
Average Age (days)	51.9	47.5	47.3	53.9	56.1	53.3	58.1	
Mice (N)	9	11	10	11	10	10	10	

Table B-2: Standardized Mean Area for Control Perchloric Acid Skeletal Muscle Extracts From C57 Mice Including Standard Deviation, Group Size and Age at Time of Muscle Sample Recovery.

Control Skeletal Muscle Extract Data

	0 day (n)	1day (n)	2 day (n)	4 day (n)	7 day (n)	9 day (n)	14 day (n)	N
unknown1.25	35.13 (4)	37.29 (10)	25.02 (6)	37.81 (6)	38.35 (8)	15.23 (6)	24.14 (5)	50
st dev	2.23	3.15	3.24	3.76	3.86	1.53	1.32	
lactate1.32	817.02 (5)	997.87 (11)	1084.46 (7)	1181.65 (8)	1219.54 (8)	1001.02 (8)	1082.20 (8)	55
st dev	139.03	271.53	104.53	125.76	158.87	117.89	135.13	
alanine1.47	42.37 (5)	66.14 (11)	50.19 (7)	66.44 (8)	51.87 (8)	55.99 (8)	73.49 (8)	55
st dev	16.38	12.52	11.31	13.44	11.6	21.26	32.55	
acetate1.92	98.65 (5)	142.87 (11)	77.25 (7)	80.73 (8)	165.20 (8)	94.47 (8)	103.25 (8)	55
st dev	101.59	133.25	31.67	36.49	159.67	39.62	59.08	
glutamate2.34	36.71 (5)	28.82 (10)	26.37 (7)	41.52 (8)	30.48 (7)	29.42 (8)	32.61 (8)	53
st dev	15.5	13.7	9.29	22.33	13.6	12.26	12.36	
succinate2.41	13.89 (5)	22.51 (10)	9.85 (7)	18.42 (8)	12.90 (7)	11.25 (8)	19.18 (8)	53
st dev	6.49	3.27	3.39	13.15	1.95	6.24	12.31	
creatine3.04	904.06 (5)	983.91 (11)	973.25 (7)	1041.68 (8)	1044.30 (8)	898.20 (8)	1125.18 (8)	55
st dev	273.74	333.63	231.31	310	223.33	212.7	172.1	
choline3.21	44.13 (3)	42.76 (6)	47.79 (5)	47.80 (7)	54.26 (5)	35.08 (5)	37.80 (5)	36
st dev	15.77	23.76	17.92	15.49	10	9.72	15.01	
carnitine3.23	90.49 (2)	86.53 (7)	91.08 (5)	102.63 (7)	97.72 (5)	73.03 (6)	103.59 (5)	37
st dev	63.33	12.35	32.92	29.5	17.05	11.68	53.41	
taurine3.26	694.08 (5)	840.73 (10)	883.52 (7)	919.53 (8)	860.79 (7)	764.25 (8)	989.69 (8)	53
st dev	285.81	337.49	193.35	127.45	120.6	143.33	103.35	
taurine3.41	680.37 (5)	838.75 (10)	836.06 (7)	901.03 (8)	838.16 (7)	716.88 (8)	926.51 (8)	53
st dev	260.31	135.23	130.92	108.21	17.31	17.95	373.06	
glycine3.56	29.61 (5)	35.31 (10)	35.60 (6)	51.67 (7)	42.89 (7)	32.91 (8)	81.54 (7)	50
st dev	13.32	12.83	15.11	12.77	7.7	11.97	35.16	
creatine3.94	591.83 (5)	650.14 (11)	680.45 (7)	677.26 (8)	725.95 (8)	543.78 (8)	659.22 (8)	55
st dev	172.7	224.18	143.49	95.21	133.5	22.39	140.37	
lactate4.11	236.48 (5)	268.50 (11)	286.45 (7)	306.14 (8)	312.67 (8)	266.89 (8)	284.64 (8)	55
st dev	77.02	103.73	113.7	129.21	110.33	30.51	120.06	
sample weight (g)	0.048	0.038	0.043	0.046	0.045	0.048	0.041	
Average Age (days)	51.9	47.5	47.3	53.9	56.1	53.3	58.1	
Mice (N)	9	11	10	11	10	10	10	

Table B-3: Standardized Mean Area for Uncrushed Perchloric Acid Skeletal Muscle Extracts From C57 Mice Including Standard Deviation, Group Size and Age at Time of Muscle Sample Recovery.

Uncrushed Skeletal Muscle Extract Data

	0 day (n)	1day (n)	2 day (n)	4 day (n)	7 day (n)	9 day (n)	14 day (n)	N
unknown1.25	46.26 (7)	27.44 (8)	84.57 (6)	70.50 (10)	58.37 (8)	36.11 (9)	125.81 (6)	54
st. dev.	32.08	27.1	65.36	59.98	15	88.18	19.15	
lactate1.32	1135.08 (7)	612.32 (8)	1046.37 (8)	1010.44 (9)	1417.46 (8)	1042.14 (9)	1653.48 (7)	56
st. dev.	377.2	252.13	901.13	570.68	613.11	880.05	983.54	
alanine1.47	41.07 (7)	114.65 (7)	71.88 (8)	65.97 (9)	101.02 (8)	80.07 (9)	98.95 (7)	55
st. dev.	12.33	48.68	24.92	22.38	7.15	24.52	33.58	
acetate1.92	102.53 (7)	155.76 (8)	43.03 (8)	297.52 (10)	80.23 (8)	135.21 (9)	266.50 (7)	57
st. dev.	67.65	273.16	88.64	301	33	231.62	272.12	
glutamate2.34	20.82 (6)	40.91 (7)	50.24 (8)	48.72 (9)	80.52 (8)	58.83 (9)	67.65 (7)	53
st. dev.	11.11	15.19	28.63	19.65	33.55	11.85	21.63	
succinate2.41	16.84 (7)	12.31 (7)	17.55 (8)	16.01 (9)	18.08 (8)	17.81 (9)	19.24 (7)	55
st. dev.	9.98	7.3	2.72	8.02	9.32	7.81	11.46	
creatine3.04	525.69 (7)	302.30 (8)	653.57 (8)	555.43 (9)	916.72 (8)	613.46 (9)	1186.97 (7)	56
st. dev.	189.27	181.67	501.67	246.11	333	351.97	692.69	
choline3.21	48.23 (4)	10.81 (4)	29.35 (6)	29.06 (9)	76.23 (5)	30.90 (7)	48.13 (5)	40
st. dev.	61.02	5.22	18.66	12.69	87.5	17.23	21.12	
carnitine3.23	42.07 (3)	30.89 (4)	80.95 (5)	65.05 (8)	126.16 (4)	76.55 (6)	119.86 (5)	35
st. dev.	33.65	13.01	36.2	22.18	89.15	36.27	72.65	
taurine3.26	404.37 (7)	229.54 (8)	640.29 (8)	548.47 (9)	1033.35 (8)	695.27 (9)	1093.38 (7)	56
st. dev.	156.7	92.61	289.49	246.41	231	215.7	525.6	
taurine3.41	380.28 (7)	247.89 (7)	644.89 (6)	534.47 (9)	1007.74 (8)	673.65 (9)	1067.26 (7)	53
st. dev.	166.23	111.66	264.88	288.88	307.72	163.9	272.9	
glycine3.56	22.46 (6)	38.31 (7)	60.13 (6)	41.58 (6)	75.60 (8)	55.35 (9)	65.11 (7)	49
st. dev.	7.77	33.715	19.17	12.27	38.7	13.21	20.63	
creatine3.94	343.50 (7)	183.14 (8)	438.32 (8)	355.43 (9)	588.33 (8)	388.65 (9)	739.00 (7)	56
st. dev.	119.91	130.71	184.19	167.8	260.12	108.66	519.59	
lactate4.11	322.08 (7)	180.32 (8)	309.91 (8)	257.18 (9)	384.97 (8)	281.60 (9)	452.12 (7)	56
st. dev.	112.67	69.01	98.72	81.16	182.28	77.52	187.27	
sample weight (g)	0.02	0.022	0.019	0.019	0.018	0.02	0.018	
Average Age (days)	51.9	47.5	47.3	53.9	56.1	53.3	58.1	
Mice (N)	9	11	10	11	10	10	10	

Table B-4: Analysis of Variance Tables for each NMRS-Visible Metabolite Studied.

Lactate1.32

Source of Variation	SS	df	MS	F	P-value	F-critical
DAYS	1.18E+07	62	190291.6	0.9	0.668125	1.52
TREATMENTS	3557771	1	3557771	16.73	0.000126	4
Error	1.32E+07	62	212609.3			
Total	2.85E+07	125				

Lactate4.11

Source of Variation	SS	df	MS	F	P-value	F-critical
DAYS	727432.4	61	11925.12	0.75	0.865186	1.53
TREATMENTS	243150.4	1	243150.4	15.34	0.000229	4
Error	966655.3	61	15846.81			
Total	1937238	123				

Creatine3.04

Source of Variation	SS	df	MS	F	P-value	F-critical
DAYS	7253428	62	116990.8	0.9	0.667605	1.53
TREATMENTS	8523803	1	8523803	65.23	2.91E-11	4
Error	8101160	62	130663.9			
Total	2.39E+07	125				

Creatine3.94

Source of Variation	SS	df	MS	F	P-value	F-critical
DAYS	3594352	62	57973.43	0.87	0.707946	1.53
TREATMENTS	3685197	1	3685197	55.28	3.78E-10	4
Error	4133070	62	66662.41			
Total	1.14E+07	125				

Taurine3.26

Source of Variation	SS	df	MS	F	P-value	F-critical
DAYS	5299456	57	92972.91	0.95	0.570391	1.55
TREATMENTS	4299297	1	4299297	44.11	1.26E-08	4.01
Error	5555560	57	97465.96			
Total	1.52E+07	115				

Taurine3.41

Source of Variation	SS	df	MS	F	P-value	F-critical
DAYS	4808761	58	82909.67	0.9	0.655421	1.55
TREATMENTS	4070000	1	4070000	44.17	1.15E-08	4.01
Error	5343933	58	92136.78			
Total	1.42E+07	117				

Alanine1.47

Source of Variation	SS	df	MS	F	P-value	F-critical
DAYS	50220.91	61	823.2936	1.1	0.352844	1.53
TREATMENTS	1027.745	1	1027.745	1.38	0.245402	4
Error	45572.68	61	747.0931			
Total	96821.33	123				

Glycine3.56

Source of Variation	SS	df	MS	F	P-value	F-critical
DAYS	190168.8	53	3588.09	0.84	0.742926	1.58
TREATMENTS	2131.182	1	2131.182	0.5	0.484337	4.02
Error	227717.6	53	4296.558			
Total	420017.5	107				

Acetate1.92

Source of Variation	SS	df	MS	F	P-value	F-critical
DAYS	1311346	62	21150.74	0.87	0.711205	1.53
TREATMENTS	30375.13	1	30375.13	1.25	0.268643	4
Error	1511556	62	24379.94			
Total	2853277	125				

Unknown1.25

Source of Variation	SS	df	MS	F	P-value	F-critical
DAYS	114356.9	56	2042.087	0.8	0.800252	1.56
TREATMENTS	11618.65	1	11618.65	4.54	0.037582	4.01
Error	143415.3	56	2560.988			
Total	269390.8	113				

Choline3.21

Source of Variation	SS	df	MS	F	P-value	F-critical
DAYS	17564.8	36	487.9112	1.16	0.332168	1.74
TREATMENTS	9211.846	1	9211.846	21.84	4.06E-05	4.11
Error	15183.07	36	421.7519			
Total	41959.72	73				

Succinate2.41

Source of Variation	SS	df	MS	F	P-value	F-critical
DAYS	9383.469	58	161.7839	0.94	0.598019	1.55
TREATMENTS	542.3968	1	542.3968	3.14	0.08164	4.01
Error	10018.4	58	172.731			
Total	19944.26	117				

Carnitine3.23

Source of Variation	SS	df	MS	F	P-value	F-critical
DAYS	73772.76	38	1941.389	1.45	0.126488	1.72
TREATMENTS	36973.74	1	36973.74	27.69	5.83E-06	4.1
Error	50733.04	38	1335.08			
Total	161479.5	77				

Glutamate2.34

Source of Variation	SS	df	MS	F	P-value	F-critical
DAYS	31860.88	58	549.3255	0.83	0.761465	1.55
TREATMENTS	3985.691	1	3985.691	6.01	0.017222	4.01
Error	38437.97	58	662.7237			
Total	74284.55	117				